The effect of beta-oxidation or TCA cycle inhibition on mitochondrial function and the sensitivity of high resolution respirometry detection

By:

Prisca Ofure Osiki

Student number: PRSOSI001

Supervisor: Dr. Dheshnie Keswell
Co-Supervisor: Dr. Amy E. Mendham

Thesis presented for the degree of:
Masters of Science (Med) Physiology
University of Cape Town

April 2019

Department of Human Biology,
Faculty of Health Sciences
University of Cape Town

DECLARATION

I, *Prisca Ofure Osiki,* hereby declare that the work on which this dissertation/thesis is based is my original work (except where acknowledgements indicate otherwise) and that neither the whole work nor any part of it has been, is being, or is to be submitted for another degree in this or any other university.

I empower the university to reproduce for the purpose of research either the whole or any portion of the contents in any manner whatsoever.

Signature: Signed by candidate Date: April 22nd 2019

Plagiarism Declaration

I know that plagiarism is wrong. Plagiarism is to use another's work and pretend that it is one's own.

This thesis/dissertation has been submitted to the Turnitin module (or equivalent similarity and originality checking software) and I confirm that my supervisor has seen my report and any concerns revealed by such have been resolved with my supervisor.

I have used the American Physiological Society referencing style for citation and referencing. Each contribution to and quotation in this dissertation from the work(s) of other people has been attributed, and has been sited and referenced.

Signature: Signed by candidate Date: April 22nd 2019

Acknowledgements

Firstly, I would like to thank my supervisor, Dr Dheshnie Keswell and my co-supervisor, Dr Amy Mendham without whose help this project would not have been completed. Your continuous guidance, thoroughness and genuine interest in my welfare surpassed that dictated for normal supervision. I was only able to complete this due to your insistence on my success.

I would also like to thank Prof Edward Ojuka, whose idea and plan this project was based on, I was immensely impacted by your gentleness, mentorship and guidance. Prof Vicki Lambert, the former head, division of Exercise Science and Sports Science Medicine (ESSM). Thank you for always going out of your way to help me and to ensure that I received all the necessary support that ensured successful completion of my research. Dr Tertius Kohn for your help with my protein assays and ensuring that I understood the concepts and technicalities that were required, your assistance was immeasurable. Dr Robea Ballo, for helping with tissue culturing and continued willingness to assist and advise where the need arose. Mrs Adri Winckler for your amazing support, guidance, counselling and the kindness you have shown me throughout the course of my degree. I equally thank all members of staff of the postgraduate administrative office, your friendship and kindness whilst I worked with you and even as I continued with my research was much appreciated.

Thank you to the Faculty of Health Sciences (completion grant), Department of Human Biology, ESSM (Ziphelele Mbambo scholarship) and the National Research Foundation (NRF) for the opportunity and funding to carry out this research. Many thanks to all the support staff at ESSM; Neezam Kariem and Trevino Larry for always willing to help with technicalities and taking time to explain and make lab work memorable. I am grateful Lesa Sivewright and Ayesha Hendricks for the administrative support you provided and your willingness to always assist and provide encouragement during this degree.

Words are insufficient to thank my parents, for their prayers and support and with whose help and nurturing I have become what I am. I especially thank my sister, Dr Abigail Osiki for always listening when I had complaints and bringing me out of dark moods and being a pillar of support throughout this project. Your help was an olive branch. I also appreciate my other siblings whose presence in my life has made the world many times better. I thank my friends and the members of my life group for their continued encouragement throughout this process.

Lastly, I want to acknowledge God who has made all things possible for me, even when I did not see it happening.

Table of Contents

DECLARATION 2
ACKNOWLEDGEMENTS 3
LIST OF ABBREVIATIONS 7
LIST OF FIGURES AND TABLES 10
ABSTRACT 16
CHAPTER ONE: Literature review 19
1.1 Introduction 19
1.2 Overview of oxidative metabolism within the mitochondria (β-oxidation and TCA cycle and oxidative phosphorylation) 20
1.3 Dysfunction of β-oxidation 24
1.4 Dysfunction of the TCA cycle 27
1.4.1 The role of β-oxidation and anaplerotic reactions in maintaining energy production in primary TCA cycle dysfunction 27
1.5 Summary: A stategy to investigate the relationship between β-oxidation, TCA cycle and OXPHOS by inhibiting key enzymes of β-oxidation or TCA cycle 29
1.6 Commonly used Methods for assessing β-oxidation and TCA cycle defects 31
1.7 The use of high resolution respirometry for assessing β-oxidation, TCA cycle and Oxidative phosphorylation 33
1.7.1 Principle of respirometry 33
1.7.2 Assessment of mitochondrial respiration with High resolution respirometry, HRR 33
1.7.3 Sensitivity of substrates used for assessing β-oxidation and TCA cycle with HRR 35
1.8.4 Commonly used Substrate combinations for the assessment of β-oxidation by HRR 36
1.8.4.1 Palmitoylcarnitine or Octanoylcarnitine 37
1.8.4.2 Palmitoylcarnitine or Octanoylcarnitine plus malate 37
1.8.4.3 Palmitoylcarnitine or Octanoylcarnitine plus carnitine 38
1.9 Aims 40
1.10 Objectives 40
1.11 Hypothesis 40
CHAPTER TWO: Materials and Methods 42
2.1. Justification for the use of a cell culture model 42
2.2 Experimental logistics and design 42
2.3 Experimental Protocols 42
2.3.1 Cell culture 42
2.3.2 Trypsinization 43

2.3.3 Cell Passage 43
2.3.4. Differentiation 43
2.3.5. Mycoplasma Test 44
2.3.6 Treatment regime 45
2.3.7. MTT Proliferation Assay 45
2.3.8 Protein assays 48
2.3.8.1 Protein extraction 48
2.3.8.2 Protein determination 48
2.3.8.3 MCAD activity 48
2.3.8.4 Aconitase activity 50
2.3.8.5 Citrate synthase 51
2.3.9 Respirometry 52
2.3.9.1 SUIT Protocol 1: Respiration with octanoylcarnitine + malate 53
2.3.9.2 SUIT Protocol 2: Respiration with octanoylcarnitine + carnitine 53
2.3.9.3 SUIT Protocol 3: Mitochondrial respiration with pyruvate +malate 53
2.4 statistical analysis 54
CHAPTER THREE: Results 55
3.1 The effect of inhibition on enzyme activities 55
3.1.1 MCAD activity 55
3.1.2 Aconitase activity assay 55
3.1.3 Citrate synthase activity assay 55
3.2 The effect of enzyme inhibition on mitochondrial respiration 57
3.2.1 The effect of enzyme inhibition on mitochondrial respiration using octanoylcarnitine and malate as substrates 57
3.2.1.1 The effect of MCAD inhibition 57
3.2.1.2 The effect of aconitase inhibition 61
3.2.1.3 Differences between aconitase inhibition and MCAD inhibition 62
3.2.2 The effect of enzyme inhibition on mitochondrial respiration using octanoylcarnitine and carnitine as substrates 65
3.2.2.1 The effect of MCAD and aconitase inhibition 66
3.2.3 The effect of enzyme inhibition on mitochondrial respiration using pyruvate, malate and glutamate as substrates. 72
3.2.3.1 The effect of MCAD inhibition 73
3.2.3.2 The effect of aconitase inhibition 76
3.2.3.3 Differences between aconitase inhibition and MCAD inhibition 77
CHAPTER FOUR: Discussion 81

4.1 Effect of MCAD inhibition on enzyme activity determined by spectrophotometric assay 81
4.2 Effect of Aconitase inhibition on enzyme activity..... 84
4.3 The combined effect of MCAD and Aconitase inhibition..... 86
4.4 The effect of enzyme inhibition on mitochondrial respiration 86
4.4.1 The effect of MCAD inhibition on mitochondrial respiration 87
4.4.1.1 The effect of MCAD inhibition on mitochondrial respiration using octanoylcarnitine and malate substrate combination 87
4.4.1.2 The effect of MCAD inhibition on mitochondrial respiration using pyruvate, malate and glutamate substrate combination 89
4.4.1.3 The effect of MCAD inhibition on mitochondrial respiration using octanoylcarnitine and carnitine substrate combination 91
4.4.2 The effect of aconitase inhibition on mitochondrial respiration 93
4.4.2.1 The effect of aconitase inhibition on mitochondrial respiration using pyruvate, malate and glutamate substrate combination 93
4.4.2.2 The effect of aconitase inhibition on mitochondrial respiration using octanoylcarnitine and malate 95
4.4.2.3 The effect of aconitase inhibition on mitochondrial respiration using octanoylcarnitine and carnitine as substrates..... 96
4.5 Conclusion and future consideration 98
REFERENCES 100
APPENDIX..... 117

List of Abbreviations

ADP	Adenosine diphosphate
ANOVA	Analysis of Variance
ASM	Acid soluble metabolites
ATP	Adenosine triphosphate
BSA	Bovine serum albumin
CI (CI-CIV)	Complex I
CACT	Carnitine acetyl-carnitine translocase
Car	Carnitine
CCCP	Cabonyl cyanide m-chlorophenyl hydrazine
CO_2	Carbon dioxide
CoA	Co-enzyme A
CPT	Carnitine palmitoyl transferase
DMEM	Dulbecco's Modified Eagle's Medium
$DMEM^{+}$	Differentiation media with DMEM, 2% Horse Serum and 1% antiobiotic
$DMEM^{++}$	Differentiation media with DMEM, 10% Fetal Bovine Serum and 1% antiobiotic
DMSO	Dimethyl sulfoxide
DNA	Deoxyribonucleic acid
EDTA	Ethylenediamine tetraacetic acid
ETF	Electron transfer flavoprotein
ETS	Electron transfer system
ETS^{CI}	ETS respiratory state due to Complex I alone
ETS^{CI+FAO}	ETS respiratory state due to convergent electron flow from Complex I and fatty acid oxidation
$ETS^{CI+FAO+CII}$	ETS respiratory state due to convergent electron flow from Complex I, fatty acid oxidation and Complex II
ETS^{FAO}	ETS respiratory state due to fatty acid oxidation alone
ETS^{FAO+CI}	ETS respiratory state due to convergent electron flow from fatty acid oxidation and Complex I

$ETS^{FAO+CI+CII}$	ETS respiratory state due to convergent electron flow from fatty acid oxidation, Complex I and Complex II
FA	Fatty acid
FBS	Fetal bovine serum
$FADH_2$	Flavine adenine dinucleotide
FAO	Fatty acid oxidation
GDP	Guanosine diphosphate
GTP	Guanosine triphosphate
HFHSD	High fructose high sucrose diet
H_2O_2	Hydrogen peroxide
HRR	High resolution respirometry
KAT	Ketoacyl-CoA thiolase
$KHPO_4$	Monopotassium phosphate
LCAD	Long chain acyl-CoA dehydrogenase
$Leak^{CI}$	Leak respiratory state due to Complex I alone
$Leak^{FAO}$	Leak respiratory state due to fatty acid oxidation alone
MCAD	Medium chain acyl-CoA dehydrogenase
$MgCl_2$	Magnesium chloride
MTP	Mitochondrial trifunctional protein
MTT	3-(4,5-Dimethylthiazol-2-Yl)-2,5-Diphenyltetrazolium Bromide
NADH	Nicotinamide adenine dinucleotide
NADPH	Nicotinamide adenine dinucleotide phosphate
OXPHOS	Oxidative phosphorylation
$OXPHOS^{CI}$	OXPHOS respiratory state due to Complex I alone
$OXPHOS^{FAO}$	OXPHOS respiratory state due to fatty acid oxidation alone
PBS	Phosphate buffer saline
Pi	Inorganic phosphate
Q	Ubiquinone
ROS	Reactive oxygen species
ROX	Residual oxygen consumption
SCAD	Small chain acyl-CoA dehydrogenase
SUIT	Substrate uncoupler inhibition titration
TCA	Tricarboxylic acid
TMS	Tandem mass spectrometry

UV/vis	Ultraviolet/visible
VLCAD	Very long chain acyl-CoA dehydrogenase
β-oxidation	Beta-oxidation
µl	microliter
μm^2	micrometer squared
g/l	Grams per litre
mg	milligrams
mmol	milimolar
ml	millilitres
nm	nanometers
pmol	picomolar
U/ml	units per millilitres

List of figures and tables

Figure 1.1: Relationship between β-oxidation, TCA cycle and OXPHOS: Fatty acid β-oxidation (Purple) generates shortened acyl-CoAs, acetyl-CoA, NADH and $FADH_2$ in four enzymatic reactions. The acetyl-CoA produced is utilized by the TCA cycle which also generates more NADH and $FADH_2$. Electrons derived from NADH and $FADH_2$ are used by the complexes of the Electron transport system (ETS) in OXPHOS to generate ATP. Flow of electrons in the ETS is governed by the increasing order of electronegativity of the complexes. The resulting membrane potential generated drives the synthesis of ATP from ADP and inorganic phosphate (P_i). Complex I (CI, NAD:ubiquinone oxidoreductase), Complex II (CII, succinate:ubiquinone oxidoreductase), Complex III (CIII, ubiquinol: ferricytochrome C oxidoreductase, Complex IV (CIV, cytochrome c oxidase), Complex V (ATP synthase) modified from (107).

Figure 1.2: Overview of mitochondrial β-oxidation pathway: degradation of fatty acyl-CoA esters in the matrix of the mitochondria comprises of four reactions (numbered 1-4 in black) that are catalyzed by chain-length specific enzymes (chain lengths shown in dark blue). (1) Oxidation of acyl-CoAs into enoyl-CoA by FAD-dependent acyl-CoA dehydrogenases: Short-chain (SCAD), medium-chain (MCAD), long-chain (LCAD) and very long-chain (VLCAD). (2) Hydration into 3-hydroxyl-CoA by enoyl-CoA hydratase (ECHS) or the single hetero-octamer protein, the mitochondrial trifunctional protein (MTP) (3) Dehydrogenation into 3-ketoacyl-CoA by medium/short chain hydroxyacyl-CoA dehydrogenase (HADH) or MTP (4) Thiolysis by ketoacyl-CoA thiolase (KAT) or (MTP) to produce a 2-carbon shortened acyl-CoA and acetyl-CoA (107).

Figure 1.3: Overview of the TCA cycle: Oxidative decarboxylation of acetyl-CoA, reducing equivalents are generated that transfer electrons to the ETS to generate ATP; modified from (126).

Figure 1.4: Reactions of the TCA cycle including exogenous supply of TCA cycle carbon intermediates (126).

Figure 1.5: Reconstitution of the TCA cycle using exogenous supplied pyruvate, malate, glutamate and succinate (51).

Figure 2.1: Changes in cell morphology in response to myogenic differentiation in control C2C12 cells. Light microscope images of C2C12 cells before and after induction of differentiation at 70% confluency with DMEM containing 2% horse serum. Cells reach 70% confluency approximately 24 hours after seeding cells onto a tissue culture flask. The cells are spindle-shaped, replication increases with time till the tissue culture flasks is fully saturated with cells at Day 2. Cells fuse together to form elongated and branched multi-nucleatated myotubes; increasing with number of days till after the 8^{th} day, where they start to gradually die off (Day 10). Cells were treated with inhibitors on the 7^{th} day after differentiation was initiated.

Figure 2.2: Experimental design. C2C12 cells were grown till a passage number of 7 ($1x10^6$ cells), after which they were differentiated into myotubes for 7 days. On the 7^{th} day, myotubes were treated with a low or high concentration of either inhibitor for MCAD or aconitase versus vehicle for 12 hours. Thereafter flasks were pooled together and separated for use in either high resolution respirometry (HRR) or for protein extraction. For all experiments, 2 technical repeats and 3 biological repeats was employed. Octanoylcarnitine (Oct), malate (Mal), carnitine (Car), pyruvate (Pyr), glutamate (Glut)

Figure 2.3: The activity of Medium chain acyl-CoA dehydrogenase (MCAD) in control C2C12 myotubes relative to Octanoyl-CoA concentrations (104.2, 160.7, 106.4, 163.6 and 86.2 mM).

Figure 2.4: The activity of aconitase in control C2C12 myotubes relative to sample volume.

Figure 3.1: The effect of MCAD and aconitase inhibition on MCAD, aconitase and citrate synthase activities. A, C, E are enzyme assays where MCAD was inhibited while B, D, F are enzyme assays where aconitase was inhibited. All data reported as Mean ± Standard Deviation. * $P < 0.05$, ** $P < 0.01$*** $P < 0.001$.

Figure 3.2: Representative trace for a high resolution respirometry protocol with octanoylcarnitine and malate substrate combination. Graph represents oxygen (O_2) concentration (blue line [µM] and changes in Oxygen flux (red line; [pmol/(s*million cells)]) with time (h: min) in a single oxygraph chamber (oroboros-2K; Oroboros instruments; Austria). ADP (Adenosine di phosphate), CCCP (carbonyl

cyanide m-chlorophenyl hydrazone), OXPHOS (oxidative phosphorylation), ETS (electron transport system), ROX (residual oxygen consumption).

Figure 3.3: The effect of MCAD inhibition on O_2 flux with octanoylcarnitine and malate as substrates. A) O_2 flux corrected to approximate number of cells (pmol O_2/s/million cells). B) O_2 flux corrected to protein concentration (pmol O_2/s/mg protein). FAO (fatty acid oxidation), OXPHOS (Oxidative phosphorylation), ETS (Electron transport system), CI (Complex I), CII (Complex II), car (Carnitine), ROX (Residual oxygen consumption). All data reported as mean ± standard deviation; n = 3; *p < 0.05, **p < 0.01.

Figure 3.4: The effect of MCAD inhibition on flux control ratio (FCR) with octanoylcarnitine and malate as substrates. Diagram shows flux control ratios (FCR) normalized relative to A) maximum ETS capacity ($ETS^{FAO+CI+CII}$) as a result of convergent electron flow from fatty acid oxidation (FAO), Complex I (CI) and complex II (CI) B) ETS capacity as a result of FAO (ETS^{FAO}). ETS (Electron transport system), OXPHOS (Oxidative phosphorylation). All data reported as mean ± standard deviation; n = 3; *p < 0.05, **p < 0.01.

Figure 3.5: The effect of MCAD inhibition on $Leak^{FAO}$/$OXPHOS^{FAO}$ coupling control ratio with octanoylcarnitine and malate as substrates. All data reported as mean ± standard deviation; n = 3.

Figure 3.6: The effect of aconitase inhibition on O_2 flux with octanoylcarnitine and malate as substrates. A) O_2 flux corrected to approximate number of cells per oxygraph chamber (pmol O_2/s/million cells) B) O_2 flux corrected to protein concentration (pmol O_2/s/mg protein). FAO (fatty acid oxidation), OXPHOS (Oxidative phosphorylation), ETS (Electron transport system), CI (Complex I), CII (Complex II), ROX (Residual oxygen consumption). All data reported as mean ± standard deviation; n = 3; *p < 0.05.

Figure 3.7: The effect of aconitase inhibition on flux control ratio (FCR) with octanoylcarnitine and malate as substrates. Diagram shows flux control ratios (FCR) normalized relative to A) maximum ETS capacity ($ETS^{FAO+CI+CII}$) as a result of convergent electron flow from fatty acid oxidation (FAO), Complex I (CI) and complex II (CI) B) ETS capacity as a result of FAO (ETS^{FAO}). ETS (Electron transport system),

OXPHOS (Oxidative phosphorylation). All data reported as mean ± standard deviation; n = 3; *p < 0.05, **p < 0.01.

Figure 3.8: The effect of aconitase inhibition on $Leak^{FAO}$/$OXPHOS^{FAO}$ coupling control ratio with octanoylcarnitine and malate as substrates. All data reported as mean ± standard deviation; n = 3.

Figure 3.9: Representative trace for a high resolution respirometry protocol with octanoylcarnitine and carnitine substrate combination. Graph represents oxygen (O_2) concentration (blue line [µM] and changes in Oxygen flux (red line; [pmol/(s*million cells)]) with time in a single oxygraph chamber (oroboros-2K; Oroboros instruments; Austria). ADP (Adenosine di phosphate), CCCP (carbonyl cyanide m-chlorophenyl hydrazone), OXPHOS (oxidative phosphorylation), ETS (electron transport system), ROX (residual oxygen consumption).

Figure 3.10: The effect of MCAD inhibition on O_2 flux with octanoylcarnitine and carnitine as substrates. A) O_2 flux corrected to approximate number of cells per oxygraph chamber (pmol O_2/s/million cells) B) O_2 flux corrected to protein concentration (pmol O_2/s/mg protein). FAO (fatty acid oxidation), OXPHOS (oxidative phosphorylation), ETS (Electron transport system), CI (Complex I), CII (Complex II), ROX (Residual oxygen consumption). All data reported as mean ± standard deviation; n= 3.

Figure 3.11: The effect of MCAD inhibition on flux control ratio (FCR) with octanoylcarnitine and carnitine as substrates. Diagram shows flux control ratios (FCR) normalized relative to A) maximum ETS capacity ($ETS^{FAO+CI+CII}$) as a result of convergent electron flow from fatty acid oxidation (FAO), Complex I (CI) and complex II (CI) B) ETS capacity as a result of FAO (ETS^{FAO}). ETS (Electron transport system), OXPHOS (Oxidative phosphorylation). All data reported as mean ± standard deviation; n = 3; *p < 0.05.

Figure 3.12: The effect of MCAD inhibition on $Leak^{FAO}$/$OXPHOS^{FAO}$ coupling control ratio with octanoylcarnitine and carnitine as substrates. All data reported as mean ± standard deviation; n = 3.

Figure 3.13: The effect of aconitase inhibition on O_2 flux with octanoylcarnitine and carnitine as substrates. A) O_2 flux corrected to approximate number of cells per oxygraph chamber (pmol

O_2/s/million cells) B) O_2 flux corrected to protein concentration (pmol O_2/s/mg protein). FAO (fatty acid oxidation), OXPHOS (oxidative phosphorylation), ETS (Electron transport system), CI (Complex I), CII (Complex II), ROX (Residual oxygen consumption). All data reported as mean ± standard deviation; n= 3.

Figure 3.14: The effect of aconitase inhibition on flux control ratio (FCR) with octanoylcarnitine and carnitine as substrates. Diagram shows flux control ratios (FCR) normalized relative A) maximum ETS capacity ($ETS^{FAO+CI+CII}$) as a result of convergent electron flow from fatty acid oxidation (FAO), Complex I (CI) and complex II (CI) B) ETS capacity as a result of FAO (ETS^{FAO}). ETS (Electron transport system), OXPHOS (Oxidative phosphorylation). All data reported as mean ± standard deviation; n = 3; **p < 0.005.

Figure 3.15: The effect of aconitase inhibition on $Leak^{FAO}$/$OXPHOS^{FAO}$ coupling control ratio with octanoylcarnitine and carnitine as substrates. All data reported as mean ± standard deviation; n = 3.

Figure 3.16: Representative trace for a high resolution respirometry protocol with pyruvate, malate and glutamate substrate combination. Graph represents oxygen (O_2) concentration (blue line [μM] and changes in oxygen flux (red line; [pmol/(s*million cells)]) with time in a single oxygraph chamber (oroboros-2K; Oroboros instruments; Austria). ADP (Adenosine di phosphate), CCCP (carbonyl cyanide m-chlorophenyl hydrazone), OXPHOS (oxidative phosphorylation), ETS (electron transport system), ROX (residual oxygen consumption).

Figure 3.17: The effect of MCAD inhibition on O_2 flux with pyruvate, malate and glutamate as substrates. A) O_2 flux corrected to approximate number of cells per oxygraph chamber (pmol O_2/s/million cells) B) O_2 flux corrected to protein concentration (pmol O_2/s/mg protein). FAO (fatty acid oxidation), OXPHOS (Oxidative phosphorylation), ETS (Electron transport system), CI (Complex I), CII (Complex II), ROX (Residual oxygen consumption). All data reported as mean ± standard deviation; n = 3; *p < 0.05, **p < 0.01, ***p < 0.001.

Figure 3.18: The effect of MCAD inhibition on flux control ratio (FCR) with pyruvate, malate and glutamate as substrates. Diagram shows flux control ratios (FCR) normalized relative to A) maximum

ETS capacity ($ETS^{CI+FAO+CII}$) as a result of convergent electron flow from Complex I (CI), fatty acid oxidation (FAO) and complex II (CI) B) ETS capacity as a result of CI (ETS^{CI}). All data reported as mean ± standard deviation; n = 3; *p < 0.05.

Figure 3.19: The effect of MCAD inhibition on $Leak^{CI}/OXPHOS^{CI}$ coupling control ratio with pyruvate, malate and glutamate as substrates. All data reported as mean ± standard deviation; n = 3.

Figure 3.20: The effect of aconitase inhibition on O_2 flux with pyruvate, malate and glutamate as substrates. A) O_2 flux corrected to approximate number of cells per oxygraph chamber (pmol O_2/s/million cells) B) O_2 flux corrected to protein concentration (pmol O_2/s/mg protein). FAO (fatty acid oxidation), OXPHOS (Oxidative phosphorylation), ETS (Electron transport system), CI (Complex I), CII (Complex II), ROX (Residual oxygen consumption). All data reported as mean ± standard deviation; n = 3; *p < 0.05, **p < 0.01.

Figure 3.21: The effect of aconitase inhibition on flux control ratio (FCR) with pyruvate, malate and glutamate as substrates. Diagram shows flux control ratios (FCR) normalized relative to A) maximum ETS capacity ($ETS^{CI+FAO+CII}$) as a result of convergent electron flow from Complex I (CI), fatty acid oxidation (FAO) and complex II (CI) B) ETS capacity as a result of CI (ETS^{CI}). All data reported as mean ± standard deviation; n = 3; *p < 0.05, **p < 0.01.

Figure 3.22: The effect of aconitase inhibition on $Leak^{CI}/OXPHOS^{CI}$ coupling control ratio with pyruvate, malate and glutamate as substrates. All data reported as mean ± standard deviation; n = 3.

Figure A.1: Plate layout for MTT assay

Table A.1: Concentration and volume of inhibitor

Table A.2: Aconitase assay reagent solutions

Table A.3: NADPH standard curve

Table A.4: Determination of ferrocenium ($Fe^{+}PF_6^{-}$) standard

Table A.5: Development of NADH standards

Abstract

INTRODUCTION: A dysfunction in fatty acid beta-oxidation (β-oxidation), particularly medium chain acyl-CoA dehydrogenase (MCAD) dysfunction is a major cause of mortality and its diagnosis is usually achieved by measuring specific protein activities or metabolites in blood and/or urine samples. However, these methods do not account for secondary defects that accompany primary deficiency; such as where measures of disruption in fatty acid metabolism do not account for defects in the TCA cycle and oxidative phosphorylation. These metabolic pathways are connected and dysfunction in one pathway (primary) could lead to dysfunction in the other (secondary). We propose the use of methods that combines all aspects of the bioenergetics module (enzyme activity in substrate oxidation within each individual pathway, transfer of electrons through the electron transport system (ETS) and oxidative phosphorylation for ATP generation) may be a more effective assessment technique. High resolution respirometry (HRR) is a recently developed technique that accounts for substrate oxidation, electron transfer via the ETS and oxidative phosphorylation. It measures the rate of oxygen consumption or flux at different respiratory states when appropriate substrates, uncouplers and inhibitors (SUIT protocols) are used. With this method, two substrate combinations are commonly used to assess medium-chain fatty acid β-oxidation; a) Octanoylcarnitine and carnitine, which is partial to the β-oxidation cycle alone, and b) Octanoylcarnitine and malate, which assesses the influence of the TCA cycle. Additionally, a combination of pyruvate, glutamate and malate is used to assess oxidation within the TCA cycle. We investigated the sensitivity of commonly used substrate combinations in HRR assessment to detect changes in mitochondrial respiration and dysfunction induced by the inhibition of either β-oxidation or the TCA cycle in C2C12 myotubes. Furthermore, we assessed MCAD, citrate synthase and aconitase enzyme activities when β-oxidation or TCA cycle was inhibited in C2C12 myotubes.

METHODS: C2C12 myotubes were differentiated for 6 days and treated for 12 hours with a high or a low concentration of one of two inhibitors as follows; a) 2 mM or 8 mM 2-mercaptoacetate to inhibit medium chain acyl-CoA dehydrogenase (MCAD); b) 6 mM or 9 mM fluorocitrate to inhibit aconitase. Each treatment was compared to control myotubes grown for the same length of time without the addition of inhibitors. The activities of MCAD, aconitase and citrate synthase were determined. In addition, mitochondrial respiration measured as O_2 flux at Routine, Leak, OXPHOS and ETS respiratory states were assessed in an Oxygraph-2K after inhibition or in control treatments using; i) Octanoylcarnitine and carnitine ii) Octanoylcarnitine and malate iii) pyruvate, malate and glutamate substrate combinations. For each assessment we corrected O_2 flux recorded at each state to; a)

approximate number of cells (pmol O_2/s/million cells) b) protein concentration (pmol O_2/s/mg protein) c) Flux control ratio (FCR) of each state to the maximum ETS capacity; $ETS^{FAO+CI+CII}$ (convergent electron flow from Fatty acid oxidation (FAO), Complex I (CI) and CII) d) FCR to either FAO-linked ETS capacity; (ETS^{FAO}) or CI-linked ETS capacity (ETS^{CI}).

RESULTS: Treatment of cells with either a low or high concentration of 2-mercaptoacetate to inhibit MCAD resulted in no significant difference in MCAD activity. Fluorocitrate treatment decreased aconitase activity with low treatment ($p = 0.011$) compared to control, and conversely it increased MCAD activity in high treatment compared to control ($p = 0.024$). Both 2-mercaptoacetate ($p = 0.03$) and fluorocitrate ($p < 0.01$) treatment at high concentrations resulted in increased citrate synthase activity, compared to low concentration and control.

Mitochondrial respiration with octanoylcarnitine and carnitine substrate combination was not altered with MCAD or aconitase inhibition. Octanoylcarnitine and malate substrate combination showed a decrease in mitochondrial respiration at the following respiratory states with both MCAD and aconitase inhibition; Routine ($p = 0.01$), $Leak^{FAO}$ ($p = 0.029$), $OXPHOS^{FAO}$ ($p = 0.006$), ETS^{FAO} ($p = 0.008$), ETS^{FAO+CI} ($p = 0.017$). FCR of each state to the maximum capacity ($ETS^{FAO+CI+CII}$) revealed a decrease with both MCAD and aconitase inhibition at the following states; routine ($p = 0.001$), $OXPHOS^{FAO}$ ($p = 0.003$), ETS^{FAO} ($p = 0.018$), $ETS^{FAO+CAR}$ ($p = 0.008$) and ETS^{FAO+CI} ($p = 0.027$).

Pyruvate, malate and glutamate substrate combination showed decreased mitochondrial respiration with MCAD inhibition at the following respiratory states; Routine ($p = 0.004$), $Leak^{CI}$ ($p = 0.007$), $OXPHOS^{CI}$ ($p = 0.003$), ETS^{CI} ($p = 0.003$), ETS^{CI+FAO} ($p = 0.01$) and $ETS^{CI+FAO+CII}$ ($p = 0.003$). FCR of each state to the maximum capacity ($ETS^{CI+FAO+CII}$) decreased with both MCAD and aconitase inhibition at Routine ($p = 0.024$), $OXPHOS^{CI}$ ($p = 0.024$) and ETS^{CI} ($p = 0.035$) states.

DISCUSSION: The main finding of this study was related to two of the SUIT protocols 1) octanoylcarnitine and malate, and 2) pyruvate, malate and glutamate. These protocols were sensitive in showing decreased respiratory capacity and coupling control ratios and may be appropriate for assessing changes in oxidative metabolism when there is a defect in β-oxidation and/ or the TCA cycle. On the other hand, octanoylcarnitine and carnitine substrate combination is not sensitive to detect dysfunction induced by inhibition of either β-oxidation or TCA cycle. Irrespective of the enzyme inhibited, HRR detected dysfunction in complex I (CI), although, when aconitase was inhibited, reduced CI-linked respiration was more pronounced compared to MCAD inhibition. Furthermore, primary inhibition of

MCAD to inhibit β-oxidation may have caused secondary inhibition of TCA cycle via aconitase, shown in decreased TCA cycle CI-linked respiration where MCAD was inhibited. In contrast, primary inhibition of aconitase seemed to be compensated for by increased MCAD activity and mitochondrial respiration related to β-oxidation. Lastly, enzyme assays should not be used as standalone techniques for assessing metabolic dysfunction at the level of TCA, β-oxidation and the mitochondria since they are not sensitive to low level defects, nor do they account for secondary interactions that influence either TCA or beta-oxidation. HRR is useful to assess mitochondrial respiration and dysfunction, when using an appropriate substrate combination and should be used in combination with the more traditional enzyme activity assays.

CHAPTER ONE

Literature Review

1.1 Introduction

Skeletal muscle is highly dependent on oxidative metabolism via the tricarboxylic acid cycle (TCA) and beta-oxidation (β-oxidation). These systems collectively support oxidative phosphorylation (OXPHOS) to produce adenosine triphosphate (ATP) necessary for energy production, tissue function and thermogenesis (59). Diseases associated with the TCA cycle are rare and often related to dysfunction in certain TCA cycle enzymes (96, 126). Conversely, diseases associated with β-oxidation are common and relate to defects in proteins required for the transport of fatty acids (FA) into the mitochondrial matrix and/or with the chain shortening process itself (107, 170). Although there is a genetic component, the most common diseases that cause defects in oxidative metabolism are acquired conditions resulting from complications associated with ageing, neurodegenerative diseases, cardiovascular diseases, and metabolic syndrome (hypertension, dyslipidemia, insulin resistance, Type II diabetes, obesity) (12, 31, 67, 85, 105, 118, 176). These conditions cause a reduction in whole body and tissue specific metabolic flexibility, which compromises the ability to adapt to energy demands and nutrient availability; further exacerbating the disease and contributing to the development of co-morbidities (67).

Assessment of dysfunction in either β-oxidation or TCA cycle typically involves measurement of accumulating organic acids in blood or urine or the activity of defective enzymes in fibroblasts or muscle biopsies (171). However, because β-oxidation, TCA cycle and OXPHOS are connected, dysfunction in one pathway (primary) could lead to dysfunction in the other (secondary), which potentially complicates assessment (and ultimately treatment) of a primary dysfunction using any of the aforementioned methods (21, 47, 105, 107). We propose that a method that combines all aspects of the bioenergetics module, which includes enzyme activity in substrate oxidation within each individual pathway, transfer of electrons through the electron transport system and oxidative phosphorylation for ATP generation may be a more effective assessment technique. Correct assessment of dysfunction is important because advances in therapeutic treatment of dysfunctions in metabolism have resulted from understanding the functional impairment associated with disease pathogenesis (21).

This review will firstly provide an overview of oxidative metabolism via the TCA cycle and β-oxidation, highlighting existing literature on diseases associated with either pathway as well as the methods through which they are assessed. In doing so, we discuss the functional relationship between β-oxidation, the TCA cycle and oxidative phosphorylation and the importance of a more inclusive method of assessment. Accordingly, we present a strategy to induce a dysfunction in β-oxidation and the TCA cycle and thus investigate the relationship between the TCA cycle, β-oxidation and oxidative phosphorylation in a defective sate. Lastly, we investigate the sensitivity of high resolution respirometry (HRR) in detecting alterations in mitochondrial respiration that reflect a dysfunction in β-oxidation and/or the TCA cycle.

1.2 Overview of oxidative metabolism within the mitochondria (β-oxidation and TCA cycle and oxidative phosphorylation)

The mitochondrion employs three main enzymatic pathways for energy generation; β-oxidation, the TCA cycle and OXPHOS; the connections between these are shown in figure 1.1. β-oxidation accounts for the oxidation of FAs of carbon chain-length, 20 or fewer in a series of four reactions that consecutively removes two carbon acetyl-CoA units. The complete cycle is illustrated in figure 1.2 (107). Briefly, free FAs of different chain lengths are activated to their respective acyl-CoA moieties in the cytosol, which allows them to cross the outer mitochondrial membrane into the intermembrane space. Acyl-CoAs are then converted into their corresponding acyl carnitine esters by carnitine palmitoyltransferase I (CPT I) that aids transport across the inner mitochondrial membrane into the matrix (172). Here, they are converted back into their CoA forms by CPT II; using up matrix CoA whilst releasing carnitine that is transferred out across the inner membrane by carnitine-acyl carnitine translocase (CACT), and acyl-CoA enters the β-oxidation pathway. Acyl-CoAs are degraded in a repeated series of four enzymatic reactions; dehydrogenation, hydration, a second dehydrogenation and thiolysis. The products being; reducing equivalents (NADH and $FADH_2$) which enter OXPHOS, a 2- carbon shortened acyl-CoA that serves as the starting block for the next cycle of β-oxidation and acetyl-CoA which is oxidized in the TCA cycle (107).

Acetyl-CoA in the TCA cycle undergoes a progressive sequence of oxidative decarboxylation reactions (126). Acetyl-CoA is additionally (mainly) supplied by the breakdown of glucose through glycolysis as well as other anaplerotic reactions that supply acetyl-CoA and carbon intermediates of the cycle. The TCA cycle consists of 8 enzyme-catalyzed biochemical reactions that generate reducing equivalents

NADH and $FADH_2$ that are transferred to the electron transport system (ETS) (96, 126). The complete cycle is depicted in figure 1.3.

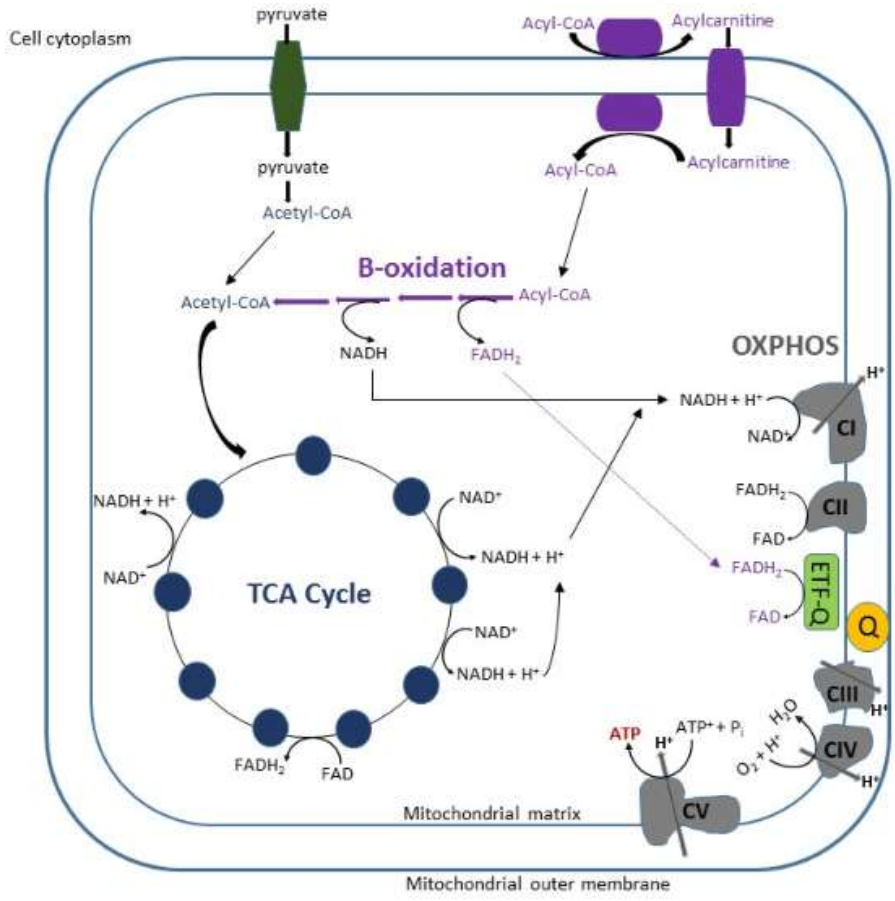

Figure 1.1: Relationship between β-oxidation, TCA cycle and OXPHOS: *Fatty acid β-oxidation (Purple) generates shortened acyl-CoAs, acetyl-CoA, NADH and $FADH_2$ in four enzymatic reactions. The acetyl-CoA produced is utilized by the TCA cycle which also generates more NADH and $FADH_2$. Electrons derived from NADH and $FADH_2$ are used by the complexes of the Electron transport system (ETS) in OXPHOS to generate ATP. Flow of electrons in the ETS is governed by the increasing order of electronegativity of the complexes. The resulting membrane potential generated drives the synthesis of ATP from ADP and inorganic phosphate (P_i). Complex I (CI, NAD:ubiquinone oxidoreductase), Complex II (CII, succinate:ubiquinone oxidoreductase), Complex III (CIII, ubiquinol: ferricytochrome C oxidoreductase, Complex IV (CIV, cytochrome c oxidase), Complex V (ATP synthase) modified from* (107)

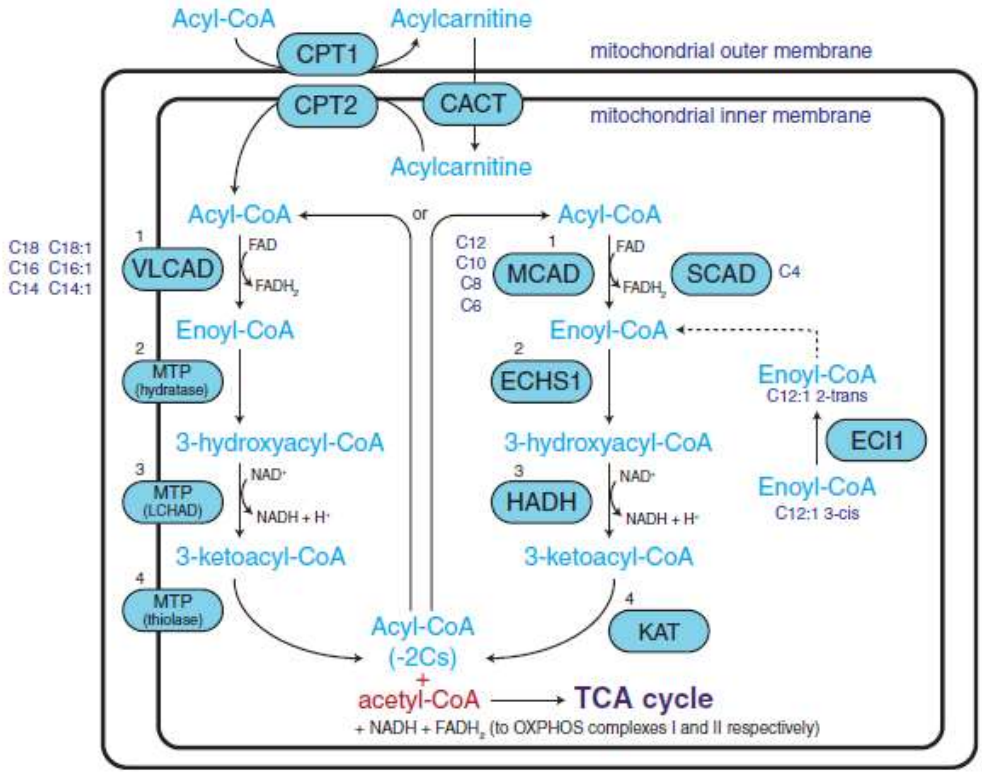

Figure 1.2: Overview of mitochondrial β-oxidation pathway: *Degradation of fatty acyl-CoA esters in the matrix of the mitochondrion comprises of four reactions (numbered 1-4 in black) that are catalyzed by chain-length specific enzymes (chain lengths shown in dark blue). (1) Oxidation of acyl-CoAs into enoyl-CoA by FAD-dependent acyl-CoA dehydrogenases: Short-chain (SCAD), medium-chain (MCAD), long-chain (LCAD) and very long-chain (VLCAD). (2) Hydration into 3-hydroxyl-CoA by enoyl-CoA hydratase (ECHS) or the single hetero-octamer protein, the mitochondrial trifunctional protein (MTP) (3) Dehydrogenation into 3-ketoacyl-CoA by medium/short chain hydroxyacyl-CoA dehydrogenase (HADH) or MTP (4) Thiolysis by ketoacyl-CoA thiolase (KAT) or (MTP) to produce a 2-carbon shortened acyl-CoA and acetyl-CoA* (107).

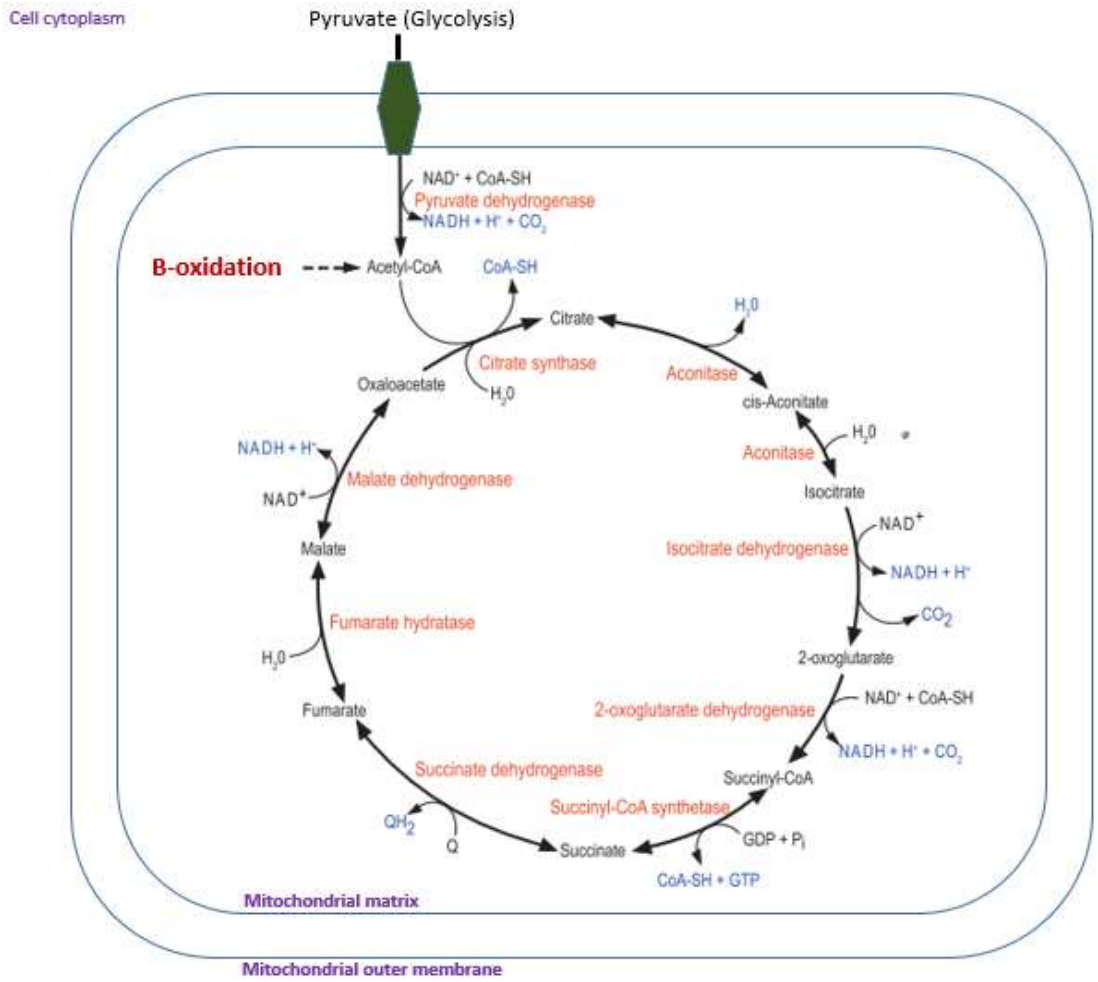

Figure 1.3: Overview of the TCA cycle: *Oxidative decarboxylation of acetyl-CoA, reducing equivalents are generated that transfer electrons to the ETS to generate ATP; modified from* (126).

OXPHOS results from coupling of a series of oxidation-reduction reactions within complexes (I-V) arranged on the inner mitochondrial membrane that facilitate phosphorylation of ADP to ATP (figure 1.1). NADH and $FADH_2$ from either β-oxidation or the TCA cycle transfer electrons sequentially to molecular oxygen, the final acceptor of electrons attached to the heme group of complex IV. The electron pair from $FADH_2$ is transferred to electron transfer flavoprotein (ETF), the Q junction, complex III, cytochrome C and finally, complex IV. Moreover, NADH is transferred to the Q junction via complex I (49). The sequential transfer of electrons is enabled because complexes are arranged in increasing order of electronegativity. Oxygen has the highest electronegativity and is a primary driving force for electron flow, in its reduced form it reacts with H^+ to form H_2O, which detaches from the complex IV binding site to allow for another O_2 to bind in its place. As electrons are transferred from one complex to the next, free energy generated is used to pump protons across the inner mitochondrial membrane

by complexes I, III and IV to create a proton motive force. This force is used by ATP synthase (complex V) to drive the phosphorylation of ADP and inorganic phosphate to produce ATP (111).

1.3 Dysfunction of β-oxidation

At least 22 disorders of β-oxidation have been implicated in human diseases, involving transport proteins or enzymes of the chain shortening process. (4, 124). Of these, a defect in medium chain acyl-CoA dehydrogenase (MCAD is reported as the most common, which affects ~1 in every 10,000 births in a Caucasian population (120, 170). Disorders affecting β-oxidation typically become apparent during specific conditions that stress tissues to increase reliance on β-oxidation. This can occur during fasting, mild to moderate prolonged exercise, fever with infection or cold exposure (158). Thus, clinical presentation is attributed to energy deficiency in β-oxidation-dependent tissues such as heart, liver and skeletal muscle. They are characterized by a spectrum of clinical disorders including; skeletal myopathy, progressive lipid storage myopathy, myoglobinuria, neuropathy, progressive cardiomyopathy, hypotonia, coma, rhabdomyolysis, exercise intolerance, recurrent Reye-like syndrome alongside hypoglycemia, hypoketonemia, hepatic encephalopathy and microvesicular steatosis of the liver and other tissues (108, 145, 159, 170)

Genetic abnormalities of β-oxidation normally present in infancy and early childhood; children are less able to cope with the high energy demands required during periods of stress (11). This is because they have low activity of many key enzymes involved in energy production, a larger brain compared to body size that is dependent on glucose metabolism, a larger surface area compared to body mass and hence a higher energy requirement to sustain body temperature, which relies on shivering thermogenesis provided primarily by fat oxidation(158). The severity of the disease symptom depends on the enzyme that is affected or the presence of residual activity (40, 94, 170). Thus some individuals are asymptomatic and are suddenly impacted later in life under aggravating conditions (35, 170). In all cases the oxidative capacity under challenging conditions is impaired (94).

Interestingly, recent investigations into these disorders revealed complications not attributed to defects in the β-oxidation pathway alone. Case reports of patients have demonstrated a complex interrelationship between the ETS and the β-oxidation cycle (124). Accordingly, defects in specific β-oxidation proteins can result in secondary OXPHOS defects (32, 128, 160, 165). Furthermore,

mitochondrial dysfunction (mitochondrial alterations and disruption of redox homeostasis) is a secondary complication of β-oxidation deficiency, which contributes to the pathophysiology of deficiency (36, 41, 104). Two hypotheses are proposed as the cause of secondary defects associated with primary β-oxidation defects;

i) *i) sequestration of CoA and the build-up of toxic intermediates resulting from a primary defect* (47, 136–139, 161)*:* Experimental data demonstrated that toxic metabolites that accumulated in FAO disorders caused disruption of mitochondrial homeostasis (deficient energy production, oxidative stress) (2, 47, 107, 130, 170). Scaini et al., (2012) investigated the *in-vitro* effects of octanoic acid and decanoic acids (metabolites that accumulate in MCAD deficiency) on various bioenergetics and oxidative stress markers, and found that these caused decreased activity of complexes I-IV in the liver and inhibited complex IV activity in skeletal muscle. Furthermore, they showed increased thiobabituric acid reactive substances (TBARS) levels and carbonyl content in both liver and skeletal muscle as well as decreased glutathione levels in rat skeletal muscle (47). Another study using blood samples from MCAD deficient patients found that parameters of lipid protein oxidative damage (sulfhydryl content) was increased and antioxidant defense system (glutathione, superoxide, dismutase, catalase activity) was decreased in these patients (36).

ii) *ii) physical interactions of fatty acid oxidation proteins and OXPHOS complexes, where loss of interactions may cause secondary defect and contribute to pathology of the disease* (32, 106, 128, 154, 157, 165). β-oxidation enzymes co-migrating with OXPHOS complexes present a physical association of β-oxidation enzymes with OXPHOS complexes. Wang et al. (2010) showed that in rat liver mitochondria, fatty acid proteins (VLCAD, ETF, LCHAD and MCAD) co-migrated with complex I and I/III/IV OXPHOS super complex with blue native polyacrylamide gel electrophoresis and by sucrose density gradients (174). They further showed that acyl-CoA substrates (for enzymes; VLCAD, LCAD and MCAD) were metabolized in fractions of purified OXPHOS supercomplexes (174). In another study where MCAD knockout was generated using 143B osteosarcoma cells, loss of MCAD function was shown to be associated with loss of stability of complex I and OXPHOS super complex (86).

Overall, a defect in energy efficiency seems to be the most important outcome of β-oxidation disorders, where oxidative stress and oxidative damage to proteins may worsen disease presentation, explaining why increased feeding or energetic substrate supply does not correct symptoms seen in some cases (149). Furthermore, the majority of these studies show the associations between β-oxidation, ETS and OXPHOS, and suggest that the function of the TCA cycle may be equally affected. Where β-oxidation is defective there is reduced supply of acetyl-CoA to the TCA, aggravating the decrease in reducing equivalents that are supplied to the ETS for OXPHOS and ultimately ATP generation (107). Accordingly, in β-oxidation defects, there is increased carbohydrate feeding and avoidance of fasting or any stressors that increase demand for fat catabolism. However, this does not explain the persistence of symptoms found in some cases (107, 149, 158). Notably, oxidative stress is particularly detrimental to Iron-sulphur cluster (Fe-S) containing proteins, one of which is aconitase of the TCA cycle (22). Aconitase can be inactivated by oxidative stress limiting the TCA cycle (75, 85). In support of this, Shuck et al (2010), showed that in rat brain, cis-4-decenoic acid, a key MCAD deficiency metabolite decreased the activity of aconitase as well as TCA-cycle linked respiration (138). Dhami et al. (2018) also showed that aconitase knockout proved to be the most lethal deletion of any TCA cycle enzyme, limiting the functioning of the entire system (37). Others have also reported that inactivation of aconitase aggravates the negative impact of an oxidative environment (27, 37, 112, 177). When aconitase is oxidized, an iron atom is released from its active site which in turn catalyzes hemolysis of hydrogen peroxide (H_2O_2) that generate free radicals by the Fenton reaction (27). This further oxidizes mitochondrial proteins, DNA and lipids (37, 112, 177). Therefore, where β-oxidation is already defective, aconitase inactivation (or inhibition) would worsen the condition. Thus, secondary TCA cycle dysfunction may indeed play a role in the pathophysiology of some β-oxidation deficiencies. However, the effect of direct MCAD inhibition or deficiency on the TCA cycle in other tissues such as skeletal muscle is unknown. In summary, primary β-oxidation defect may cause secondary, OXPHOS and TCA cycle defect leading to overall mitochondrial dysfunction and energy deficiency.

Hence, the implication of secondary dysfunction is the worsening of symptoms where β-oxidation is defective (primary dysfunction). Thus, a secondary dysfunction may go undetected since diagnosis of disease is mostly associated with measuring characteristic fatty acids as well as their carnitine or glycine derivatives that accumulate in blood or urine or assessment of enzyme activity. Indeed, the appropriate management of many β-oxidation disorders is hindered by the failure to recognize clear biochemical abnormalities (107). Accordingly, correct investigative assessment may offer new perspectives for therapeutic intervention. For example, if the extent of oxidative damage to aconitase is a direct correlation of MCAD dysfunction, intervention that protects aconitase from oxidative inactivation could

improve disease symptoms. Therefore, the effect of MCAD dysfunction (or inhibition) on the TCA cycle and especially aconitase is worth further investigation.

1.4 Dysfunction of the TCA cycle

Unlike β-oxidation, genetic human diseases associated with the TCA cycle are rare (126). These diseases are connected with either the inability of pyruvate metabolism to supply acetyl-CoA to the TCA cycle for the complete oxidation of carbohydrate or inactivity of enzymes within the TCA cycle to metabolize acetyl-CoA (53, 96, 126). Diseases of the TCA cycle involve deficiency of pyruvate dehydrogenase, phosphoenoylpyruvate carboxykinase, dihydrolipoamide dehydrogenase, 2-ketoglutarate dehydrogenase, fumarase, succinate dehydrogenase or a combined succinate dehydrogenase and aconitase deficiency (53, 57, 96, 126). These deficiencies are associated with altered functioning of the central nervous system and neuromuscular system as a result of impaired energy production (20, 96, 126). The classical features include; encephalopathy, neonatal lactic acidosis, Leighs's syndrome, progressive hypotonia, psychomotor retardation, Kearns-Sayre syndrome, growth retardation, pulmonary oedema, muscle weakness, and exercise intolerance to mention a few (20, 96, 126).

1.4.1 The role of β-oxidation and anaplerotic reactions in maintaining energy production in primary TCA cycle dysfunction.

The pattern of disease with TCA cycle dysfunction shows a characteristic organ specific impairment, which seems to exclude other organs or tissues (heart, liver or kidney) that are predominantly dependent on oxidative metabolism(126). Indeed, we know that β-oxidation is a major fuel source in many organs including the heart, liver and skeletal muscle (38, 45, 124) and could explain why patients with TCA cycle dysfunction survive or why defects are associated with specific organ/tissue impairment. The role of β-oxidation in TCA cycle-associated defects is exemplified in cases of pyruvate dehydrogenase deficiency where a ketogenic diet can improve symptoms (122, 146). Wexler et al. (1997), showed that the earlier the restriction of carbohydrates the better the outcome of mental development and survival (64). In contrast to the idea that β-oxidation may compensate for energy deficiency in TCA cycle associated defects, Yudoff et al. (1994) suggests that sustained life is due to the TCA cycle being made up of two 'mini-cycles' as follows; i) running from oxaloacetate, citrate, isocitrate, α-ketoglutarate and back to oxaloacetate, ii) from α-ketoglutarate, succinoyl-CoA, succinate, fumarate, malate, oxaloacetate and back to α-ketoglutarate (126). Accordingly, many of the defects that have

been found with the enzymes of the TCA cycle involve enzymes limited to either one part of the 'mini-cycle', suggesting that the unaffected 'mini-cycle' is bypassed, in part metabolizing pyruvate and allowing for cell survival (126). According to the discussion in section 1.3 above, secondary defects in the TCA cycle arising from a primary defect in β-oxidation are associated with the 'first mini cycle', a path that connects reducing equivalents to complex I of the ETS. Where β-oxidation is defective, there is reduced acetyl-CoA supply to the TCA cycle as well as likely inhibition of aconitase. The implication would be the worsening of energy deficiency and reliance on the 'second mini cycle' for energy production. However, it remains to be seen what effect the second mini cycle would have on energy compensation where β-oxidation is already defective and may not compensate for energy production. It is likely that cell survival could result from anaplerotic reactions that supply carbon intermediates beyond the point of enzyme defect that allows for TCA cycle metabolism to continue (14). For example, in fumarase deficiency the blockade of the TCA cycle may be partially corrected by the transamination of α-ketoglutarate into oxaloacetate, thereby allowing pyruvate oxidation (14). To provide more insight into the potential supply of carbon intermediates where TCA cycle enzymes are defective, a schematic diagram is provided in figure 1.4 (126). Overall, in TCA cycle deficiencies, energy compensation may fuel cell survival, however the mechanism, as well as the organ/tissue specifications for compensation, is not clear and needs to be further investigated.

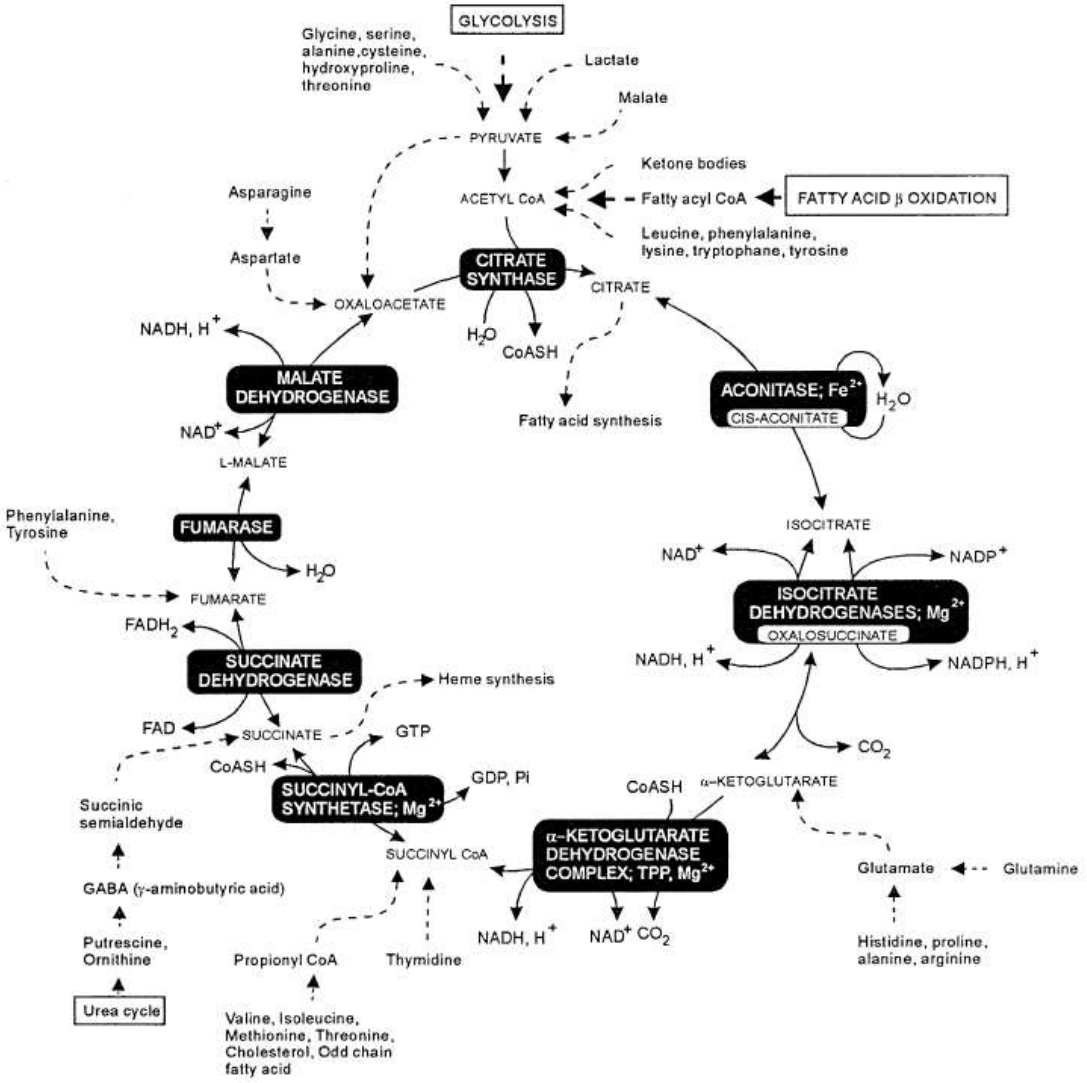

Figure 1.4 Reactions of the TCA cycle including exogenous supply of TCA cycle carbon intermediates (126)

1.5 Summary: A strategy to investigate the relationship between β-oxidation, TCA cycle and OXPHOS by inhibiting key enzymes of β-oxidation or TCA cycle

Conditions that affect energy efficiency and the supply of fuel would cause loss of organ/tissue function that would adversely impact the whole body (111). β-oxidation, TCA cycle and oxidative phosphorylation are key processes in maintaining energetic homeostasis. Although it is evident that defects in these pathways can cause devastating illnesses in humans, however, the relationship that exists in an attempt to maintain homeostasis when one pathway is defective is insufficient and requires further investigation.

MCAD deficiency can elicit devastating effects on the β-oxidation pathway (41, 107, 155, 170). A defect in longer chain acyl-CoA dehydrogenases causes an increased supply of medium chain fatty acids to bypass the defect, however, during MCAD deficiency there is no bypass. As such, toxic metabolites accumulate that exacerbate energy deficiency, cause oxidative stress leading to oxidative damage of proteins contributing to the pathology of disease (46, 147–149, 168). The unexplained characteristic in many β-oxidation defects including MCAD has led to investigations into the pathophysiology of the disease (4, 107, 110, 140). Several studies have shown the impact on energy machinery (including OXPHOS and TCA cycle) of toxic metabolites that accumulate where MCAD is deficient (36, 107, 128, 138). However, to our knowledge no study has investigated the impact of directly inhibiting MCAD on β-oxidation, TCA cycle and OXPHOS; the assessment of which may contribute to understanding MCAD and β-oxidation dysfunction. To investigate this, 2-mercaptoacetate may be used to inhibit MCAD as it has been shown to directly inhibits acyl-CoA dehydrogenases including MCAD (9). Studies using 2-mercaptoacetate report that inhibition of 2-mercaptoacetate was limited to the acyl-CoA dehydrogenase enzyme, but not electron transfer flavoprotein (ETF) or in the transport of fatty acids into the mitochondria (7–9). Therefore, the use of 2-mercaptoacetate may be an appropriate model of MCAD deficiency.

With regards to the TCA cycle, genetic defects in the pathway are less common, with acquired defects being the most important contributors to the dysfunction of the pathway (21, 53, 105, 126). To this end, aconitase is suggested as an important enzyme affected under conditions of oxidative stress (5, 27, 58, 85, 143). Furthermore, aconitase has been implicated in MCAD dysfunction, where its activation contributes to worsening energy deficiency (138). Moreover, clarity is lacking into the impact of a TCA cycle dysfunction on β-oxidation and OXPHOS. Aconitase may be directly inhibited using fluorocitrate, a toxic inhibitor of aconitase (43, 85). Fluorocitrate has been used in many studies to understand the impact of energy deficiency seen in some neurological diseases and also in understanding the impact of hypoxia on cell physiology (43, 83, 97, 162). Thus, fluorocitrate is ideal for investigating the relationship between β-oxidation, TCA cycle and OXPHOS in a TCA cycle defective state.

1.6 Commonly used methods for assessing β-oxidation and TCA cycle defects

The assessment of TCA cycle dysfunction is similar to that of β-oxidation where accumulating organic acids in blood or urine samples as well as in fibroblast are assessed by biochemical evaluation, TMS or enzymatic analysis (53, 96). These are usually indicative of the point in the pathway where a defect is present. The methods used to assess β-oxidation dysfunction have already been extensively reviewed (10, 61) and a short summary is provided below:

Enzymology: Classical enzymological determinations involve monitoring the transfer rate of electrons from appropriate fatty acyl-CoAs to electron acceptors by enzymes in mitochondrial preparations or total cell homogenates using spectrometry or fluorometry (65). For example, in determining the activity of acyl-CoA dehydrogenases (enzymes that catalyze the first step of β-oxidation) the rate of re-oxidation of the reduced enzyme is measured by monitoring the charge transfer to a suitable electron acceptor at a specific wavelength. During β-oxidation, acyl-CoA dehydrogenases are reduced by appropriate acyl-CoAs and then re-oxidized by FAD+, which donates the electrons to electron transfer flavo protein (ETF) in a two-step one electron process. Experimentally, the rate of transfer of electrons to the ETF is a measure of the activity of the enzyme. In these reactions, the acyl-CoA dehydrogenases are incubated in a reaction mix containing hexafluorophosphate (a commercially available alternative to the ETF) and the addition of acyl-CoAs are used to determine the activity of the enzyme at a given wavelength using spectrophotometry (80, 172). However, enzyme assays alone may not explain the nature of β-oxidation dysfunction that is presented in some scenarios. For example, partial defect in the activity of one enzyme may not be reflected on such assays (10). Furthermore, additional steps are required for the interpretation and performance of these enzyme assays depending on the nature of the sample. This is because there is a distinct overlap between enzymes i.e. between MCAD and SCAD in disrupted cells (10). Additionally, measuring the enzyme activity excludes other contributing factors involved in β-oxidation impairment such as defect in transport proteins or of mitochondrial dysfunction. Enzymology is thus used in combination with one or more detection technique/s.

Metabolite method: The production rate of carbon dioxide (CO_2) is the end product of complete β-oxidation and monitored by use of appropriate carbon-radiolabeled fatty acid substrates (4, 63, 68). In this method, tissue homogenates or cultured cells are incubated in oxidation reaction medium together with ^{14}C-labelled fatty acid, usually palmitate or oleate, for an amount of time at 37^0C. During incubation, the fatty acid is oxidized in the mitochondrion to generate acetyl-CoA, which can then enter the TCA cycle and be oxidized to CO_2. In addition to CO_2, acid soluble metabolites (ASM) such as; acetyl-carnitine, acetyl-CoA, ketone bodies, glucogenic intermediates and short chain fatty acyl-CoAs ($^<$C6)

can be generated from incomplete oxidation (measured using a scintillation counter). The radioactive CO_2 and ASMs are measures of fatty acid oxidation (63). Diagnosis of β-oxidation by this method assumes that there is an association between the accumulations of specific chain length intermediates (ASMs) with the deficiency of a distinct acyl-CoA dehydrogenase (10). This method only provides an indication of the presence of dysfunction, but no understanding as to the energy produced from the oxidative process or how efficiently oxidation is coupled to energy production. Accordingly, it may be used as a confirmation of an already suspected dysfunction.

Tandem mass spectroscopy (TMS): TMS is used to measure the accumulation rate of β-oxidation intermediates, usually acyl-carnitines of various lengths. The acyl-carnitine profile obtained is analyzed and compared with profiles from samples of known β-oxidation defects (103, 142). However, two acylcarnitine compounds may have the same mass but are associated with different conditions, which cannot be differentiated using TMS (10). Analysis of urine organic acids may be used to differentiate species and identify disease by biochemical evaluation (123, 142).

Biochemical evaluation: This method typically involves acidification of urine, addition of appropriate internal standards, extraction into an organic solvent and derivatization, and analysis by gas chromatography/electron impact mass spectrometry. It is used for investigating suspected metabolic disease in patients presenting a range of clinical symptoms (71). A broad range of metabolites in urine are detected using gas chromatography/mass spectrometry. For example, the detection of medium chain dicarboxylic acids, produced when flux through β-oxidation pathway is impaired at the level of 3-hydroxyacyl CoA dehydrogenase or 3-ketoacyl CoA thiolase (10). The limitation of this method is that it does not detect longer chain-length dicarboxylic acids that are not found in urine and will hence be undetected in cases where these accumulate in disease. This method also relies on detecting acylcarnitine profiles by using isotope-labelled internal standards that are not commercially available for all acylcarnitine species. Again, this method is restricted to already suspected defects in β-oxidation.

1.7 The use of high resolution respirometry for assessing β-oxidation, TCA cycle and Oxidative phosphorylation

1.7.1 Principle of respirometry

Unlike the aforementioned methods which only measure one aspect of metabolism (by product of metabolism, intermediates, or enzyme activity), mitochondrial respirometry offers a dynamic measurement of metabolic flux rates (114). The principle of respirometry is based on the coupling of changes in metabolite levels, membrane permeability, and activity of individual enzymes to oxidative phosphorylation (114). As previously mentioned, oxidation of substrates in β-oxidation or TCA cycle produces electron carriers, NADH and $FADH_2$ that donate their electrons to complexes of the electron transfer system (ETS) (see figure 1.1- 1.3). Oxygen is the major driving force for electron flow and is also the ultimate acceptor of electrons. As long as O_2 supply is continuous, the flow of electrons along the ETS will be maintained. The flow of electrons through the ETS is coupled to the phosphorylation of ADP and inorganic phosphate into ATP (51). Hence, if the ADP and O_2 are kept constant, the rate of oxygen consumption by the mitochondria will be restricted singularly by the rate at which NADH and $FADH_2$ are supplied from substrate oxidation (in β-oxidation or TCA cycle). This is the underlying principle of respirometry; a technique that measures the rate of O_2 consumption (or O_2 flux) by mitochondria from biological samples such as cells, isolated mitochondria and permeabilized tissues or biopsies (49)

1.7.2 Assessment of mitochondrial respiration with high resolution respirometry, HRR

Recent advancement in respirometry has led to the development of HRR that allows accurate measurement of oxygen consumption in very small samples at various respiratory states (e.g. leak, intrinsically coupled, pathologically dyscoupled or experimentally non-coupled respiratory states) in an Oxygraph (Oroboros-2k) (48, 50). This technology employs sensitive polagraphic oxygen sensors to accurately measure the rate of oxygen consumption under controlled conditions that mimic physiological conditions of temperature (37^0C), ionic concentration and substrates availability (15, 62). A carefully designed sequence of titrating substrates, uncouplers and inhibitors (SUIT protocols) makes possible assessment of rates of oxygen consumption for desired respiratory states (72, 119). For example, in intact cells (e.g blood cells, fibroblasts, stem cells, muscle cells etc), it is possible to determine routine respiration (physiological resting respiration), uncoupled respiration (when ATP synthase is inhibited), and experimentally noncoupled respiration (by titrating non-physiologic uncouplers) (166). These are the only respiratory states that can be measured in these cell types because the plasma membrane is impermeable to exogenously added ADP and mitochondrial substrates (114, 135). Routine respiration here is because of endogenous substrates; as such, the

capacity for oxidative phosphorylation cannot be measured (92). However controlled membrane permeabilization with an agent such as digitonin allows for entry of exogenous substrates (61, 112, 127, 147, 149). This permeabilization leads to the loss of cytosolic molecules such as adenylates, substrates and cytosolic enzymes making it possible for exogenous substrates to gain access into the mitochondria. There is therefore a drop in oxygen consumption from routine state after the addition of digitonin (114). This drop is then rescued by the addition of exogenous substrate in leak state (49).

In permeabilized fibers, cells and isolated mitochondria, leak respiration is usually determined at the start of the experiment after addition of substrate but not ADP (51, 75). Leak respiration is the non-phosphorylating resting state of intrinsic uncoupled or dyscoupled respiration when oxygen flux is minimized by the back-pressure of a high chemiosmotic potential generated when ATP synthase is not active (49, 52). The addition of saturating concentration of ADP activates ATP synthase and stimulates oxygen consumption. This rate of oxygen consumption represents the maximum capacity of oxygen consumption when substrate oxidation is coupled to phosphorylation of ADP to generate ATP, which is referred to as OXPHOS capacity (49, 51). Another leak state of respiration may be induced by titrating an inhibitor of ATP synthase such as oligomycin. This leak state measures oxygen consumption due to proton leak, electron slip or cation recycling at a maximum membrane potential (51). A low oxygen flux at this state indicates that mitochondria maintain a sufficiently high protonmotive force, which restricts electron transport, whereas a high flux reflects proton leakiness of the mitochondria. This state is a measure of the coupling efficiency of the mitochondrial OXPHOS system. Addition of non-physiologic uncouplers at this state induces maximal oxygen consumption and is referred to as ETS capacity. Uncouplers, such as FCCP and CCP, are protonophores that allow the movement of protons down a concentration gradient (protons move from the intermembrane space into the matrix) and dissipate the membrane potential. Dissipation of the membrane potential in this way stimulates maximal activity of the ETS to pump H^+ back to the intermembrane space, an activity that stimulates electron flow through the ETS thus consuming more O_2 above OXPHOS. Inhibition of electron flow through the ETS by an appropriate inhibitor, allows measurement of residual O_2 consumption (ROX). It accounts for O_2 consumed by reactions not associated with the ETS. ROX is used as a correction factor and subtracted from ROUTINE, LEAK, OXPHOS and ETS respiratory (50).

The SUIT protocol provides insight into the effects of experimental treatments or disease conditions on specific components of the OXPHOS system. SUIT protocols allow for the evaluation of cell viability; membrane integrity (cytochrome c release), respiratory inhibition caused by defects in the ETS, including respiratory complexes and activities of enzymes and substrate transporters across the inner

mitochondrial membrane (49). For example, changes in ETS and OXPHOS capacities recorded after exercise training in muscle reflect changes in substrate oxidation and ATP synthesis (169). On the other hand, a change in LEAK indicates a change in proton conductance (18, 44, 117). The ratio of different respiratory states also yields valuable information regarding respiratory control. For example, the ratio of respiration in the coupled state to respiration in the leak state is referred to as the respiratory control ratio (RCR) (18, 50) and indicates the ability of the mitochondria to respond to ADP stimulation. A high RCR implies that the mitochondria have a high capacity for substrate oxidation and ATP production (51, 114). HRR can detect small changes in RCR due to experimental treatments or mitochondrial dysfunction and hence it an excellent tool for revealing the effects of treatments, diseases or adaptations to physiological conditions or stressors.

1.7.3 Sensitivity of substrates used for assessing β-oxidation and TCA cycle with HRR

Pyruvate, glutamate, malate and succinate are commonly used to reconstitute the TCA cycle function in HRR assessment and is depicted in figure 1.5 (51). These substrates are anions that cannot cross the lipid membrane and hence their entrance into the inner mitochondria is aided by anion carriers in the inner mitochondria membrane (49). Pyruvate, glutamate and malate are NADH generating CI-linked substrates, while succinate is directly linked to CII. Together these substrates represent the convergent electron flow from CI and CII to the Q-junction and then to CIII and finally CIV of the ETS (51). Because pyruvate, glutamate and malate are CI-linked, they were used alone in the past to stimulate CI-linked respiration; i.e. either pyruvate, malate or glutamate and succinate for CII. However, the use of any substrates alone underestimate OXPHOS capacity. Irrespective, separating CI-linked substrates from that of CII or grouping CI-linked substrates allows testing of specific hypotheses in mitochondrial research, for example, where a defect in particular enzymes or complex of the ETS is suspected (114).

However, unlike the TCA cycle, there are some uncertainties with assessing β-oxidation using HRR, and these issues are discussed below.

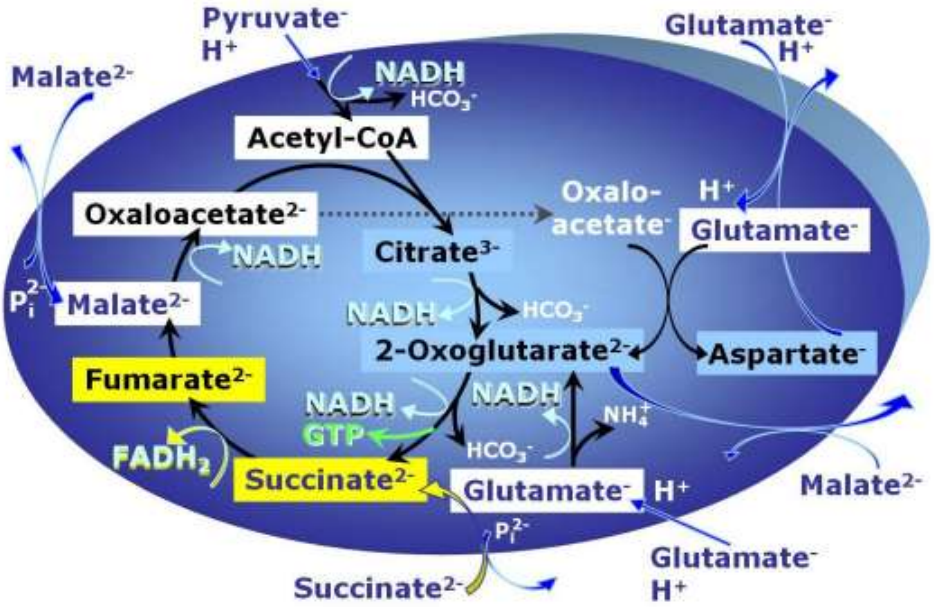

Figure 1.5: Reconstitution of the TCA cycle using exogenous supplied pyruvate, malate, glutamate and succinate (51).

1.8.4 Commonly used substrate combinations for the assessment of β-oxidation by HRR

Over the years different substrates have been used in assessing β-oxidation. Researchers initially used palmitoylcarnitine (long chain fatty acyl-carnitine) alone but there has been a gradual evolution to include either malate or carnitine along with palmitoylcarnitine (38, 60, 109, 164). Recently, use of octanoylcarnitine (medium chain fatty acyl-carnitine) instead of, or in addition to, palmitoylcarnitine has become popular (12, 77, 134). Oxidation of octanoylcarnitine has been found to have an approximately equal effect as using palmitoylcarnitine in respirometry determinations (134). Octanoylcarnitine and palmitoylcarnitine are active forms of FAs that are able to cross the mitochondrial membrane into the matrix where they are broken down to produce acetyl-CoAs, shorter chain acyl-CoAs, NADH and $FADH_2$ (6). Acyl-CoAs are recycled back into the β-oxidation cycle for further degradation, while $FADH_2$ and NADH feed into the ETS. The acetyl-CoA produced may build up in the mitochondrial matrix and inhibits the thiolase reaction of β-oxidation if not continually removed (79). Inclusion of malate or carnitine along with palmitoylcarnitine/octanoylcarnitine prevents accumulation of acetyl-CoA. Malate is easily transported into the mitochondrial matrix by the dicarboxylate carriers (51) and oxidized to oxaloacetate by malate dehydrogenase enzyme. Oxaloacetate reacts with acetyl-CoA to form citrate which is metabolized in the TCA cycle. Alternatively, carnitine may also be used to prevent accumulation of acetyl-CoA when octanoylcarnitine or palmitoylcarnitine are metabolized in beta oxidation. Carnitine is transported into the mitochondrial matrix by carnitine - acyl carnitine

translocase where it reacts with acetyl-CoA to form acetyl-carnitine that is transported out of the matrix via carnitine-acetyl carnitine translocase (6).

1.8.4.1 Palmitoylcarnitine or octanoylcarnitine

Research conducted by Perevoschika et al. (2013) revealed that oxidation of palmitoylcarnitine alone is not sufficient to support respiration as shown by oxygen consumption (115). In this study, isolated rat muscle mitochondria were employed to determine the rate of oxygen consumption. Results showed that palmitoylcarnitine was unresponsive to ADP and uncoupler titrations. This response was attributed to a build-up of acetyl-CoA that inhibits the thiolase reaction in β-oxidation. Other research by Van Eunen et al. (2013) verifies that palmitoylcarnitine alone is not sufficient to support beta oxidation (40). Using both computational and experimental models involving palmitoylcarnitine oxidation, they revealed that the β-oxidation pathway is vulnerable to substrate overload (40). At high palmitoyl-CoA concentrations, the shorter CoA esters accumulate (since they are not being utilized in the TCA cycle), resulting in a depletion of the CoA pool and preventing further oxidation of acyl-carnitine (40). The above observations suggest that use of palmitoylcarnitine/octanoylcarnitine alone for assessing β-oxidation is not viable and thus researchers have used carnitine or malate in addition to either palmitoylcarnitine or carnitine for β-oxidation assessment.

1.8.4.2 Palmitoylcarnitine or octanoylcarnitine plus malate

Octanoylcarnitine/ palmitoylcarnitine plus malate has been used often as substrate combinations in the assessment of β-oxidation. These substrate combinations have been used under a variety of physiological conditions. Perevoschika et al. (2013) showed that in mitochondria from skeletal muscle of healthy rats, leak respiration after the addition of palmitoylcarnitine and malate was 71 ± 10 nmol O/min/mg protein and addition of ADP increased oxygen consumption to 376 ± 28 nmol O/min/mg protein. OXPHOS capacity, measured in the presence of octanoylcarnitine and malate, increased from 76.8 ± 15.6 to 86.3 ± 17.9 pmol/s/mg protein and Flux control ratio (FCR) increased from 1.9 ± 0.6 to 2.8 ± 0.2 AU in permeabilized fibres from adults after endurance training (116). Bonnard et al. (2008) used respirometry to measure changes in mitochondrial function in mice fed a high fat and high sucrose (HFHSD) diet for 16 weeks (12). Their results indicated a reduction in OXPHOS capacity and FCR using both palmitoylcarnitine + malate and octanoylcarnitine and malate as substrates; indicating that a HFHSD diet supressed β-oxidation. Additionally, reduced β-oxidation was not linked to altered availability of substrates because genes involved in muscle fatty acid uptake (FAT/CD36) and entry into the mitochondria were remarkably increased in the skeletal muscle of the mice. The authors attributed

this to excessive reactive oxygen species (ROS) production; treatment with an antioxidant decreased ROS production and restored mitochondrial function (12).

Palmitoylcarnitine + malate is favoured as a substrate combination in assessing β-oxidation. It is effective in determining changes in OXPHOS capacity that result from different physiologic conditions. However, it remains unclear whether the readings recorded are valid measures of β-oxidation, under all physiological conditions, due to metabolism of malate. Upon entry into the mitochondrial matrix, malate is oxidized to oxaloacetate by malate dehydrogenase in the TCA cycle. Oxaloacetate condenses with acetyl CoA to produce citrate which is further metabolized in the TCA cycle. Thus, the complete oxidation of a fatty acid moiety could be calculated as the energy generated as a result of reducing equivalents from the β-oxidation pathway itself and from the complete oxidation of acetyl-CoA in the TCA cycle. It could therefore be suggested that the rate of β-oxidation (including removal of acetyl-CoA) is influenced in part by the TCA cycle.

Remarkably, a computational model of β-oxidation predicts that decreased acetyl-CoA concentration should raise the concentration of free CoAs that facilitate continued β-oxidation (40). Conversely, a defect in enzymes of the TCA cycle such as, malate dehydrogenase, citrate synthase or aconitase may affect the rate of removal of acetyl-CoA contributing to a decline in the rate of β-oxidation (111); this however remains to be tested. Interestingly, there are only a limited number of diseases that are associated with primary isolated or multiple defects in TCA cycle enzymes (126). However, as previously mentioned, secondary dysfunction in the TCA cycle and especially inactivation of aconitase in many primary deficiencies including MCAD dysfunction can inhibit aconitase. This inhibition is likely to reduce flux through the TCA cycle and decrease the rate of oxidation of octanoylcarnitine.

Based on the above observations, it can be hypothesized that conditions that affect the metabolism of malate in the TCA cycle would reduce the measured oxygen flux, giving a false reading of the rate of β-oxidation when malate is used as a co-substrate. For example, if a primary MCAD deficiency results in the inhibition of aconitase, it would be difficult to differentiate the effect of primary deficiency versus secondary. Therefore, it is necessary to evaluate the validity of using acylcarnitine + malate as substrates under conditions of mitochondrial dysfunction that arise from TCA cycle defects.

1.8.4.3 Palmitoylcarnitine or octanoylcarnitine plus carnitine

It has long been established that long- or medium-chain FAs or their CoA derivatives are only oxidized by mitochondria if carnitine is present, whereas their corresponding carnitine esters are excellent

substrates by themselves (29, 87). Recent research verified this observation polarographically using human muscle mitochondria and myoblasts. They showed that oxidation of palmitoyl-CoA was dependent on the presence of carnitine whereas palmitoylcarnitine oxidation occurred in its absence. As mentioned earlier, carnitine is needed for transportation of fatty acids into the mitochondrial matrix. Inside the mitochondrial matrix, palmitoylcarnitine is converted to palmitoyl-CoA by CPT II. Use of optimal concentrations of palmitoyl-CoA and carnitine in these experiments ensure that both palmitoylcarnitine and carnitine are present to drive β-oxidation.

Inclusion of carnitine has been shown by several studies to increase palmitoylcarnitine oxidation. The effects of carnitine on the metabolism of palmitoylcarnitine was studied by using isolated healthy rat liver mitochondria (19). They found that carnitine concentrations less than 1.25 mM resulted in an increased production of acetylcarnitine and increased palmitoylcarnitine oxidation. Recently Perevoshchikova et al. (2013) measured the rate of oxygen consumption with carnitine + palmitoylcarnitine as substrates (167). Oxygen consumption using a polarographic Clark electrode was measured from skeletal muscle mitochondria of female Wistar rats. The addition of carnitine (2 mM) to palmitoylcarnitine (15 μM) resulted in an increase in basal respiration from an 11 ± 1 to 57 ± 6 nmol O/min/mg protein and OXPHOS capacity from 11 ± 1 to 96 ± 15 nmol O/min/mg protein (115). It has been explained that carnitine increases respiration by preventing acetyl-CoA accumulation during palmitoylcarnitine oxidation. Carnitine reacts with acetyl-CoA to form acetylcarnitine in a reaction catalysed by carnitine acetyltransferase (124). Further research showed that the addition of 2 mM carnitine had no significant effect on the oxidation pyruvate/malate and glutamate/malate (TCA cycle substrates) but increased oxygen consumption with palmitoylcarnitine. Carnitine increased NAD(P)H/$NAD(P)^+$ autofluorescence during palmitoylcarnitine oxidation (141). An increase in NADH implies a greater capacity for electrons transfer into the electron transport system, oxygen utilization, and ATP production.

Although palmitoylcarnitine (or octanoylcarnitine) plus carnitine is a common substrate used for β-oxidation assessments, a critical analysis of this substrate combination leads to reservations whether it is a true representation of β-oxidation *in-vivo*. Firstly, β-oxidation produces NADH and $FADH_2$ directly and indirectly through acetyl-CoA oxidation by the TCA cycle. Hence the rate of oxygen consumption recorded during beta oxidation reflects oxidation of electron carries from both the TCA cycle and β-oxidation. However, use of palmitoylcarnitine plus carnitine (or octanoylcarnitine) does not account for FADH and NADH from acetyl-CoA since carnitine transports the acetyl CoA from β-oxidation out of the mitochondria. Therefore, oxygen flux obtained by using the substrate combination is lower than

expected from *in-vivo* assessments. Secondly, the oxidation of palmitoylcarnitine (or octanoylcarnitine) requires that there be an existing CoA pool to drive β-oxidation. It is not known whether the rate of removal of acetyl-CoA by carnitine sufficiently restores the CoA pool for optimal oxidation of palmitoylcarnitine (or octanoylcarnitine). Failure to restore the CoA pool would result in diminished oxidation of palmitoylcarnitine and manifest as a decrease in oxygen consumption and would be erroneously interpreted as a decreased capacity of the mitochondria to oxidize fatty acids. Therefore, the validity of this substrate combination in assessing β-oxidation needs to be further evaluated.

1.9 Aims

The primary aim of this study was to investigate the sensitivity of commonly used substrate combinations in HRR to detect changes in mitochondrial respiration and dysfunction, induced by the inhibition of either MCAD or aconitase to limit β-oxidation and the TCA cycle, respectively, in C2C12 myotubes.

The secondary aim was to investigate the activity of MCAD, citrate synthase and aconitase enzymes when MCAD or aconitase is inhibited in C2C12 myotubes and how it relates to β-oxidation and/ or the TCA cycle

1.10 Objectives

To evaluate the effects of low and high concentration inhibition of MCAD (using 2-mercaptoacetate) and aconitase (using fluorocitrate) on;

i. Mitochondrial respiration (β-oxidation & TCA cycle) using HRR, and employing either of the following commonly used substrate combinations:
    a) Pyruvate, malate and glutamate
    b) Octanoylcarnitine and malate
    c) Octanoylcarnitine and carnitine

ii. Activity of enzymes; MCAD, aconitase and citrate synthase.

1.11 Hypothesis

1) MCAD inhibition would reduce MCAD activity and limit β-oxidation, as well as decrease aconitase activity whilst increasing citrate synthase activity. Furthermore, MCAD inhibition will reduce mitochondrial respiration of the ETS capacity linked to complex I. This would be most significantly

shown in the complex I specific substrate combination; pyruvate, malate and glutamate and in the β-oxidation substrate combination; octanoylcarnitine and malate.

2) Aconitase inhibition would reduce aconitase activity and limit the TCA cycle, as well as increase citrate synthase enzyme activity. Furthermore, aconitase inhibition will reduce mitochondrial respiration of the ETS capacity linked to complex I. This would be most significantly shown in the complex I specific substrate combination (pyruvate, malate and glutamate) and to a lesser extent in the substrate combination that most closely links beta-oxidation and the TCA cycle (octanoylcarnitine and malate).

3) The substrate combination octanoylcarnitine and carnitine will have limited sensitivity in MCAD and aconitase inhibition.

CHAPTER TWO

Materials and Methods

2.1. Justification for the use of a cell culture model

C2C12 cells, a sub clone of the mouse myoblast cell line is widely used in various studies (24, 26, 42, 89, 98, 144).These cells readily proliferate in high-serum conditions and differentiate at low-serum conditions into extensive contracting muscle-like myotubes that express characteristic skeletal muscle proteins and properties. The ability to differentiate into myotubes is an important characteristic of C2C12 cells as an *in-vitro* model of skeletal muscle, and it is appropriate for investigating complex biochemical, molecular or pathological adaptations that occur in skeletal muscle (82, 100, 144, 178). The cells were obtained from the American Type Culture collection (Manassas VA, USA).

2.2 Experimental logistics and design

An overview of the experimental logistics and design is provided in figure 2.2 with detailed description provided below.

2.3 Experimental Protocols

2.3.1 Cell culture

All tissue culture was performed under BIOflow II Labotec laminar flow (Midrand, South Africa). C2C12 adherent myoblasts were grown on 50 ml tissue culture flasks with filtered caps (Greiner Bio-one, GMBH, Frickenhausen, Germany) containing growth medium. The growth medium comprised of 7 ml Dulbecco's Modified Eagles Medium ($DMEM^{++}$) (Sigma-Aldrich, St. Louis, MO) containing 25 mM glucose and supplemented with 1% antibiotic (10000 U/ml penicillin, 100000 µg/ml streptomycin) (Gibco, Paisley, Scotland) and 10% Fetal Bovine Serum (FBS) (Life technologies, Carlsbad, Canada). The cultures were maintained in a humidified incubator (Labotec, USA) at 37^0C and 5% CO_2. Growth medium was changed every 2 days. Myoblasts were routinely passaged once 70-80% confluency was reached and were sub cultured in a 1:4 split ratio. The cells were observed at critical time intervals, such as the undifferentiated stage and at day 2, 4, 6, 7 and 10 of differentiation (figure 2.1) with a Zeiss Stemi 305

stereo microscope and photographed with a digital camera, Zeiss, AuxioCam ERc5s (Zeiss, Oslo, Norway).

2.3.2. Trypsinization

Trypsin-EDTA, 0.25% (Gibco, Paisley, Scotland) was used to dislodge anchorage-dependent cells once cells reached 70 – 80% confluency. Trypsinization was performed as follows:

$DMEM^{++}$ was aspirated from the adherent cells. Thereafter, cells were washed with 5 ml of Phosphate-Buffered Saline (0.01 M Phosphate buffer, 0.0027 M potassium chloride, 0.137 M sodium chloride, pH 7.4 at 25^0C) (Sigma-Aldrich, St. Louis, MO) and 1 ml of concentrated Trypsin-EDTA was added to trypsinize the cells. The cells were immediately incubated for ~2 min at 37^0C and fresh $DMEM^{++}$ was added to inactivate trypsin action. The cell suspension was transferred to a 15 ml falcon tube and centrifuged (1500 g, 25^0C for 4 min) using a micro centrifuge (Heraeus instruments, Newton, CT USA) to obtain pellets.

2.3.3 Cell Passage

The pellets obtained after trypsinization were carefully re-suspended in $DMEM^{++}$. To achieve a split ratio of 1:4, a pellet from a single flask was re-suspended in 4 ml $DMEM^{++}$ and 1 ml of cell suspension was added to 4 flasks each containing 6 ml of $DMEM^{++}$. For all experiments, cells were maintained at a passage number of 7.

2.3.4. Differentiation

To induce differentiation to form multinucleated myotubes, cultured cells were allowed to reach ≥90% confluence in the growth medium. The growth medium was then replaced with a differentiation medium (DMEM with supplemented 2% Horse serum, 1% antibiotic-10000 unit/ml penicillin and 10000 µg/ml streptomycin) and changed every 48 hours for seven days prior to treatment. From day 8 post differentiation we observed gradual increase in cell death and hence all treatment was done at day 7 post differentiation (figure 2.1).

2.3.5. Mycoplasma Test

Mycoplasma tests (30) were routinely performed to verify that cells were not contaminated. Cells were cultured in DMEM^{++} until 70-80% confluence was reached and thereafter trypsinized (section 2.3.2). The resulting pellets were re-suspended in penicillin and streptomycin free media and plated onto a cover slip in a 30 mm tissue culture dish. These cells were maintained in the antibiotic free medium for 3-5 days (humidified incubator at 37^0C and 5% CO_2). On the day of the test, cells that had been growing on coverslips were washed with PBS and fixed with glacial acetic acid: methanol (1:3) for 5 min. Thereafter, the fixative was removed and the coverslip air dried for 3 min, followed by staining with 0.5 µg/ml Hoechst solution (Hoechst 33342, trihydrochloride, trihydrate) in the dark for 10 min. Stained cells were then washed three times with PBS. The cover slip was mounted with Mowiol 4-88 (Calbiochem, San Diego, USA) onto a glass slide, and visualized on the phase contrast microscope, Axiovert 200 M microscope (Zeiss, Oslo, Norway). Images were taken using an AxioCamHR camera with Axiovision software (Version 4.7, Zeiss, Oslo, Norway). Stained nuclei appeared blue and spots around the nuclei indicated mycoplasma contamination. Further experiments were only performed upon confirmation that the cells were mycoplasma negative.

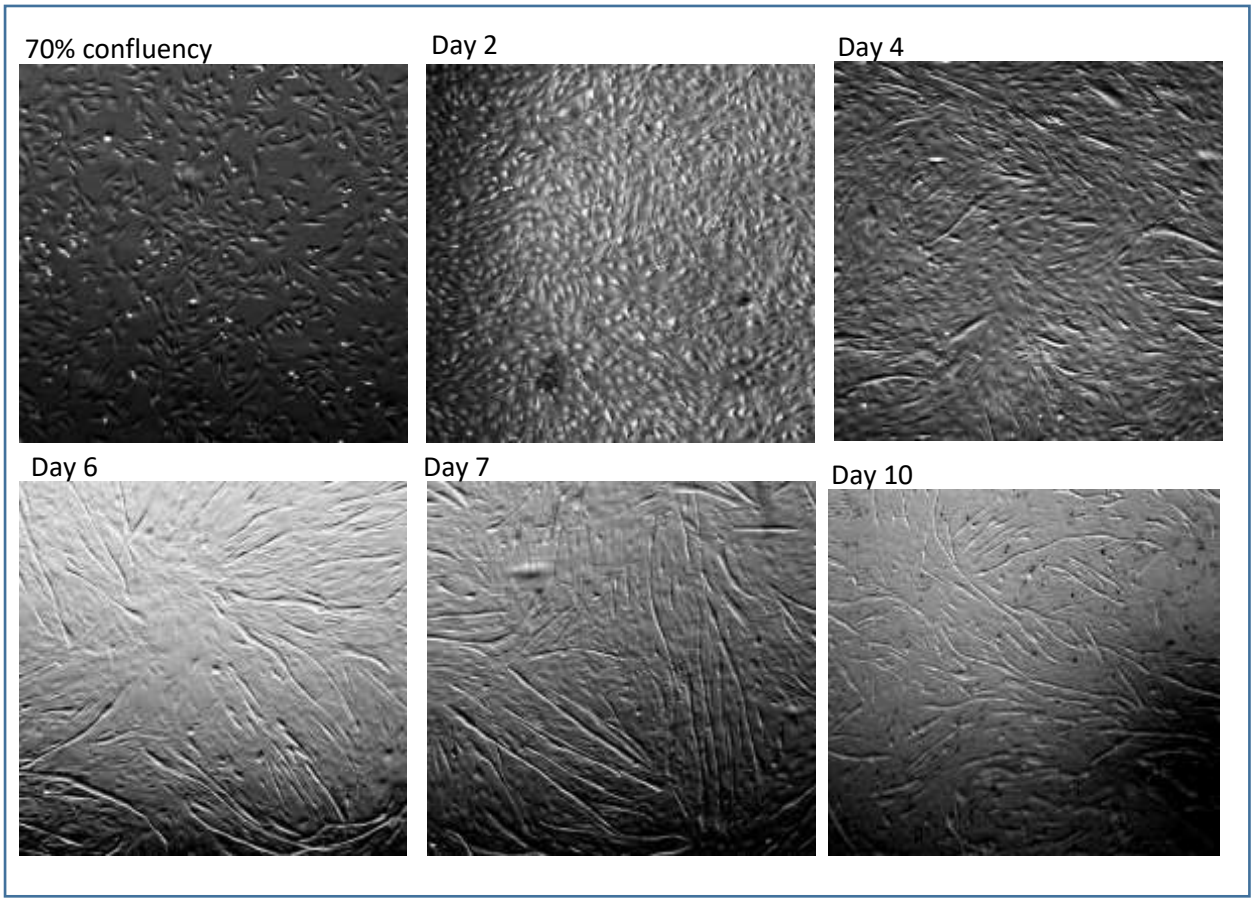

Figure 2.1: Changes in cell morphology in response to myogenic differentiation in control C2C12 cells.

Light microscope images of C2C12 cells before and after induction of differentiation at 70% confluency with DMEM containing 2% horse serum. Cells reach 70% confluency approximately 24 hours after seeding cells onto a tissue

culture flask. The cells are spindle-shaped, replication increases with time till the tissue culture flasks is fully saturated with cells at Day 2. Cells fuse together to form elongated and branched multi-nucleated myotubes; increasing with number of days till after the 8th day, where they start to gradually die off (Day 10). Cells were treated with inhibitors on the 7th day after differentiation was initiated.

2.3.6 Treatment regime

A defect in β-oxidation was induced by selective inhibition of MCAD using 2-mercaptoacetate (7, 16, 81), while fluorocitrate was used to inhibit aconitase of the TCA cycle (43, 78, 83, 175).

2-mercaptoacetate (Thioglycolic acid; Sigma-Aldrich, St. Louis, MO) was reconstituted in water up to a final concentration of 1 M at pH 7. DL-Fluorocitric acid barium salt (Fluorocitrate; Sigma-Aldrich, St. Louis, MO, USA) was activated and corrected to the purity of the powder according to a protocol by Tremblay et al. (2005) (163) Barium fluorocitrate (82.86 mg) was dispersed in 1 ml deionised water to which 50.2 µl of 37% HCl was added to dissolve the powder. Thereafter, 42.6 mg sodium sulphate and 31.8 mg anhydrous sodium carbonate were added to the barium solution. The insoluble barium sulphate was removed by centrifugation (2000 g, 5 min) and the test solution was prepared to a concentration of 0.1 M in water at 7 pH. Both inhibitors were further re-diluted in differentiation media (DMEM supplemented with 2% horse serum and 1% antibiotic) to their final concentrations.

2.3.7. MTT Proliferation Assay

This assay was used to determine effective concentrations and treatment times of inhibitors. Initially, 2-mercaptoacetate was reconstituted in DMEM to a final concentration of 0.25, 0.5, 1, 2, 4, 6, 8, 10 and 20 mM and fluorocitric acid to 0.025, 0.05, 0.1, 0.2, 0.4, 0.6, 0.8, 1 and 2 mM. Concurrently, other cells (controls) were grown without the addition of the inhibitors to DMEM. All cells were plated at a density of 3 x 10^3 cells/well in a 96 well plate (90 µl cell suspension in DMEM^{++} per well) and incubated at 37°C in a 5% CO_2 incubator. Cell proliferation and differentiation was initiated as previously described (section 2.3.4). On day 7 of differentiation, sample wells containing myotubes were treated with 10 µl of the respective concentration of either 2-mercaptoacetate or fluorocitric acid for either 4, 12 or 24 h. After treatment, 10 µl of MTT reagent (100 mg/20 ml 1 XPBS) was added to both sample and blank wells for 4 h before adding the solubilizing reagent (25 g sodium lauryl sulphate, 250 ml distilled water, 76.6 µl 37% HCL) for overnight incubation (Appendix 1).

Absorbance was measured at 595 nm using a micro plate reader (Biotek® instruments Inc. Winooski, USA) in conjunction with the Gen 5 Data analysis software (version 2.01, Biotek® instruments Inc. town, USA). The dose response curve was determined using Graph Pad-Prism software (version 5, Los Angeles, USA). Inhibition was achieved after 12 h of treatment and was used for subsequent experiments. To determine the optimum inhibitory concentration cells were incubated with increasing concentrations of the inhibitors for 12 h treatment. The cells were inhibited by 2-mercaptoacetate treatment from 1 – 10 mM. Fluorocitric acid treatment resulted in decreased proliferation from 2 mM and above. We further examined the effect of an increase in the concentration of fluorocitric acid on cell proliferation. There was a decrease in proliferation from 2 – 10 mM of fluorocitric acid. Hence, we chose to treat with a low or high concentration of either inhibitor as follow; 2 mM and 8 mM of 2-mercaptoacetate, and 6 mM and 9 mM of fluorocitric acid for 12 h in all subsequent experiments.

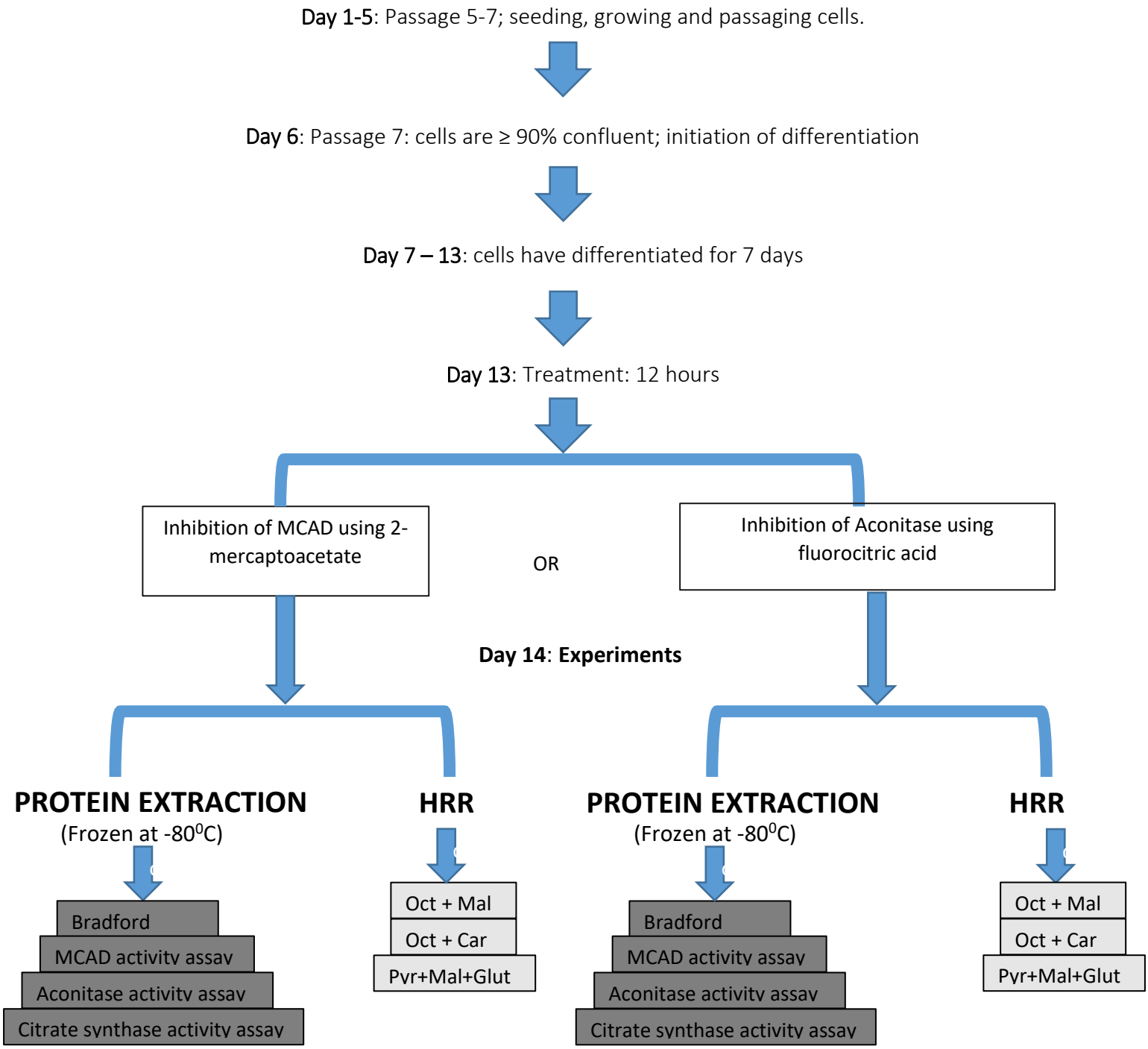

Figure 2.2: Experimental design. *C2C12 cells were grown till a passage number of 7 (1x10^6 cells), after which they were differentiated into myotubes for 7 days. On the 7th day, myotubes were treated with a low or high concentration of either inhibitor for MCAD or aconitase versus vehicle for 12 hours. Thereafter flasks were pooled together and separated for use in either high resolution respirometry (HRR) or for protein extraction. For all experiments, 2 technical repeats and 3 biological repeats was employed. Octanoylcarnitine (Oct), malate (Mal), carnitine (Car), pyruvate (Pyr), glutamate (Glut)*

2.3.8 Protein assays

2.3.8.1 Protein extraction

Protein was extracted from each flask containing myotubes. They were first washed with PBS, scrapped off the bottom of the flask using a Nunc™ cell scraper (ThermoFischer Scientific) into another 5 ml PBS. The suspension containing myotubes was transferred to a clean 15 ml falcon tube which was centrifuged at 1500 g, for 3 mins at 25^0C. Thereafter, the supernatant was discarded and pellets obtained. The pellets were re-suspended in 150 µl of ice cold extraction buffer (containing 0.1 M Tris-HCL, 15 mM tricarballylic acid, final pH 7.8) (173), transferred to a clean 1.5 ml microfuge tube and homogenised on ice. Homogenisation was achieved by sonicating at 80 HZ for 3 x 10 s bursts (Qsonica sonicator, Newton, CT, USA). The homogenates were left on ice for 20 min followed by centrifugation (13000 g 4^0C and 20 min). The supernatant containing lysate was collected and stored at -80^0C until further analyses.

2.3.8.2 Protein determination

The protein concentration of all previously frozen lysates was measured using the Bradford protocol (17). Briefly, lysates were re-diluted (1:1) in extraction buffer; 10 ul of diluent was added to 250 ul of Bradford reagent (Bradford reagent was purchased from Sigma-Aldrich Co®. St. Loius, USA) and the absorbance measured at 595 nm using a microplate reader (Biotek® instruments Inc. Winooski, USA). BSA was used to make standards of known concentration and the protein concentration was determined from BSA standard curve. The unknown protein concentration (mg) was calculated using the formula;

$$\frac{Absorbance\ of\ unknown\ sample\ X\ dilution}{Slope\ of\ standard\ curve}$$

2.3.8.3 MCAD activity

The assay was performed according to modifications to a procedure (173). Briefly, MCAD activity was determined spectrophotometrically by monitoring the decrease in ferrocenium ion absorbance at 300 nm using an extinction coefficient of 4300 M^{-1}. The reaction medium (0.24 ml final volume, 7.4 pH) contained: 100 mM potassium phosphate (KH_2PO_4), 1mM EDTA, 0.5mM sodium tetrathionate, 0.0716

mM ferrocenium hexafluorophosphate (Sigma-Aldrich Co®. St. Loius, USA) and 10 µl C2C12 homogenate (1.2-3.6 mg/ml protein). The reaction was started by addition of 104.2 mM octanoyl-CoA. Absorbance measurements were made on a microplate reader (Biotek® instruments Inc. USA) for ~30 min with absorbance read every 5 min (Appendix 4). Microsoft Excel (2012) was used to draw a standard curve of known ferrocenium hexafluorophosphate concentrations. Reaction rates were calculated from the linear portions of the absorbance versus time plots and the following formula applied to get the specific activity (µmol/min/mg Protein) of MCAD in each sample;

$$\frac{dilution\ X\ slope\ of\ sample}{slope\ of\ STD\ curve\ X\ protein\ concentration}$$

In initial experiments with controls, we used the acyl-CoA dehydrogenase reaction medium as described by Wang et al. (2013) (173) which followed modifications to a method by Lehman and co-workers (80). This included, 10 µl of sample homogenate, 500 µl of reaction mix containing 100 mM KH_2PO_4, 1 mM EDTA, 0.5 mM sodium tetrathionate and 200 µM ferrocenium hexafluorophosphate, pH 7.4 to which 50 µl of 0.5 mM octanoyl-CoA was added. The decrease in absorbance at 300 nm was measured over 5 min in a UV/vis spectrophotometer (Beckman Coulter, Fullerton, CA, USA) and activity was then determined by multiplying the slope to the molar concentration constant for ferrocenium hexafluorophosphate (4300 M^{-1}). Under these conditions the rate of reduction in our C2C12 myotubes were found to follow no trend after 5 min. We then switched to determining the activity of MCAD in a microplate reader (Biotek® instruments Inc. Vermont, USA), after first determining the absorbance of standards of known ferrocenium hexafluorophosphate concentrations. A trend towards linearity in MCAD activity was observed at a lower concentration of 71.6 µM of ferrocenium hexafluorophosphate. We therefore decided to study the effect of increasing the concentration of octanoyl-CoA on the linearity of the enzyme assay with time, at 71.6 µM of ferrocenium hexafluorophosphate. Linearity was optimal at higher octanoyl-CoA concentrations for ~30 min (figure 2.3). Our results showed that MCAD activity with octanoyl-CoA as substrate was best measured at an acyl-CoA concentration of 104.2 mM (based on the concentration of acyl-CoA that resulted both in the highest activity of MCAD as well as sample volume with the least standard error). We measured MCAD activities in C2C12 myotubes of all treated and control samples using these optimized conditions.

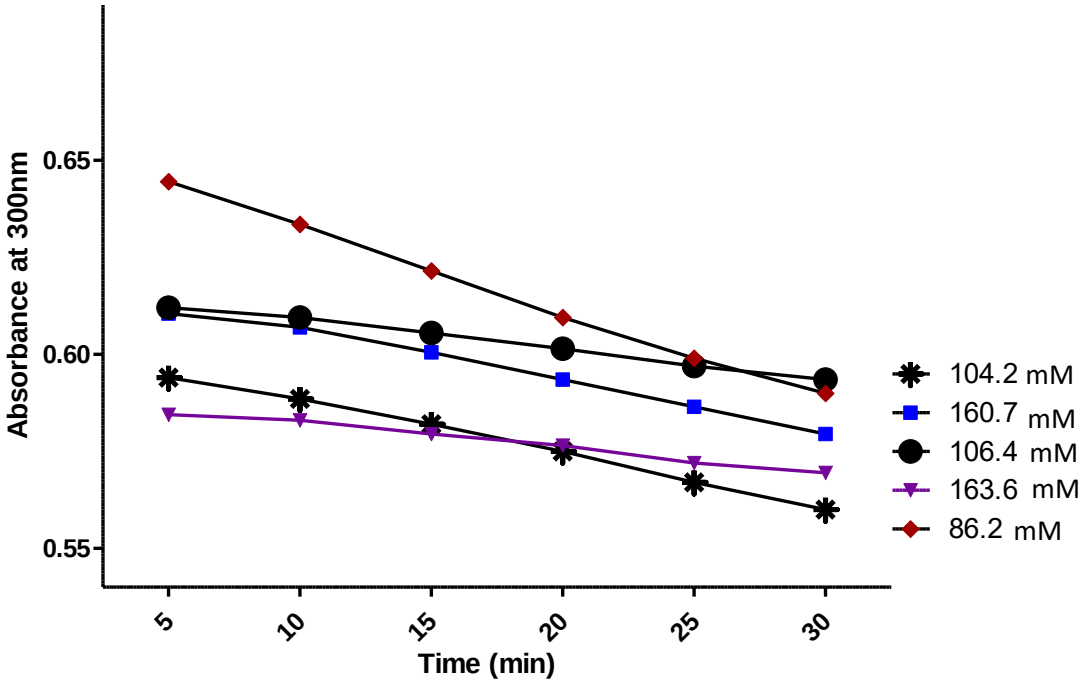

Figure 2.3. The activity of Medium chain acyl-CoA dehydrogenase (MCAD) in control C2C12 myotubes relative to Octanoyl-CoA concentrations (104.2, 160.7, 106.4, 163.6 and 86.2 mM).

2.3.8.4 Aconitase activity

Protocol was adapted from Gardener et al. (1992) (43). Briefly, aconitase activity was measured by monitoring the increase in absorbance at 340 nm, 25^{0}C. The reaction medium (total volume 0.25 ml, 7.4 pH) contained: 50 mM Tris-Buffer, 2 mM Tri-sodium citrate, 0.5 mM $MgCl_2$, 0.2 mM β-$NADP^+$, 1.5 U/ml isocitrate dehydrogenase. The reaction started by adding 15 µl of sample homogenate containing protein. Absorbance measurements were made on a microplate reader (Biotek® instruments, Vermont, USA) every 60 s for at least 1 h (Appendix 3). Reaction rates were calculated from the linear portions of the absorbance versus time plots. Microsoft excel was used to draw a standard curve of known NADPH concentrations and the following formula applied to get the specific activity (µmol/min/mg protein) of aconitase in each sample;

$$\frac{dilution\ X\ slope\ of\ sample}{slope\ of\ STD\ curve\ X\ protein\ concentration}$$

To determine the best assay conditions, we initially studied the effect of altered concentration of the sample on the linearity of aconitase activity over 2 h in control cells. Increasing sample concentrations resulted in a proportional increase in linearity with time. Linearity reduced after ~ 1 h (figure 2.4) and a mid-point was identified (15 µl sample in a total reaction volume of 250 µl, measured over 1 h). These optimized conditions (based on both sample economy and sample volume that resulted in the highest aconitase activity) were used to determine aconitase activity for all control and treated myotubes.

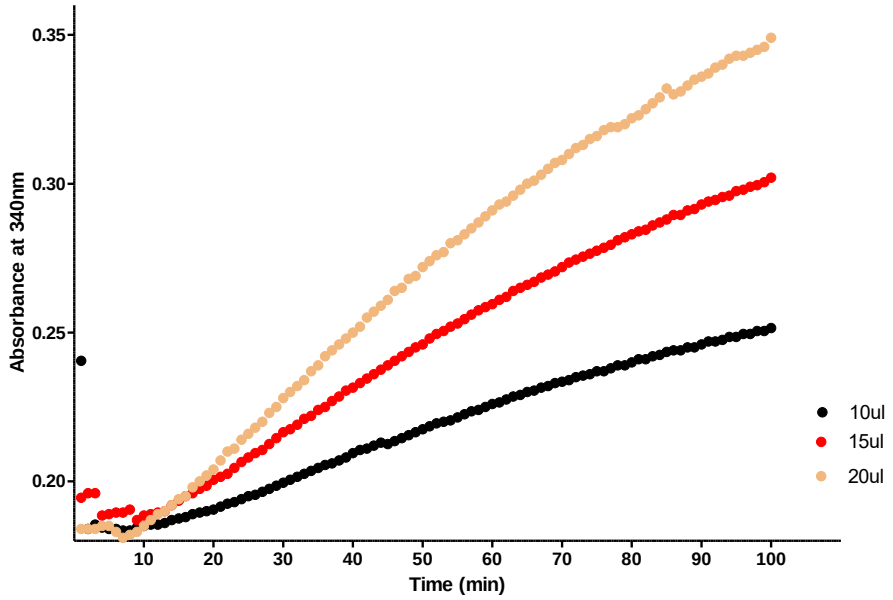

Figure 2.4: The activity of aconitase in control C2C12 myotubes relative to sample volume

2.3.8.5 Citrate synthase

This was completed according to a modified protocol by Kohn et al. (2007) (69). The activity of citrate synthase was determined by monitoring the increase in fluorescence of NADH at 25^{0}C, every 30 s for 5 min. The reaction mix (total volume 0.26 ml, pH 8) contained 0.1 M Tris-buffer, 2.5 mM EDTA, 0.5 mM NAD^+, 1 mM L-malate and 8 µg/ml malate dehydrogenase was added to 10 µl sample and 5 µl acetyl-CoA (Appendix 5). Reaction rates were calculated from the linear portions of the absorbance versus time plots. Microsoft Excel (2012) was used to draw a standard curve of known NADH concentrations and the following formula applied to get the specific activity (µmol/min/mg protein) of citrate synthase in each sample;

$$\frac{dilution\ X\ slope\ of\ sample}{slope\ of\ STD\ curve\ X\ protein\ concentration}$$

2.3.9 Respirometry

The rate of mitochondrial respiration in C2C12 myotubes was measured using Oxygraph-2K High resolution respirometry (Oroboros® instruments, Innsbruck, Austria). A substrate-uncoupler-inhibitor titration (SUIT) protocols was applied as previously described (102). This oxygraph has two chambers, equipped with a Peltier thermostat, electromagnetic stirrers and a gas-tight stopper ensuring minimum oxygen diffusion between the chamber solution and surroundings. Oxygen concentration (µmol/L) in the chamber and oxygen flux (pmol O_2/s/million cells) were recorded using DatLab software (Version 7.3, Oroboros instruments, Innsbruck, Austria). Standard instrumental calibrations were performed timeously (≥ 3 months) to correct for instrumental background oxygen flux, which accounts for the back-diffusion of oxygen into the chamber from the various components; leak from the exterior, the chemical medium and sensor (48). Air calibration of the oxygen sensors was performed daily and before each experiment to account for the partial pressure of air and the medium (51)

On each day of experiment, cells were scrapped into 5 ml PBS and pellets obtained after centrifugation (1500 g, 25^0C, 3 mins) The pellets were then re-suspended in 2.3 ml of respiration buffer, MIR05 (containing 0.5 mM EGTA, 3 mM $MgCl_2$, 20 mM taurine, 10 mM $KHPO_4$, 20 mM HEPES, 200 mM sucrose, 0.1% BSA, final pH 7.1) (114). Two millilitres of the cell suspension was added to an oxygraph chamber ($1x10^6$ cells). Immediately, the chamber was hyper-oxygenated to a concentration of 450-500 µmol/L and the oxygen flux allowed to stabilize. Once oxygen levels were stabilised a state of routine respiration (physiological resting respiration) was recorded. The cell membrane was then permeabilized with 2 µl of digitonin (final concentration of 10 mg/ml DMSO; Appendix 2). This concentration was evaluated in optimization experiments to achieve full permeabilization of cells to allow for easy access of substrates and ADP into the mitochondria without compromising the membrane integrity and mitochondrial function. A sequence of defined respiratory states (oxygen flux resulting from titration of specific substrates) were induced experimentally by stepwise titration according to the following SUIT protocols (51):

2.3.9.1 SUIT Protocol 1: Respiration with octanoylcarnitine + malate

Octanoylcarnitine and malate (0.2 mM and 0.5 mM, respectively) were added to initiate leak respiration (non-phosphorylating resting state as a result of proton leak or slip). Thereafter, maximum oxidative phosphorylation (OXPHOS) was induced by addition of ADP (5 mM). Cytochrome C (10 µM) was added to check the integrity (<10% change in oxygen flux) of the outer mitochondrial membrane (72). The contribution of β-oxidation to the maximum capacity of the ETS was determined by titrating 1 µL (0.05 µM) of chemical uncoupler, CCCP (carbonyl cyanide m-chlorophenyl hydrazine) in stepwise additions until no further increase in respiration was observed. This was closely followed by addition of pyruvate (5 mM) and glutamate (10 mM) to obtain the contribution of complex I to the maximum capacity and afterwards 10 mM of succinate for a convergent Complex I and II linked respiration. Lastly, 2.5 µM of antimycin A, an inhibitor of complex III was added to produce a state of residual oxygen consumption (ROX) to estimate oxidative side reactions. During the course of the experiment oxygen was added to the chambers where necessary to maintain a concentration of 450-250 µmol/l.

2.3.9.2 SUIT Protocol 2: Respiration with octanoylcarnitine + carnitine

In separate experiments, all steps of the suit protocol 1 (presented above) was administered. However, leak respiration was initiated with octanoylcarnitine (0.2 mM) and carnitine (2 mM). Maximum Complex I-linked ETS capacity was measured by titrating 5 mM of pyruvate, 0.5 mM of malate and 10mM of glutamate in succession.

2.3.9.3 SUIT Protocol 3: Mitochondrial respiration with pyruvate +malate

TCA cycle-linked leak respiration was initiated by titrating 2 mM of pyruvate, 0.5 mM of malate and 10 mM of glutamate. This was followed by ADP (2 mM), cytochrome C (5 µM), and 0.05 µM steps of CCCP for maximum capacity of the Complex I-linked ETS. To determine the contribution of β-oxidation-linked substrate to ETS, octanoylcarnitine and carnitine (0.2 mM and 2 mM, respectively) was added. This was followed by 10 mM succinate for Complex II-linked ETS and 2.5 µM of antimycin A for ROX.

On completion of each respirometry assessment, the most stable portion of the oxygen flux/slope was selected at each respiratory state. Experiments that did not meet the criteria for stability of oxygen flux across respiratory states, cell viability and membrane integrity (cytochrome c release) were excluded

from statistical analysis. Thereafter, oxygen flux was corrected for ROX and normalized to protein concentration (mg) and approximate cell number (million cells; number of cells present in cell culture dish before differentiation into myotubes; as it is not possible to obtain cell number after they have fused into myotubes). Flux control ratios (FCR) were calculated as the ratio of each respiratory state to the maximum capacity as well as to maximum FA-linked or Complex I-linked respiration. (50). Lastly, the ratio of LEAK state to OXPHOS states were calculated.

2.4 Statistical analysis

Three biological repeats and two technical repeats were employed for each experimental determination. Statistical analysis was performed using IBM SPSS statistics software (Version 25) and graphical representation was made using GraphPad Prism (version 8.0.2, GraphPad Software inc., La Jolla, Ca, US). Data were first checked for normality using the Shapiro-Wilks test. Normally distributed data are presented as mean ± standard deviation. Statistical differences between control and treatment groups within each protocol were determined using repeated measures ANOVA using group and treatment concentration as main effects and interaction. Paired t-test were used to explore differences within each group. Statistical significance was accepted as $p<0.05$.

CHAPTER THREE

Results

3.1 The effect of inhibition on enzyme activities

We determined the effect of specific enzyme inhibition on the activities of MCAD, aconitase and citrate synthase. Where MCAD was inhibited, it was firstly important to evaluate the effect of inhibition on the targeted enzyme and additionally to investigate the effect of β-oxidation inhibition on the activity of TCA cycle enzymes. We equally measured the activity of aconitase, MCAD and citrate synthase where MCAD or aconitase was respectively inhibited.

3.1.1 MCAD activity

MCAD activity for MCAD and aconitase inhibition are shown in figure 3.1 A and B, respectively. No significant alteration in MCAD activity was observed with either high or low concentration of MCAD inhibitor ($p > 0.05$; figure 3.1A). However, MCAD activity was increased with high concentration of aconitase inhibitor compared to control ($p = 0.024$; figure 3.1B).

3.1.2 Aconitase activity assay

Aconitase activity for MCAD and aconitase inhibition are shown in figure 3.1 C and D, respectively. We observed a trend towards a main effect of concentration ($p = 0.059$) where aconitase was inhibited. Post hoc analysis revealed a significant decrease in aconitase activity with aconitase inhibition in the low treatment compared to control ($p = 0.011$). No significant change in aconitase activity was observed where MCAD was inhibited.

3.1.3 Citrate synthase activity assay

Citrate synthase activity where MCAD or aconitase was inhibited is shown in figure 3.1 E and F, respectively. MCAD inhibition showed a significant increase in citrate synthase activity with high concentration treatment compared to control ($p = 0.03$) and low treatment ($p = 0.015$). Similarly, aconitase inhibition showed an increase in citrate synthase activity with both low ($p = 0.001$) and high ($p < 0.001$) concentration treatment groups, compared to control. Additionally, a trend towards

increased citrate synthase activity was observed in high compared to low treatment with aconitase inhibitor (p = 0.053).

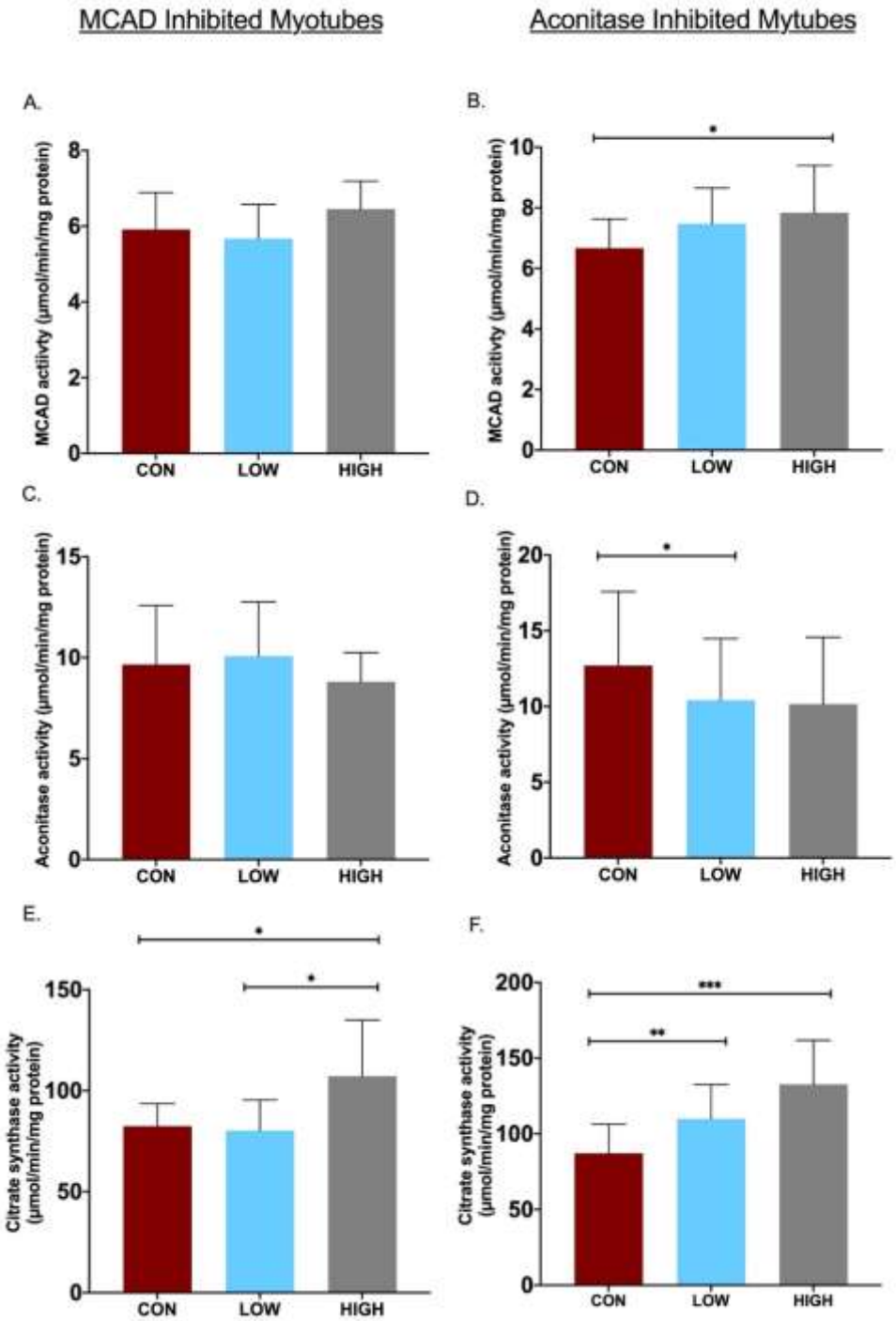

FIGURE 3.1: The effect of MCAD and aconitase inhibition on MCAD, aconitase and citrate synthase activities respectively. A, C, E are enzyme assays where MCAD was inhibited while B, D, F are enzyme assays where aconitase was inhibited. *All data reported as mean ± standard deviation*. * P < 0.05, ** P < 0.01*** P < 0.001.

3.2 The effect of enzyme inhibition on mitochondrial respiration

3.2.1 The effect of enzyme inhibition on mitochondrial respiration using octanoylcarnitine and malate as substrates.

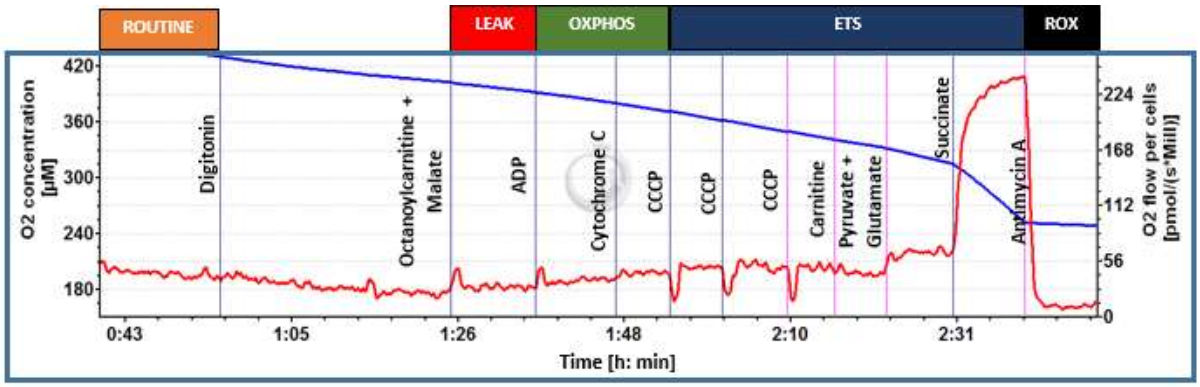

Figure 3.2. Representative trace for a high resolution respirometry protocol with octanoylcarnitine and malate substrate combination. *Graph represents oxygen (O_2) concentration (blue line [µM] and changes in Oxygen flux (red line; [pmol/(s*million cells)]) with time (h: min) in a single oxygraph chamber (oroboros-2K; Oroboros instruments; Austria). ADP (Adenosine di phosphate), CCCP (carbonyl cyanide m-chlorophenyl hydrazone), OXPHOS (oxidative phosphorylation), ETS (electron transport system), ROX (residual oxygen consumption).*

3.2.1.1 The effect of MCAD inhibition

Mitochondrial respiration was normalised to the approximate number of cells (pmol O_2/s/million cells) and results are shown in figure 3.3A. There was a main effect of concentration at all respiratory states except ROX as follows: Routine ($p = 0.01$), $Leak^{FAO}$ ($p = 0.029$), $OXPHOS^{FAO}$ ($p = 0.006$), ETS^{FAO} ($p = 0.008$), $ETS^{FAO+CAR}$ ($p = 0.009$), ETS^{FAO+CI} ($p = 0.017$), $ETS^{FAO+CI+CII}$ ($p = 0.012$). At routine respiration, O_2 flux decreased in low treatment compared to control ($p = 0.023$). $OXPHOS^{FAO}$ significantly decreased in the high treatment compared to control ($p = 0.048$) with a trend to decrease in the low treatment group compared to control ($p = 0.056$). Likewise, there was a trend towards decreased at ETS^{FAO} in low treatment compared to control ($p = 0.067$). $ETS^{FAO+CI+CII}$ significantly decreased in high treatment compared to control ($p = 0.044$) and low treatment ($p = 0.009$).

Oxygen flux normalised to protein concentration (pmol O_2/s/mg protein) are shown in figure 3.3B. This provided a more accurate estimation of mitochondrial respiration, accounting for cell loss through enzyme inhibition. There was a main effect of concentration at routine state alone, however, post hoc analysis revealed no significant difference in O_2 flux with increased inhibition. There was no main effect or interaction effect for all other respiratory states ($p > 0.05$).

Flux control ratios (FCR) at all respiratory states relative to $ETS^{FAO+CI+CII}$ or ETS^{FAO} are shown in figure 3.4A and B, respectively. There was a main effect of concentration at routine, $OXPHOS^{FAO}$, ETS^{FAO}, $ETS^{FAO+CAR}$ and ETS^{FAO+CI} FCR. FCR for routine respiration decreased in low treatment compared to control ($p = 0.002$) and increased in high treatment compared to both control ($p = 0.006$) and low treatment ($p = 0.003$). $OXPHOS^{FAO}$ FCR decreased in both low ($p = 0.013$) and high ($p = 0.023$) treatment compared to control. Lastly, FCR decreased in low treatment compared to control for both ETS^{FAO} ($p = 0.028$) and $ETS^{FAO+CAR}$ ($p = 0.037$). FCR of all respiratory states relative to ETS^{FAO} showed no significant main effect, however, a trend at ETS^{FAO+CI} was observed ($p = 0.052$). Finally, we measured the coupling control ratio of $Leak^{FAO}$ to $OXPHOS^{FAO}$; no significant main effect with MCAD inhibition was observed (figure 3.5)

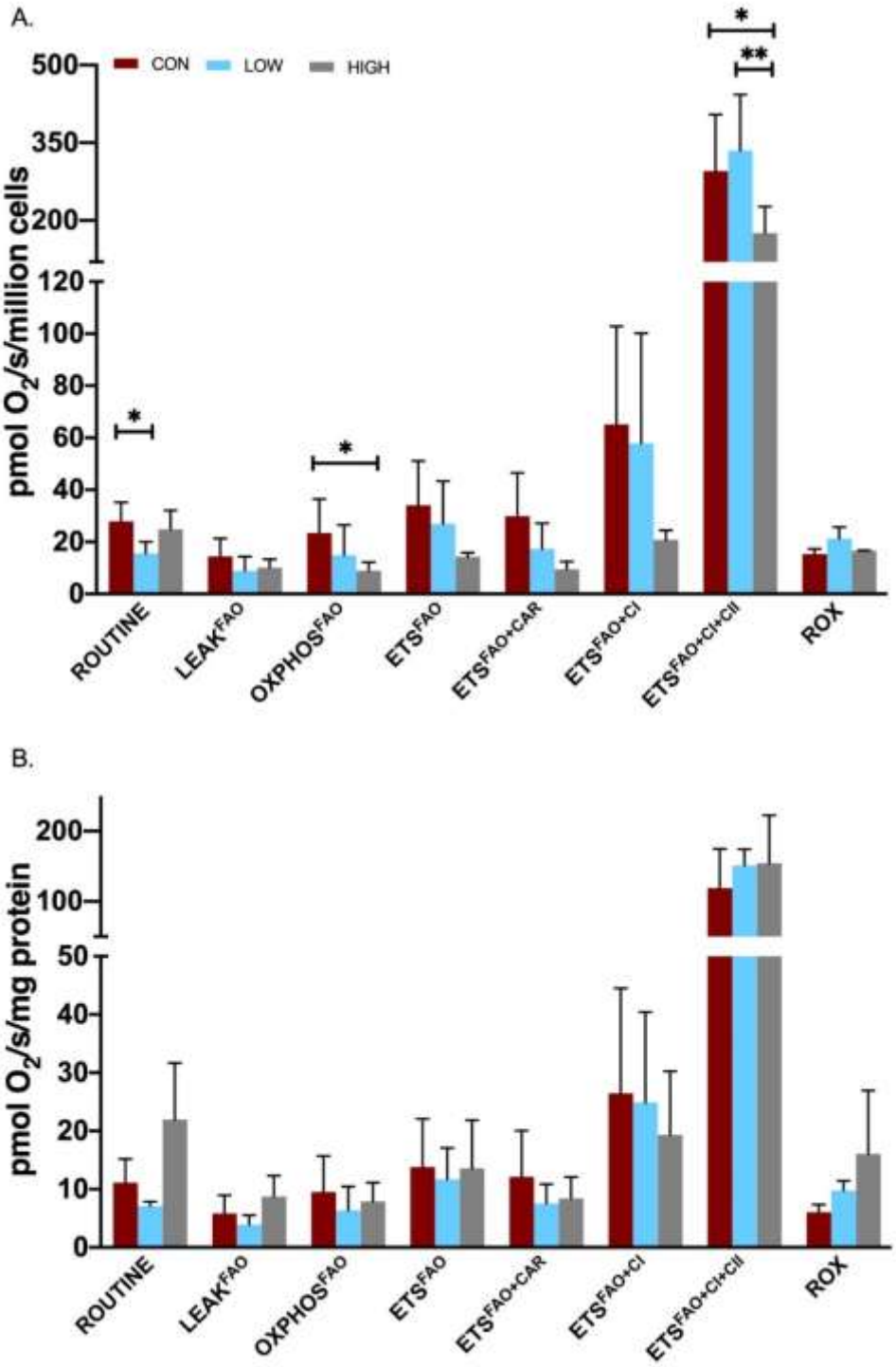

Figure 3.3: The effect of MCAD inhibition on O_2 flux with octanoylcarnitine and malate as substrates. *A) O_2 flux corrected to approximate number of cells (pmol O_2/s/million cells). B) O_2 flux corrected to protein concentration (*pmol O_2/s/mg protein*). FAO (fatty acid oxidation), OXPHOS (Oxidative phosphorylation), ETS (Electron transport system), CI (Complex I), CII (Complex II), car (Carnitine), ROX (Residual oxygen consumption). All data reported as mean ± standard deviation; N= 3; *p < 0.05, **p < 0.01.*

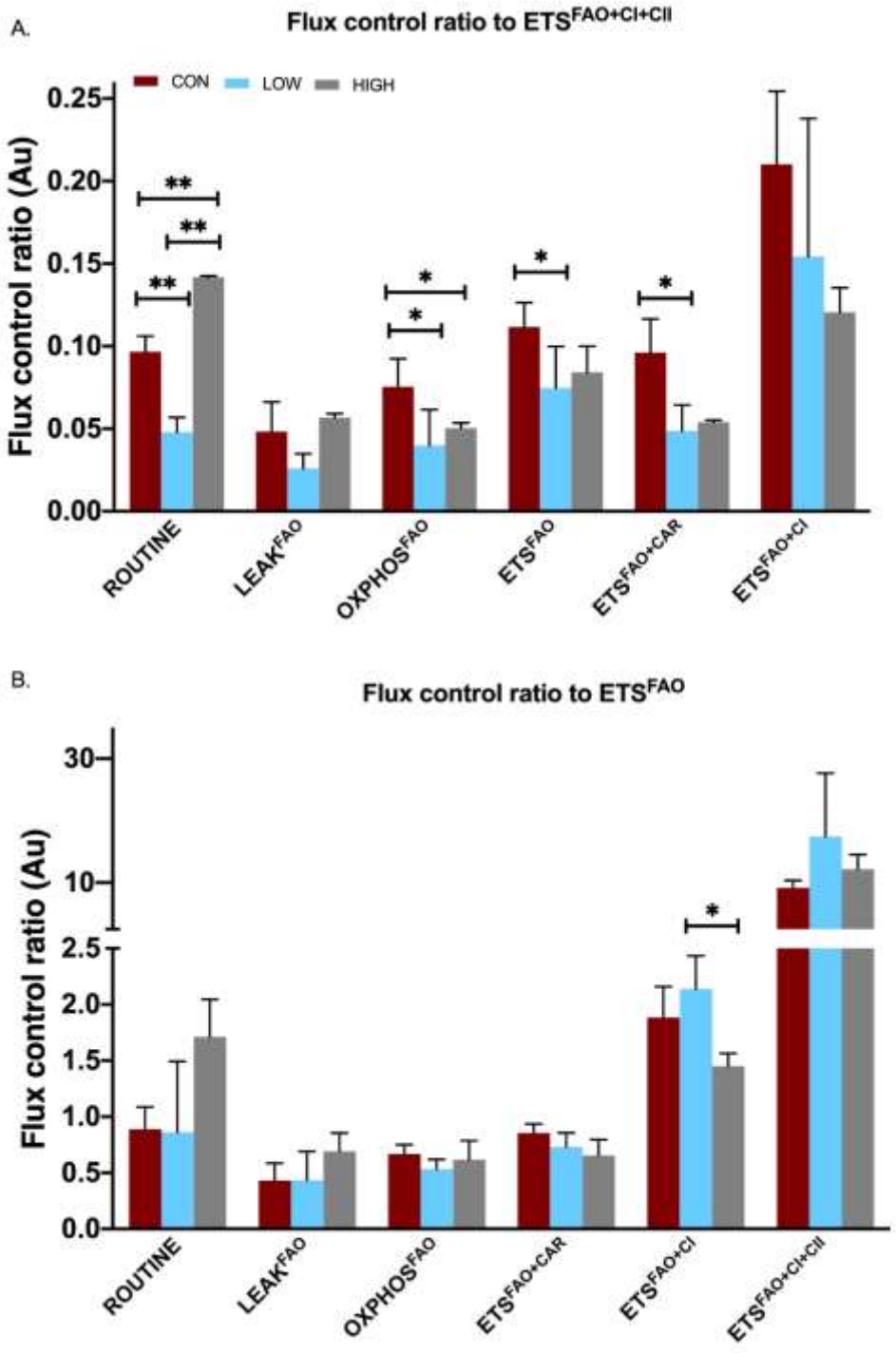

Figure 3.4: The effect of MCAD inhibition on flux control ratio (FCR) with octanoylcarnitine and malate as substrates. *Diagram shows flux control ratios (FCR) normalized relative to A) maximum ETS capacity ($ETS^{FAO+CI+CII}$) as a result of convergent electron flow from fatty acid oxidation (FAO), Complex I (CI) and complex II (CI) B) ETS capacity as a result of FAO (ETS^{FAO}). ETS (Electron transport system), OXPHOS (Oxidative phosphorylation). All data reported as mean ± standard deviation; n = 3; *p < 0.05, **p < 0.01.*

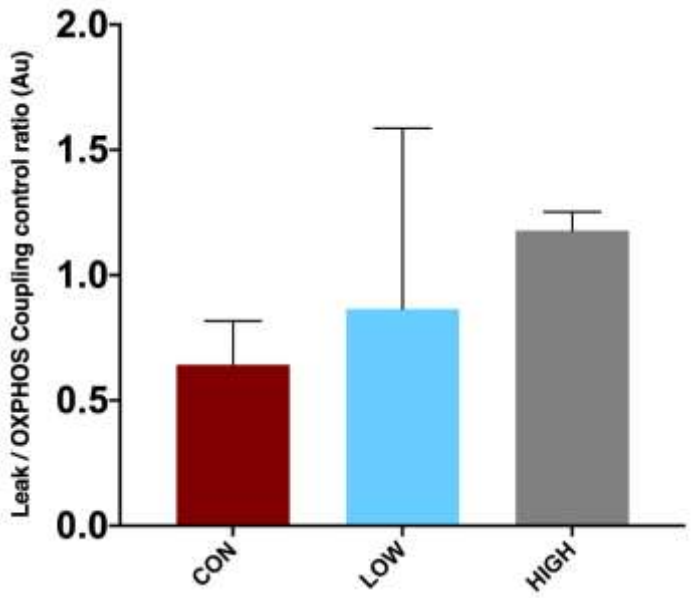

Figure 3.5: The effect of MCAD inhibition on Leak^{FAO}/OXPHOS^{FAO} coupling control ratio with octanoylcarnitine and malate as substrates. *All data reported as mean ± standard deviation; n = 3.*

3.2.1.2 The effect of aconitase inhibition

Respiration normalised to approximate number of cells (pmol O_2/s/million cells) and protein concentration (pmol O_2/s/mg protein) are shown in figure 3.6 A and B, respectively. There was a main effect of concentration in O_2 flux (pmol O_2/s/million cells) at the following respiratory states; Routine ($p = 0.01$), Leak^{FAO} ($p = 0.029$), OXPHOS^{FAO} ($p = 0.006$), ETS^{FAO} ($p = 0.008$). Routine respiration significantly decreased in the high treatment compared to control ($p = 0.032$), however, the decrease in the low treatment compared to control ($p = 0.088$) and in the high compared to low treatment ($p = 0.074$) was not significant. Leak^{FAO} decreased in high treatment compared to control ($p = 0.047$). Similarly, OXPHOS^{FAO} decrease in high treatment compared to both control ($p = 0.042$) and low treatment ($p = 0.037$). Although not significant, there was a trend towards decreased O_2 flux at ETS^{FAO} in high compared to low treatment ($p = 0.066$). Routine respiration (pmol O_2/s/mg protein) revealed a main effect of concentration ($p = 0.037$). There was a decreased flux in the high treatment compared to low treatment ($p = 0.042$), but there was a trend towards a decrease in the low treatment compared to control without reaching significance ($p = 0.058$).

The FCR relative to maximum capacity of the ETS (ETS$^{FAO+CI+CII}$) or ETS^{FAO} are shown in figure 3.7 A and B, respectively. There was a main effect of concentration at routine ($p = 0.001$), OXPHOS^{FAO} ($p = 0.003$),

ETS^{FAO} (p = 0.018), $ETS^{FAO+CAR}$ (p = 0.008) and ETS^{FAO+CI} (p = 0.027). Routine FCR was significantly decreased in both low (p = 0.009) and high (p = 0.004) treatment compared to control; however, there was a trend to decrease in the high compared to low treatment (p = 0.055). $OXPHOS^{FAO}$ FCR decreased in the high treatment compared to control (p = 0.006) and low treatment (p = 0.046). Additionally, ETS^{FAO} showed a trend to decrease in the low (p = 0.054) and high (p = 0.05) treatment compared to control. Post hoc analysis revealed no significant change in FCR at $ETS^{FAO+CAR}$ and ETS^{FAO+CI}. Finally, we measured the coupling control ratio of $LEAK^{FAO}$ to $OXPHOS^{FAO}$. No significant main effects (p = 0.121 concentration; p = 0.703 treatment) or interaction (p = 0.699) was shown with aconitase inhibition (figure 3.8).

3.2.1.3 Differences between aconitase inhibition and MCAD inhibition

There was an interaction effect between aconitase inhibitor treatment and MCAD inhibitor treatment at Routine respiration (pmol O_2/s/million cells; p = 0.037), however, this interaction was driven by a significant effect of concentration within groups and no difference between treatment groups (p > 0.05). Furthermore, O_2 flux normalised to protein concentration (pmol O_2/s/mg protein) showed a main effect of treatment at Routine respiration (p = 0.037). Post hoc analysis did not reveal any significant difference with inhibitor treatment. The FCR calculated to $ETS^{FAO+CI+CII}$ showed interaction effects of routine (p < 0.001), $Leak^{FAO}$ (p = 0.013) and $OXPHOS^{FAO}$ (p = 0.015). Routine respiration showed a difference between aconitase treatment and MCAD treatment at high concentration (p = 0.040). $Leak^{FAO}$ and $OXPHOS^{FAO}$ showed no difference between aconitase and MCAD treatment concentrations (all p > 0.05). Therefore, the interactions were driven by significant changes within each treatment group. Lastly, there was an interaction effect in ETS^{FAO+CI} to ETS^{FAO} ratio (p = 0.017). Similarly, the interaction effects were driven by the significant effect of concentration within the groups.

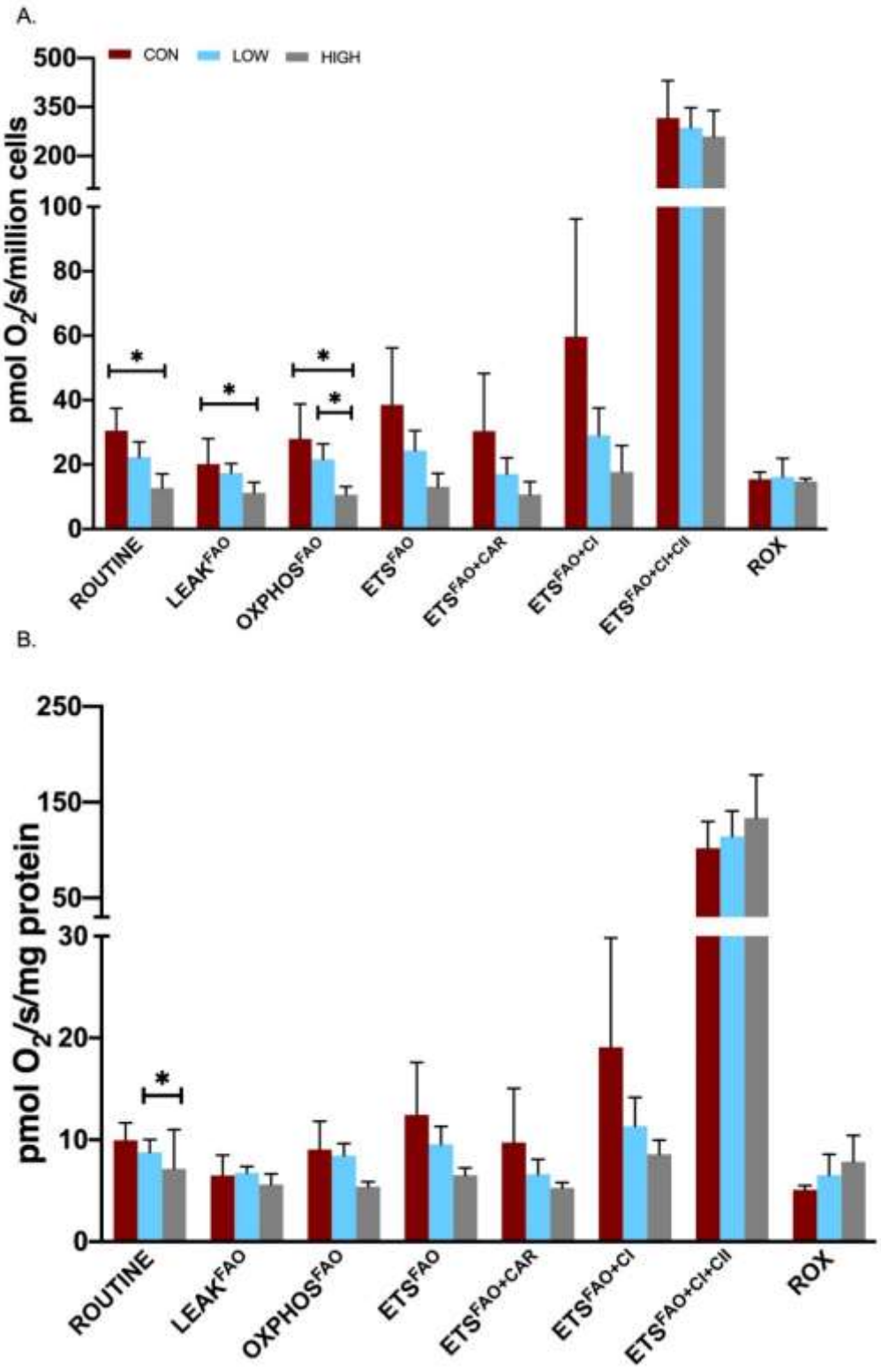

Figure 3.6: The effect of aconitase inhibition on O_2 flux with octanoylcarnitine and malate as substrates.

*A) O_2 flux corrected to approximate number of cells per oxygraph chamber (pmol O_2/s/million cells) B) O_2 flux corrected to protein concentration (*pmol O_2/s/mg protein*). FAO (fatty acid oxidation), OXPHOS (Oxidative phosphorylation), ETS (Electron transport system), CI (Complex I), CII (Complex II), ROX (Residual oxygen consumption). All data reported as mean ± standard deviation; n= 3; *p < 0.05.*

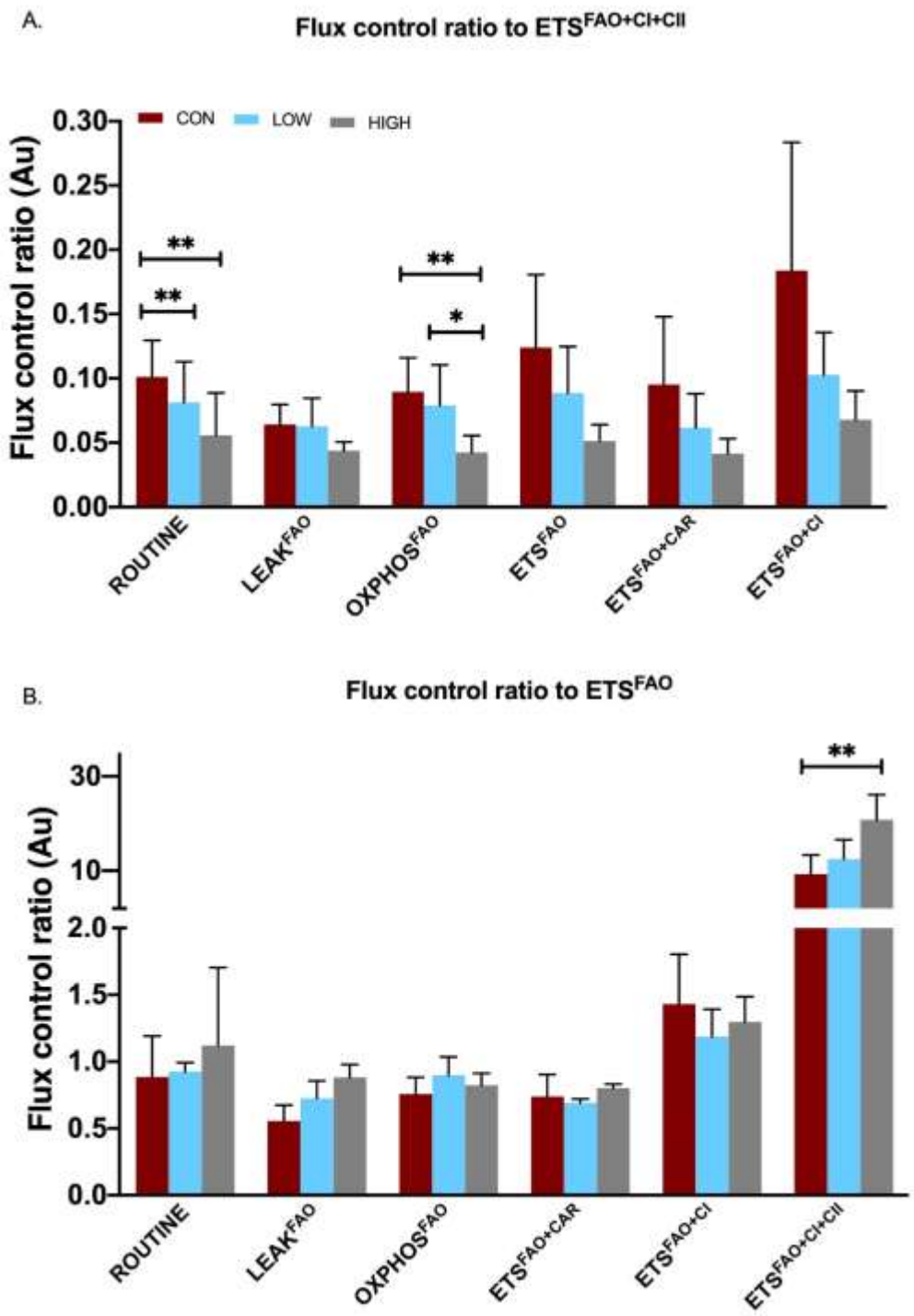

Figure 3.7: The effect of aconitase inhibition on flux control ratio (FCR) with octanoylcarnitine and malate as substrates. *Diagram shows flux control ratios (FCR) normalized relative to A) maximum ETS capacity ($ETS^{FAO+CI+CII}$) as a result of convergent electron flow from fatty acid oxidation (FAO), Complex I (CI) and complex II (CI) B) ETS capacity as a result of FAO (ETS^{FAO}). ETS (Electron transport system), OXPHOS (Oxidative phosphorylation). All data reported as mean ± standard deviation; n = 3; *p < 0.05, **p < 0.01.*

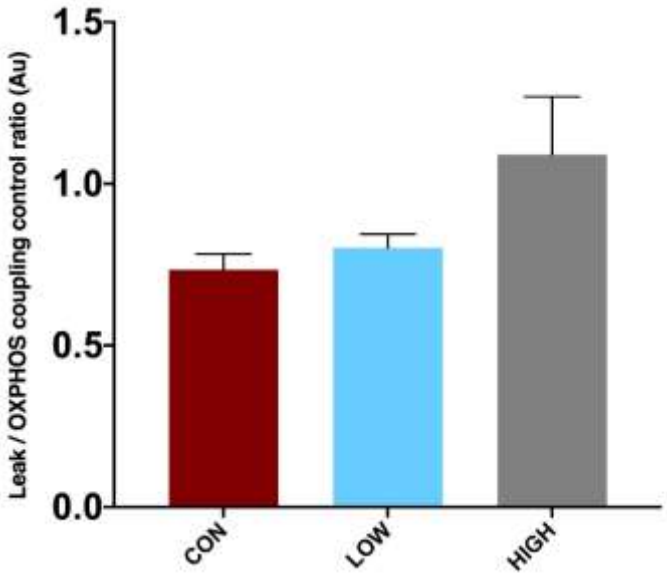

Figure 3.8. The effect of aconitase inhibition on Leak^{FAO}/OXPHOS^{FAO} coupling control ratio with octanoylcarnitine and malate as substrates. *All data reported as mean ± standard deviation; n = 3*

3.2.2 The effect of enzyme inhibition on mitochondrial respiration using octanoylcarnitine and carnitine as substrates.

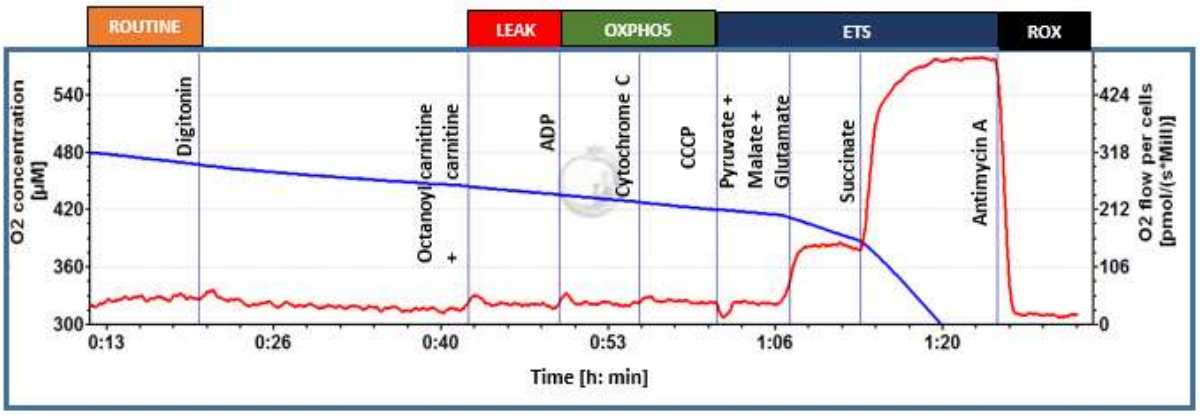

Figure 3.9. Representative trace for a high resolution respirometry protocol with octanoylcarnitine and carnitine substrate combination. *Graph represents oxygen (O_2) concentration (blue line [µM] and changes in Oxygen flux (red line; [pmol/(s*million cells)]) with time in a single oxygraph chamber (oroboros-2K; Oroboros instruments; Austria). ADP (Adenosine di phosphate), CCCP (carbonyl cyanide m-chlorophenyl hydrazone), OXPHOS (oxidative phosphorylation), ETS (electron transport system), ROX (residual oxygen consumption).*

3.2.2.1 The effect of MCAD and aconitase inhibition

Mitochondrial respiration using octanoylcarnitine and carnitine substrate combination are shown in figures 3.10-3.15. MCAD and aconitase inhibition showed no main effect or interaction ($p>0.05$) for most respiratory states when respiration was normalised to cell number (pmol O_2/s/million cells), protein concentration (pmol O_2/s/mg protein), and FCR. The only observed change was a main effect of concentration when FCR was calculated to maximum ETS capacity for FAO alone (ETS^{FAO}; $p = 0.04$) at $Leak^{FAO}$ state. There was a significant increase in the low treatment compared to control when MCAD ($p = 0.017$; figure 3.11B) and aconitase were inhibited ($p = 0.001$; figure 3.15 B).

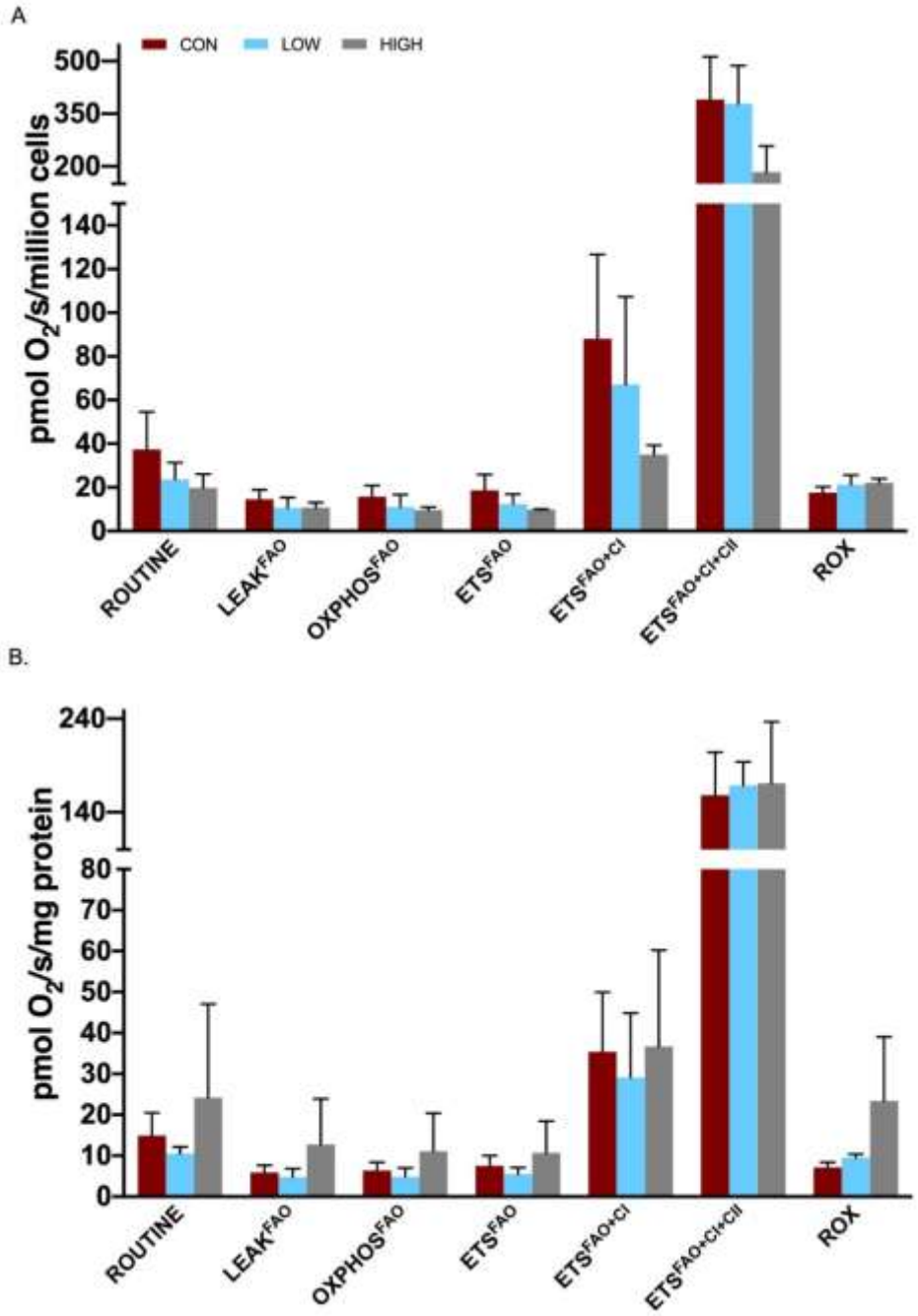

Figure 3.10: The effect of MCAD inhibition on O_2 flux with octanoylcarnitine and carnitine as substrates.

*A) O_2 flux corrected to approximate number of cells per oxygraph chamber (pmol O_2/s/million cells) B) O_2 flux corrected to protein concentration (*pmol O_2/s/mg protein*). FAO (fatty acid oxidation), OXPHOS (oxidative phosphorylation), ETS (Electron transport system), CI (Complex I), CII (Complex II), ROX (Residual oxygen consumption). All data reported as mean ± standard deviation; n= 3.*

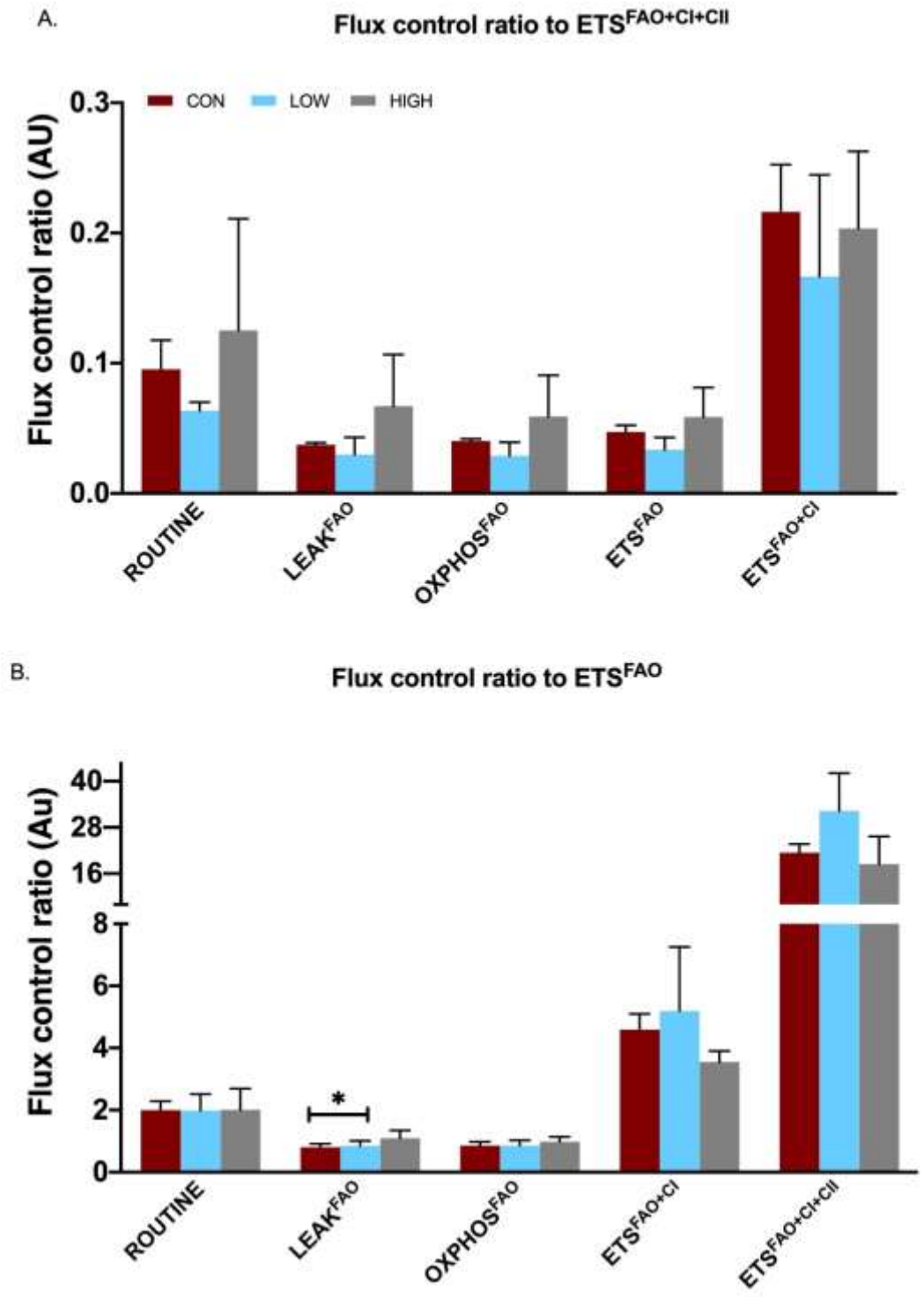

Figure 3.11: The effect of MCAD inhibition on Flux control ratio (FCR) with octanoylcarnitine and carnitine as substrates. *Diagram shows flux control ratios (FCR) normalized relative to A) maximum ETS capacity ($ETS^{FAO+CI+CII}$) as a result of convergent electron flow from fatty acid oxidation (FAO), Complex I (CI) and complex II (CI) B) ETS capacity as a result of FAO (ETS^{FAO}). ETS (Electron transport system), OXPHOS (Oxidative phosphorylation). All data reported as mean ± standard deviation; n = 3; *p < 0.05.*

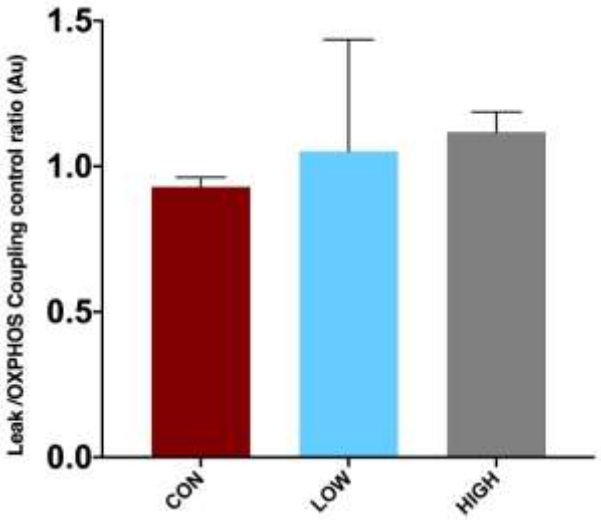

Figure 3.12: The effect of MCAD inhibition on Leak^{FAO}/OXPHOS^{FAO} coupling control ratio with octanoylcarnitine and carnitine as substrates. *All data reported as mean ± standard deviation; n = 3.*

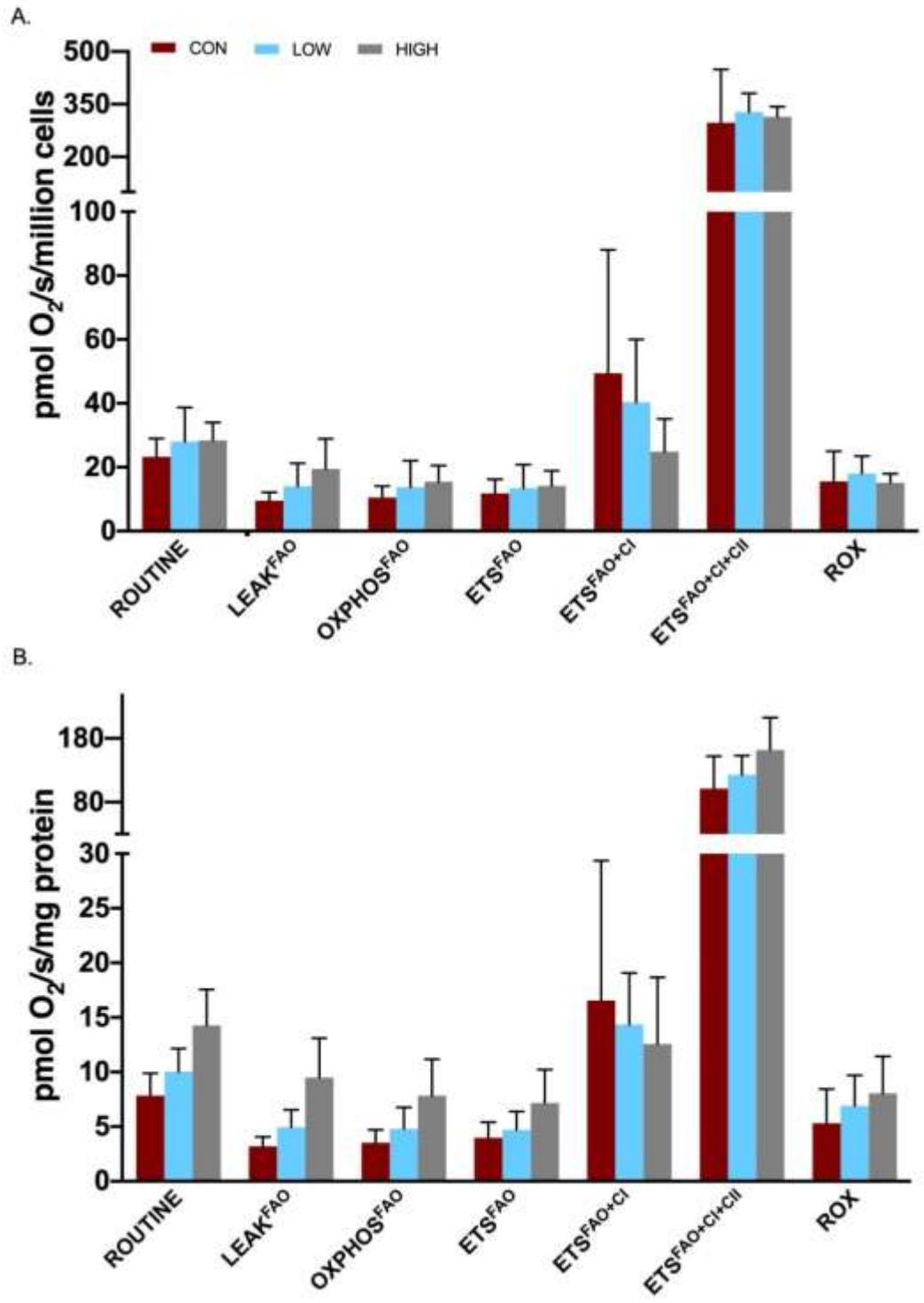

Figure 3.13: The effect of aconitase inhibition on O_2 flux with octanoylcarnitine and carnitine as substrates.

A) O_2 flux corrected to approximate number of cells per oxygraph chamber (pmol O_2/s/million cells) B) O_2 flux corrected to protein concentration (pmol O_2/s/mg protein). FAO (fatty acid oxidation), OXPHOS (oxidative phosphorylation), ETS (Electron transport system), CI (Complex I), CII (Complex II), ROX (Residual oxygen consumption). All data reported as mean ± standard deviation; n= 3.

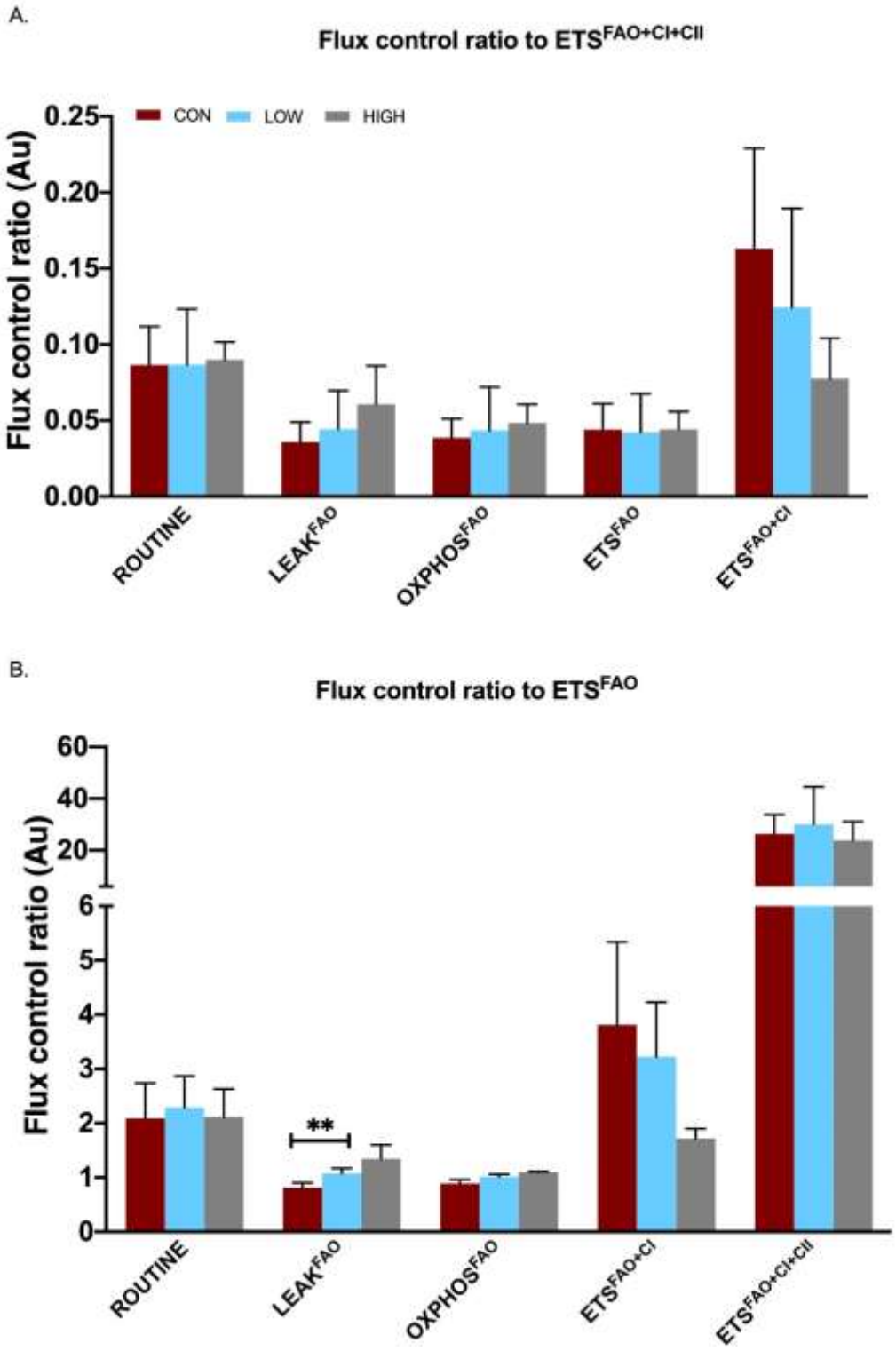

Figure 3.14: The effect of aconitase inhibition on flux control ratio (FCR) with octanoylcarnitine and carnitine as substrates. *Diagram shows flux control ratios (FCR) normalized relative A) maximum ETS capacity ($ETS^{FAO+CI+CII}$) as a result of convergent electron flow from fatty acid oxidation (FAO), Complex I (CI) and complex II (CI) B) ETS capacity as a result of FAO (ETS^{FAO}). ETS (Electron transport system), OXPHOS (Oxidative phosphorylation). All data reported as mean ± standard deviation; n = 3; **p < 0.005.*

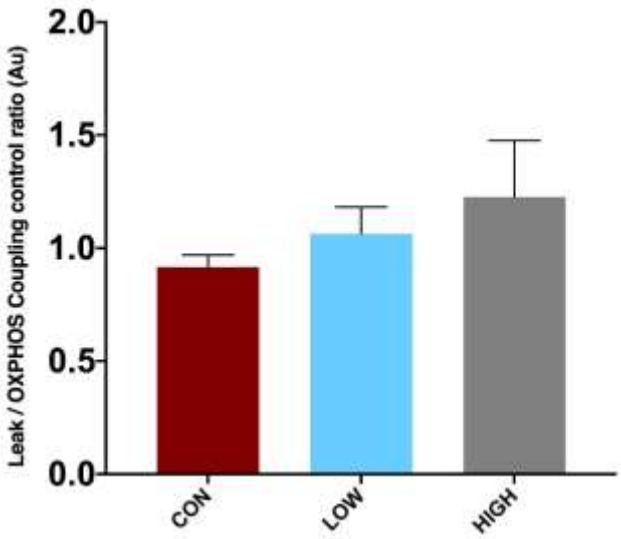

Figure 3.15: The effect of aconitase inhibition on Leak^{FAO}/OXPHOS^{FAO} coupling control ratio with octanoylcarnitine and carnitine as substrates. *All data reported as mean ± standard deviation; n = 3.*

3.2.3 The effect of enzyme inhibition on mitochondrial respiration using pyruvate, malate and glutamate as substrates.

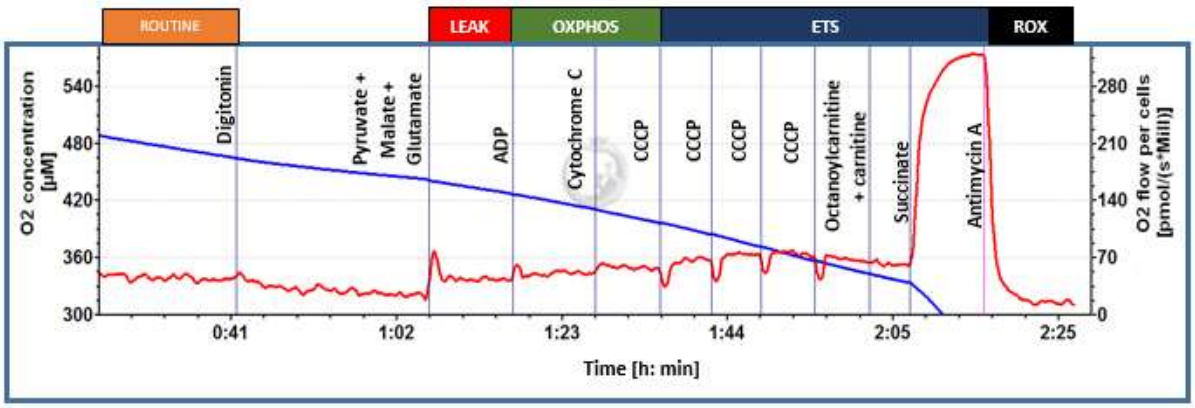

Figure 3.16. Representative trace for a high resolution respirometry protocol with pyruvate, malate and glutamate substrate combination. *Graph represents oxygen (O_2) concentration (blue line [µM] and changes in Oxygen flux (red line; [pmol/(s*million cells)]) with time in a single oxygraph chamber (oroboros-2K; Oroboros instruments; Austria). ADP (Adenosine di phosphate), CCCP (carbonyl cyanide m-chlorophenyl hydrazone), OXPHOS (oxidative phosphorylation), ETS (electron transport system), ROX (residual oxygen consumption).*

3.2.3.1 The effect of MCAD inhibition

Oxygen flux normalised to the approximate amount of cells (pmol O_2/s/million cells) are reported in figure 3.17 A. A main effect of concentration at all respiration states are as follows: Routine ($p = 0.004$), $Leak^{CI}$ ($p = 0.007$), $OXPHOS^{CI}$ ($p = 0.003$), ETS^{CI} ($p = 0.003$), ETS^{CI+FAO} ($p = 0.01$) and $ETS^{CI+FAO+CII}$ ($p = 0.003$). $Leak^{CI}$ ($p < 0.001$), $OXPHOS^{CI}$ ($p = 0.002$), ETS^{CI} ($p = 0.022$) and ETS^{CI+FAO} ($p = 0.022$) decreased in high compared to low treatment. Lastly, $ETS^{CI+FAO+CII}$ decreased in high treatment compared to both control ($p = 0.028$) and low treatment ($p = 0.008$). Oxygen flux adjusted to protein concentration (pmol O_2/s/mg protein) are reported in figure 3.17 B. There was a main effect of concentration at Routine ($p = 0.005$), ETS^{CI} ($p = 0.006$) and ETS^{CI+FAO} ($p = 0.022$). ETS^{CI} ($p = 0.024$) and ETS^{CI+FAO} ($p = 0.037$) significantly decreased in the low treatment compared to control.

The flux control ratios of each respiratory state to $ETS^{CI+FAO+CII}$ or ETS^{CI} are shown in figure 3.18 A and B, respectively. There was a main effect of concentration at Routine ($p = 0.024$) and $OXPHOS^{CI}$ ($p = 0.024$) to $ETS^{CI+FAO+CII}$. We observed a trend for decreased routine FCR with high compared to low treatment ($p = 0.06$), while $OXPHOS^{CI}$ decreased in the high compared to low treatment ($p = 0.022$). Lastly, $Leak^{CI}$ to $OXPHOS^{CI}$ ratio indicated a main effect of concentration ($p = 0.036$), however, post-hoc analysis showed no significant difference with increasing inhibitor concentration (figure 3.19).

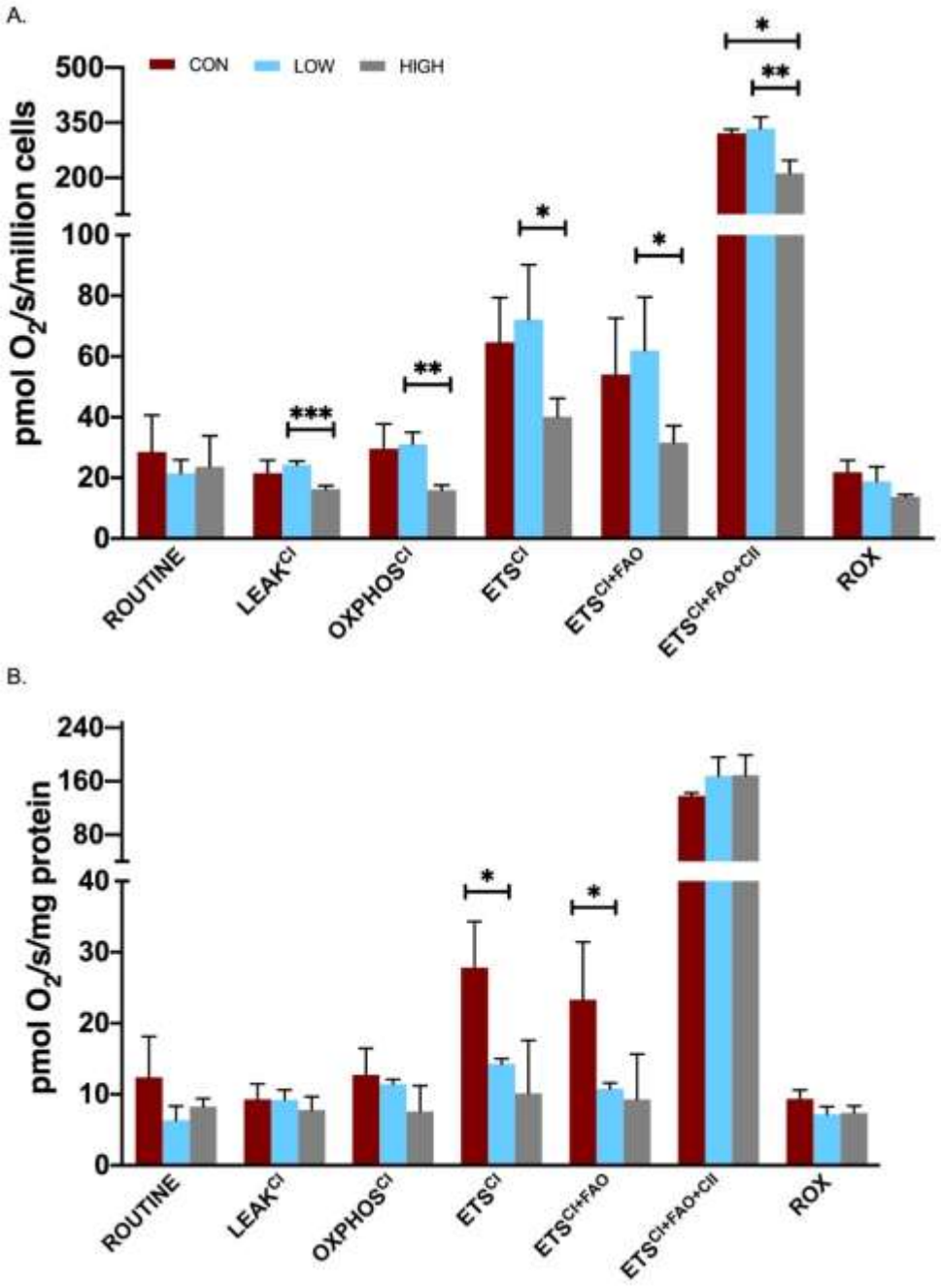

Figure 3.17: The effect of MCAD inhibition on O_2 flux with pyruvate, malate and glutamate as substrates.

*A) O_2 flux corrected to approximate number of cells per oxygraph chamber (pmol O_2/s/million cells) B) O_2 flux corrected to protein concentration (pmol O_2/s/mg protein). FAO (fatty acid oxidation), OXPHOS (Oxidative phosphorylation), ETS (Electron transport system), CI (Complex I), CII (Complex II), ROX (Residual oxygen consumption). All data reported as mean ± standard deviation; n = 3; *p < 0.05, **p < 0.01, ***p < 0.001.*

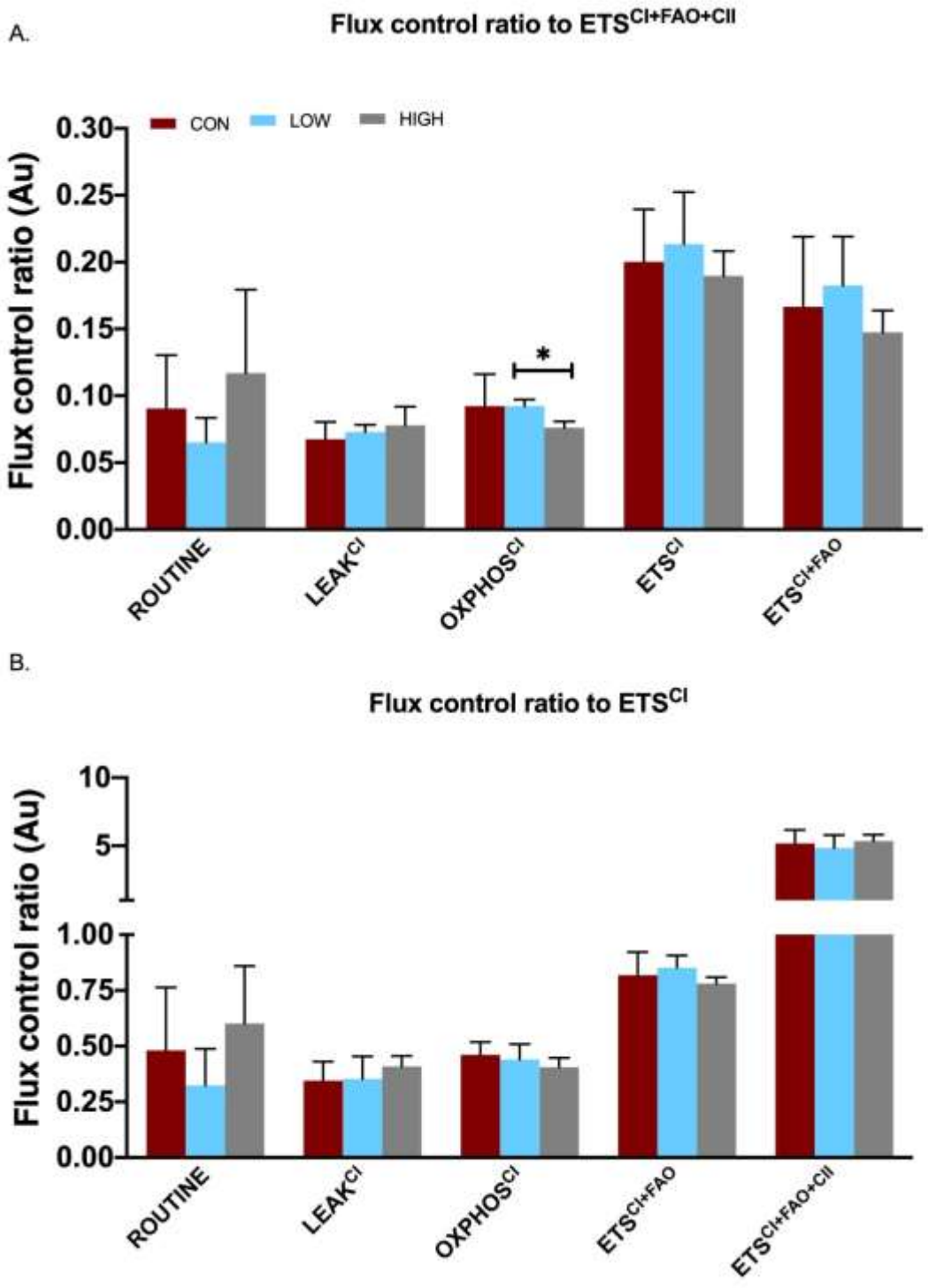

Figure 3.18: The effect of MCAD inhibition on flux control ratio (FCR) with pyruvate, malate and glutamate as substrates. *Diagram shows flux control ratios (FCR) normalized relative to A) maximum ETS capacity ($ETS^{CI+FAO+CII}$) as a result of convergent electron flow from Complex I (CI), fatty acid oxidation (FAO) and complex II (CI) B) ETS capacity as a result of CI (ETS^{CI}). All data reported as mean ± standard deviation; n = 3; *p < 0.05.*

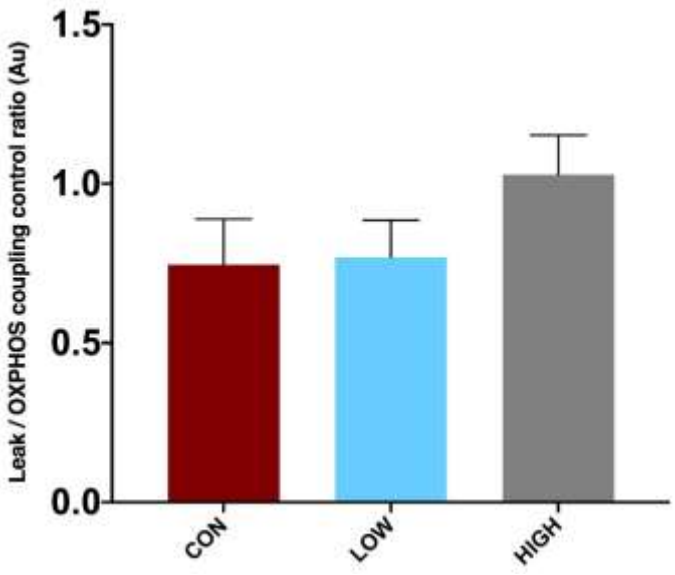

Figure 3.19: The effect of MCAD inhibition on Leak^{CI}/OXPHOS^{CI} coupling control ratio with pyruvate, malate and glutamate as substrates. *All data reported as mean ± standard deviation; n = 3.*

3.2.3.2 The effect of aconitase inhibition

Respiration normalised to the million cells (pmol O_2/s/million cells) are displayed in figure 3.20 A. There was a main effect of concentration at all respiration states except ROX as follows: Routine ($p = 0.004$), LEAK^{CI} ($p = 0.007$), OXPHOS^{CI} ($p = 0.003$), ETS^{CI} ($p = 0.003$), ETS^{CI+FAO} ($p = 0.01$) and ETS$^{CI+FAO+CII}$ ($p = 0.003$). Routine respiration was significantly decreased in both low ($p = 0.022$) and high ($p = 0.009$) treatment compared to control. Likewise, LEAK^{CI} and OXPHOS^{CI} decreased in high treatment compared to control ($p < 0.05$) and low treatment ($p < 0.05$). ETS^{CI} decreased in high ($p = 0.024$) and low ($p = 0.013$) treatment compared to control. ETS^{CI+FAO} decreased in the low treatment compared to control ($p = 0.015$), and, a trend towards decreased flux was observed in high treatment compared to controls ($p = 0.065$). Additionally, a trend towards decreased flux was also observed in the high compared to low treatment at ETS$^{CI+FAO+CII}$ ($p = 0.054$).

Oxygen flux at each respiratory state corrected to protein concentration (pmol O_2/s/mg protein) are shown in figure 3.20 B. Results show a main effect of concentration at Routine ($p = 0.005$), ETS^{CI} ($p = 0.006$) and ETS^{CI+FAO} ($p = 0.022$). Routine respiration was significantly decreased in low treatment compared to control ($p = 0.045$) but only a trend towards decrease in the high treatment compared to control ($p = 0.057$). ETS^{CI}, decreased in low treatment compared to control ($p = 0.036$). There was a trend towards decreased flux at ETS^{CI+FAO} in low treatment compared to controls ($p = 0.063$)

The FCR of each respiratory state to the maximum capacity of the ETS ($ETS^{CI+FAO+CII}$) are shown in figure 3.21 A. There was a main effect of concentration at Routine (p = 0.024), $OXPHOS^{CI}$ (p = 0.024) and ETS^{CI} (p = 0.035). Routine FCR decreased in the low treatment compared to control (p = 0.01), however, only a trend towards a decrease was observed in the high compared to low treatment (p = 0.068). $OXPHOS^{CI}$ decreased in the high treatment compared to control (p = 0.045) and low treatment (p = 0.005). Similarly, ETS^{CI} decreased in both low (p = 0.009) and high (p = 0.03) treatment, compared to control.

The FCR of each respiratory state to the maximum capacity of the ETS due to CI contribution alone (ETS^{CI}) are displayed in figure 3.21 B. There was a main effect of concentration at $ETS^{CI+FAO+CII}$. There was a significant increase in both the low (p = 0.008) and high (p = 0.035) treatment compared to control. There was a trend towards an increase in the high compared to low treatment (p = 0.06). Finally, there was a main effect of concentration in the $LEAK^{CI}$ to $OXPHOS^{CI}$ ratio, however, there was no significant effect of treatment concentration (figure 3.22).

3.2.3.3 Differences between aconitase inhibition and MCAD inhibition

There was a main effect of treatment when respiration was corrected to millions of cells (pmol O_2/s/million cells) at ETS^{CI} (p = 0.026). At low inhibitor concentration, O_2 flux was decreased with MCAD compared to aconitase inhibition (p = 0.015), however only a trend towards a decrease between groups was observed at high concentration (p = 0.055). When FCR was calculated to the maximum capacity of the ETS, $ETS^{CI+FAO+CII}$; we observed an interaction effect for $Leak^{CI}$ FCR (p = 0.018) and ETS^{CI} FCR (p = 0.046); conversely there was a main effect of treatment for $OXPHOS^{CI}$ (p = 0.046), ETS^{CI} (p = 0.003) and ETS^{CI+FAO} (p = 0.008). ETS^{CI} FCR was decreased in MCAD compared to aconitase inhibition at both low (p = 0.008) and high (p = 0.012) concentration. Similarly, ETS^{CI+FAO} FCR was decreased with MCAD inhibition compared to aconitase inhibition at both low (p = 0.005) and high (p = 0.02) concentration. Lastly, FCR calculated to the maximum capacity for complex I alone (ETS^{CI}) showed a main effect of treatment for $Leak^{CI}$ (p = 0.032), $OXPHOS^{CI}$ (p = 0.027) and $ETS^{CI+FAO+CII}$ (p = 0.041). There was a decreased FCR in MCAD compared to aconitase inhibition at low concentration for $Leak^{CI}$ (p = 0.025), $OXPHOS^{CI}$ (p = 0.002) and $ETS^{CI+FAO+CII}$ (p = 0.01).

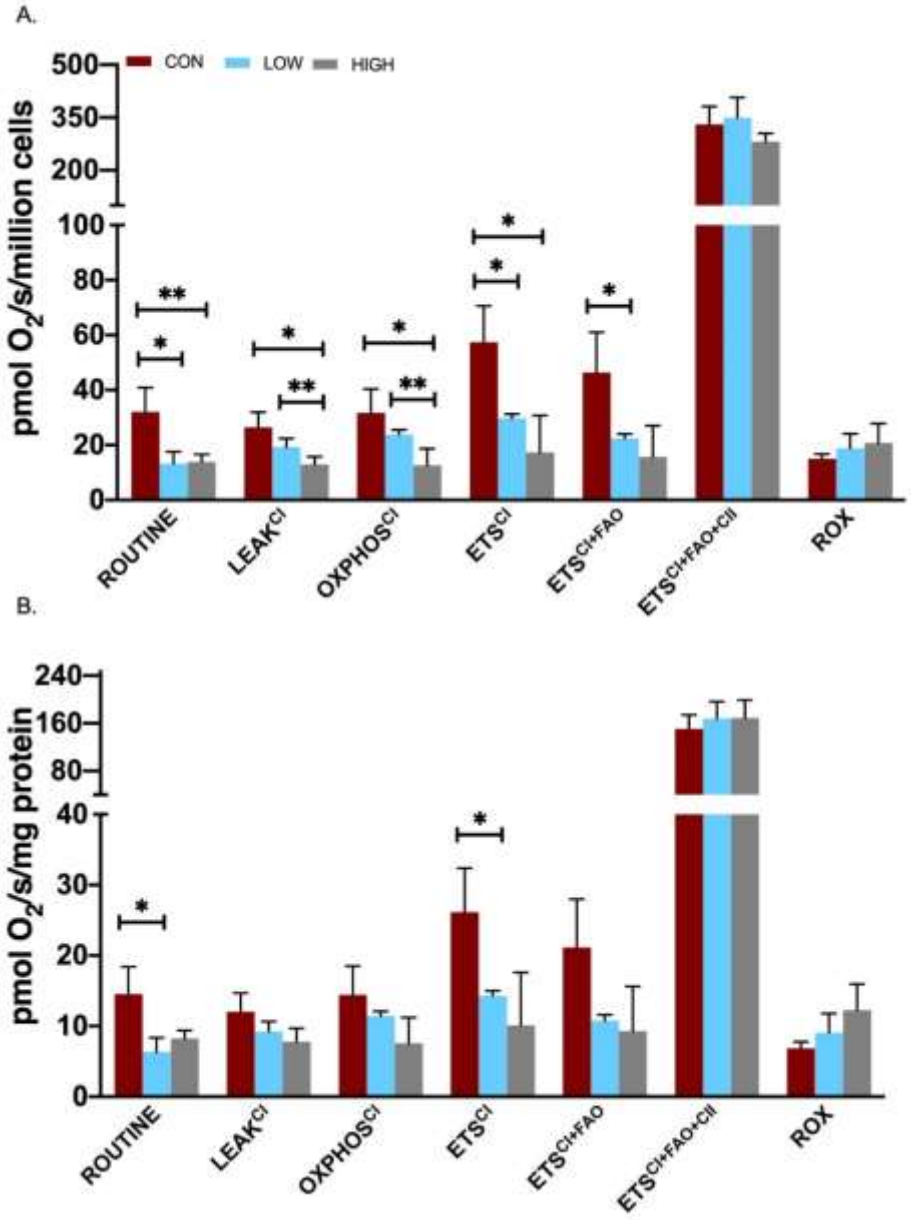

Figure 3.20: The effect of Aconitase inhibition on O_2 flux with pyruvate, malate and glutamate as substrates. *A) O_2 flux corrected to approximate number of cells per oxygraph chamber (pmol O_2/s/million cells) B) O_2 flux corrected to protein concentration (pmol O_2/s/mg protein). FAO (fatty acid oxidation), OXPHOS (Oxidative phosphorylation), ETS (Electron transport system), CI (Complex I), CII (Complex II), ROX (Residual oxygen consumption). All data reported as mean ± standard deviation; n = 3; *p < 0.05, **p < 0.01.*

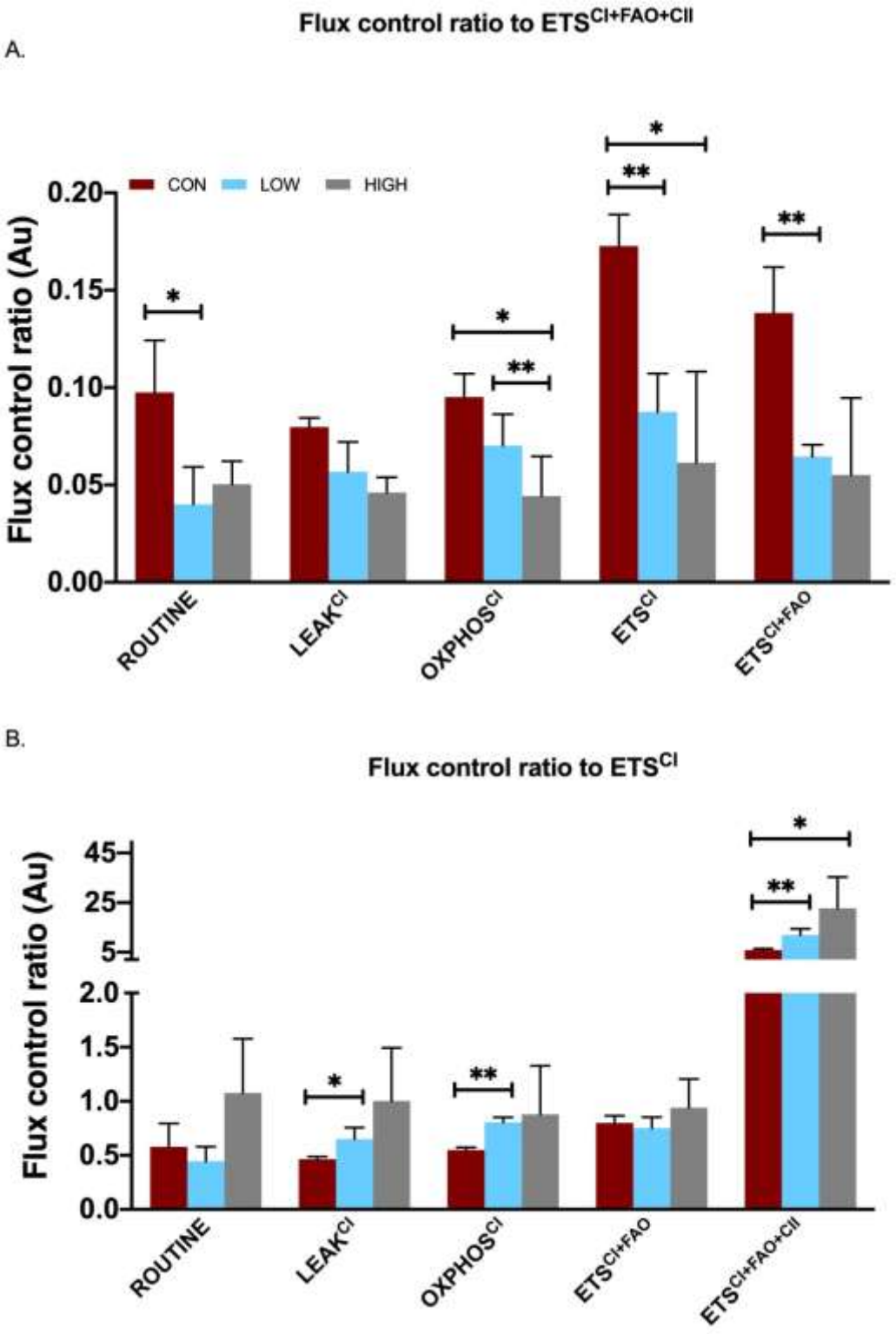

Figure 3.21: The effect of aconitase inhibition on flux control ratio (FCR) with pyruvate, malate and glutamate as substrates. *Diagram shows flux control ratios (FCR) normalized relative to A) maximum ETS capacity ($ETS^{CI+FAO+CII}$) as a result of convergent electron flow from Complex I (CI), fatty acid oxidation (FAO) and complex II (CI) B) ETS capacity as a result of CI (ETS^{CI}). All data reported as mean ± standard deviation; n = 3; *p < 0.05, **p < 0.01.*

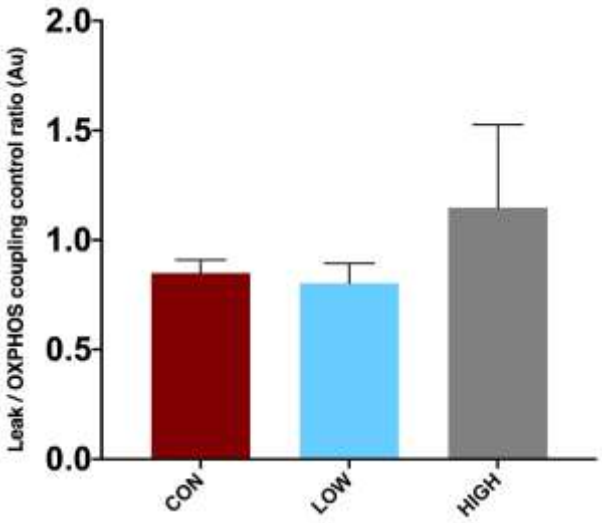

Figure 3.22: The effect of aconitase inhibition on Leak^{CI}/OXPHOS^{CI} coupling control ratio with pyruvate, malate and glutamate as substrates. *All data reported as mean ± standard deviation; n = 3.*

CHAPTER FOUR

Discussion

This thesis investigated alterations in the activity of specific enzymes and in mitochondrial respiration during the selective inhibition of rate limiting enzymes of either β-oxidation or the TCA cycle. Furthermore, we assessed the sensitivity of three different HRR protocols in detecting β-oxidation and TCA cycle dysfunction when the rate limiting enzymes were inhibited. The main finding of this study was related to two of the SUIT protocols 1) octanoylcarnitine and malate, and 2) pyruvate, malate and glutamate. These protocols were sensitive in showing decreases in mitochondrial respiration and dysfunction and may be appropriate for assessing changes in oxidative metabolism when there is a defect in β-oxidation and the TCA cycle. Secondly, enzyme assays may not be used as a standalone technique for assessing mitochondrial dysfunction and should be used to complement the results obtained from HRR, when using an appropriate substrate combination. Additionally, octanoylcarnitine and carnitine substrate combination is not a sensitive SUIT protocol to assess alterations in mitochondrial respiration when rate limiting enzymes are inhibited. Irrespective of the enzyme inhibited, HRR detected dysfunction in complex I (CI). Although, when aconitase was inhibited reduced CI-linked respiration was more pronounced when compared to MCAD inhibition. Lastly, primary inhibition of MCAD to inhibit β-oxidation may have caused secondary inhibition of TCA cycle via aconitase, shown in decreased TCA cycle, CI-linked respiration where MCAD was inhibited. In contrast, primary inhibition of aconitase seemed to be compensated for by increased MCAD activity and mitochondrial respiration related to FAO oxidation. These results are novel as they explore the effect of β-oxidation dysfunction on the TCA and vice versa in C2C12 myotubes using HRR.

4.1 Effect of MCAD inhibition on enzyme activity determined by spectrophotometric assay

In this study, treatment of C2C12 myotubes with either a low (2 mM) or high (8 mM) concentration of 2-mercaptoacetate to inhibit MCAD did not significantly alter MCAD activity assessed using the classic spectrophotometric assay that employed ferrocenium ion as electron acceptor (figure 3.1A). Other studies have shown that 2-mercaptoacetate does indeed reduce the activity of acyl-CoA dehydrogenases (ACAD) including MCAD (7–9, 16, 81, 95). Previously, Bauchè et al. (1983) found a 16%, 36% and 63% inhibition of palmitoyl-CoA, butryl-CoA and isovaleryl-CoA with 25 µM of 2-mercaptoacetate, respectively (9). More recently, 2 mM and 4 mM of 2-mercaptoacetate inhibited acyl-CoA dehydrogenase shown by reduction in CO_2 produced from [1-^{14}C] oleate in lung adenocarcinoma

cells (81). To our knowledge, the present study is the first to assess the effect of 2-mercaptoacetate on MCAD activity in skeletal muscle. One critical observation made with this study was the effect of high inhibitor concentration on cell viability. We observed that cells lifted off the tissue culture dish and were lost in the washing process when myotubes were treated for 12 hours. Thus, the results obtained here may be a reflection of partial inhibition in the remaining surviving myotubes. Nevertheless, it has been reported that measurement of MCAD activity via this method may be confounded by residual activity that produce false results even where MCAD is clearly deficient. For example, where genetic testing has revealed anomalies in enzymes of β-oxidation or where specific circulating metabolites of incomplete β-oxidation have been found (65, 133, 156). Residual activity is as a result of compounds such as free CoA that contain a free SH-group that can reduce ferricenium ion directly resulting in artificial high rates of reaction (80). To solve this problem, some researchers have added N-ethylmaleimide to their incubation medium; N-ethylmaleimide reacts with SH-group competing with free CoA, balancing out the unusual high rates of reaction when MCAD activity is assessed (65). However, addition of N-ethylmaleimide to mitochondrial matrix pre-exposed to 2-mercaptoacetate resulted in the reversion of inhibitions of palmitoyl-CoA, isovaryl-CoA and butryl-CoA dehydrogenations (7). Accordingly, its addition was omitted in our protocol, which may have caused increased variability in the results through an artificial amplification of MCAD activity. These results highlight the limitation of using the classic spectrophotometric enzyme assay in assessing MCAD activity.

Despite the unaltered MCAD activity with inhibition obtained in the spectrophotometric assay, we were able to confirm that 2-mercaptoacetate indeed influenced the C2C12 myotubes, as we found increased activity of citrate synthase with both low and high concentration treatment of MCAD inhibitor (figure 3.1E). In this study it was essential to measure the activity of citrate synthase as it is an important marker of mitochondrial function, biogenesis and a key enzyme of the TCA cycle (73, 75). However, increased citrate synthase activity was not accompanied by changes in aconitase activity, which may have indicated upregulation of the TCA cycle. We may therefore conclude that increased citrate synthase activity was not due to increased oxidative metabolism within the TCA cycle. In fact, we hypothesise that MCAD inhibition may result in partial loss of TCA cycle function from the simultaneous inhibition of aconitase. One effect of MCAD inhibition (or deficiency) is the accumulation of toxic β-oxidation metabolites (varied chain length of free fatty acids and their acyl-CoA and acyl-carnitines derivatives) that are significant contributors to oxidative stress. Aconitase is very sensitive to oxidative stress and can be inhibited when oxidative stress is induced in the mitochondria. In view of this, Schuk et al. (2010) showed that aconitase is inactivated by cis-4-decenoic acid, a representative toxic MCAD metabolite resulting from MCAD deficiency (138). Even though, we recorded no change in aconitase

activity where MCAD was inhibited using the enzymatic spectrophotometric assay, we show reduced TCA cycle CI-linked respiration where MCAD is inhibited (Section 3.2.3.1, figure 3.17), which may have been due to attenuation of aconitase activity. In support of this, where aconitase was directly inhibited we show similar pattern of decreased TCA cycle CI-linked respiration (Section 3.2.3.2, figure 3.20). Thus the reflected lack of significant change in aconitase activity where MCAD was inhibited may be as a result of the limitation of the sensitivity of the spectrophotometric assay. Overall, primary inhibition of MCAD to limit β-oxidation may have caused secondary inhibition of the TCA cycle via aconitase.

Citrate produced from increased citrate synthase activity would largely exit the mitochondria into the cytosol and cause a decrease in aconitase activity (75). To our knowledge no study has shown a concurrent increase in citrate synthase activity with β-oxidation inhibition. A possible consequence of decreased oxidative metabolism (inhibition of β-oxidation and possibly TCA cycle) may be increased activation of glycolysis, which may in part account for increased citrate synthase activity because of increased substrate supply from glycolysis. In fact, glycolytic and oxidative metabolic pathways are tightly coupled and function to maintain the cellular energetic balance (25). Many studies have shown that glycolysis is inhibited by oxidation of fatty acids and particularly by medium chain fatty acids in muscle and other tissues where it constitutes a glucose sparing process (99, 153). Therefore, when oxidation of medium chain fatty acid is inhibited (and the resultant inactivation of the TCA cycle), glycolysis may be activated as an alternative fuel source. Although, the glycolytic pathway is less energy efficient, it has been shown that glycolysis is enhanced to compensate for energy production where an oxidative pathway is weakened (179). Indeed, we showed that both β-oxidation and TCA cycle linked respiration are attenuated with 2-mercaptoacetate treatment to inhibit MCAD. Accordingly, compromised oxidative metabolism (catabolic reaction of β-oxidation and TCA cycle) may have resulted in increased involvement of the glycolytic pathway to restore homeostasis. Assessing the effect of MCAD inhibition on glycolytic enzymes or on the pathway itself was beyond the scope of this study and future research is required to test this hypothesis.

Regardless of the potential shift to support more glycolysis to restore energy balance, it seems this is not sufficient energy to support body/organ function, which is indicated by the extreme clinical manifestation particularly with MCAD deficiency (34, 41, 158, 159). Perhaps an important consideration to the consequence of dysfunction maybe tissue specific, as tissue or organs have different energy requirements. However, where β-oxidation is defective, the level of contribution from the glycolytic pathway to restore energy homeostasis is unknown. Interestingly, it has been shown that in certain

cancer cells where aerobic glycolysis is preferred over oxidative metabolism, increased glycolysis is not an attempt to increase energy production but rather to support biosynthesis of bio molecules and increased proliferation (70, 90). In contrast, enhanced glycolysis in some cancers is due to impairment of mitochondrial function including diminished expression of mitochondrial oxidative enzymes, respiratory chain and TCA cycle (28, 88, 113); this effect is equally comparable to that seen in normal cells where mitochondrial dysfunction and reduced respiration sways metabolism towards glycolysis (25). Overall, inhibition of MCAD seemed to have caused a significant reduction in oxidative metabolism where glycolysis may be up regulated to restore energetic homeostasis.

4.2 Effect of aconitase inhibition on enzyme activity

Our treatment of C2C12 myotubes with either low (2 mM) or high (9 mM) concentration of fluorocitrate to inhibit aconitase showed a trend towards a main effect of concentration. Post hoc analysis revealed a significant decrease in aconitase activity with low concentration of the inhibitor. The current study determined the total aconitase activity in our cell lysate which included both cytosolic and mitochondrial aconitase (56). Previous studies have shown that cytosolic aconitase remains unaffected by inhibition with fluorocitrate (85), which may suggest that the abundance of unaffected cytosolic aconitase in our cell lysate may have contributed to the results. Since mitochondrial, and not cytosolic, aconitase activity contributes to energy metabolism and where aconitase activity becomes rate limiting, there should be an expected deleterious effect on oxidative phosphorylation. Accordingly, we found decreased TCA cycle-linked respiration with both low and high concentration of aconitase inhibitor. Although we are the first to use fluorocitrate to inhibit aconitase in C2C12 myotubes, previous studies have shown decreased activity of aconitase on various sample types (39, 43, 78, 83, 84, 91, 93, 163, 175). In an earlier study, Gardener and colleagues treated cultured human epithelial-like lung cells (A549) with 10 mM sodium fluoroacetate or 0.1 mM sodium (±)-fluorocitrate for 24 hours. They found that the effect of fluorocitrate on aconitase inactivation mimicked the inhibitory effects of sub lethal or lethal hyperoxia induced in rat lungs. In their study, fluorocitrate caused cell swelling that was observed with hyperoxia and like the present study, treatment of fluorocitrate did not cause visible cell death (43). Another study showed that fluorocitrate acted on glial cells as a 'suicide' substrate for the enzyme aconitase, overall inhibiting the TCA cycle and temporarily depressing glial function (84). They treated the cortex of adult male Sprague-Dawley rats with 0.01, 0.02, 0.05 or 0.5 mM of fluorocitrate. Overall, our study supports previous reports that inhibition of aconitase with fluorocitrate limits the TCA cycle and oxidative phosphorylation (39, 43, 78, 83, 84, 91, 93, 163, 175).

Additionally, we have shown that where aconitase is inhibited, the activity of citrate synthase was increased; reflected in increased activity with both low and high concentration of aconitase inhibitor (figure 3.1F). This finding was similar to the study by Larsen et al. (2016); where inactivation of aconitase by oxidative stress, induced by high intensity exercise in human *m. Vastus Lateralis*, lead to increased citrate synthase activity (75). Similarly, Gardener et al (1994) showed that inhibition of aconitase with fluorocitrate or hyperoxia in lung cells lead to increased citrate levels (43). One explanation for increased activity of citrate synthase was offered by Larsen et al. (2016) where they showed that the concurrent increased citrate offers cytoprotective effects from oxidative stress (75). To test this, they added 10 mM of sodium citrate to cultured primary myotubes pre-exposed to 50-200 μM H_2O_2 and showed that addition of citrate fully abolished mitochondrial dysfunction (75). Thus, we could hypothesise that inhibition of aconitase contributed to the loss of homeostasis in the cell and increasing citrate may have contributed to restoring this balance.

Furthermore, since aconitase is a key regulator of the TCA cycle, its inhibition would lead to diminished oxidative metabolism and ATP production. Accordingly, Dhami et al. (2018), using mammalian CHO-K1 cells established that knockdown of aconitase was the most lethal amongst TCA cycle genes; its deletion impaired the entire cycle (37). As citrate cannot be metabolised further in the TCA cycle, it leaves the mitochondria and enters the cytosol where it is recruited for fatty acid synthesis (37, 75). Thus, deactivation of aconitase and resulting impairment of the TCA cycle was reported to increase fatty acid synthesis and glycolysis (37). In agreement, we found increased MCAD activity when high concentration of aconitase inhibitor was used (figure 3.1B), which may be an indication of increased substrate supply for β-oxidation. Collectively, the increase in citrate and accompanying increase in MCAD activity may reflect the conversion of glucose to lipids supported by increased glycolysis. This association of increased citrate synthase activity as well as enzymes of fatty acid oxidation is comparable to what is seen in some cancers, where decreased oxidative metabolism and increased citrate production directs substrates towards biosynthesis rather than toward oxidation to CO_2 and H_2O (132). Indeed the rate of glycolysis has been reported to increase in fluorocitrate poisoned frog and mammalian muscles, as well as in hyperoxia (43). Furthermore, others have found increased activity of lactate dehydrogenase and glucose 6-phosphate dehydrogenase, which are important enzymes involved in glycolysis, with increased activity of citrate synthase (43, 76, 132). It is worth noting that C2C12 myotubes in this study were grown in a high glucose medium, which would mean that the cells had enough substrates to support glucose metabolism via glycolysis. However, as this was beyond the scope of this study, we were unable to determine whether the inhibition of the TCA cycle leads to increased glycolysis. Overall

it seems that inhibition of aconitase resulted in oxidative imbalance, which may have up regulated β-oxidation and glycolysis as a mechanism to restore homeostasis

4.3 The combined effect of MCAD and aconitase inhibition

This study aimed to explore the relationship between a defect in β-oxidation and the TCA cycle. We have shown that where MCAD activity was inhibited, the increase in citrate synthase was not due to increased metabolism within the TCA cycle, shown by the lack of concurrent increase in aconitase activity. Indeed, where aconitase was inhibited and its activity was shown to decrease, citrate synthase as well as MCAD activity increased. This is the first study to show these enzyme interactions, although understanding/exploring the mechanism by which this occur was beyond the scope of this study. We suspect that in both cases of inhibition, increase in citrate synthase activity was an attempt by the cell to restore the redox balance (58, 75). This loss of homeostasis was more pronounced with inhibition of aconitase reflected by the higher degree of increase in citrate synthase activity (figure 3.1 F). We can therefore hypothesize that where MCAD is deficient, the TCA cycle may not compensate for decreased oxidative metabolism but is rather negatively impacted by loss of β-oxidation, leading to overall dysfunction in the mitochondrial energetic machinery. Furthermore, where aconitase is inhibited, the cell attempts to improve redox balance partially through increased activity in β-oxidation. The relationship between β-oxidation and the TCA cycle and the impact of inhibition of each pathway on mitochondrial function was further investigated by assessing mitochondrial respiration with HRR.

4.4 The effect of enzyme inhibition on mitochondrial respiration

Recently, it has been reported that energy deficiency and/or disruption is involved in the pathophysiology of some FAO defects including MCAD (86, 107). We show here that MCAD inhibition with 2-mercaptoacetate decreases mitochondrial respiration assessed by HRR using both β-oxidation linked substrates (octanoylcarnitine and malate) and TCA cycle linked substrates (pyruvate, malate and glutamate). This confirms that β-oxidation inhibition affects overall mitochondrial energetic machinery irrespective of the substrates oxidized. Additionally, we investigated the impact of aconitase inhibition on mitochondrial respiration when adding TCA cycle linked substrates. We showed that aconitase is a key regulator of the TCA cycle and resulted in a decrease in respiratory capacity as well as energetic efficiency of the mitochondria when using a pyruvate, malate and glutamate substrate combination. Furthermore, β-oxidation with octanoylcarnitine and malate combination was also decreased with aconitase inhibition but the pyruvate, malate and glutamate substrate combination was most sensitive

to the inhibition. The use of octanoylcarnitine and carnitine seemed to have inhibited multiple respiratory states at the concentrations used in this study, affecting both control and inhibited myotubes. We suspect that there was an imbalance in the rate of octanoylcarnitine oxidation and the removal of its intermediate by carnitine thereby causing a metabolic block. Accordingly, careful consideration of the optimum concentration of both octanoylcarnitine and carnitine should be taken into account when using this substrate combination in the future. Overall, SUIT protocols using octanoylcarnitine and malate or pyruvate, malate and glutamate showed to be effective in detecting a dysfunction resulting from inhibition of rate limiting enzymes beyond classic enzymatic assays.

4.4.1 The effect of MCAD inhibition on mitochondrial respiration

4.4.1.1 The effect of MCAD Inhibition on mitochondrial respiration using octanoylcarnitine and malate substrate combination

The use of octanoylcarnitine and malate has been demonstrated as an effective method for assessing β-oxidation by respirometry (12, 101, 115, 116). In agreement, we have shown that in healthy C2C12 myotubes, respiration measured as oxygen flux increased in response to the addition of substrates, ADP and uncoupler titrations (figure 3.2). Following MCAD inhibition, this substrate combination resulted in decreased respiratory capacity at routine, $OXPHOS^{FAO}$, ETS^{FAO} and $ETS^{FAO+CI+CII}$ with high and low concentration inhibitor treatment (section 3.2.1.1; figure 3.3). This indicated that metabolism using octanoylcarnitine and malate substrate combination was efficient in responding to altered substrate oxidation, membrane potential and ATP demands. However, altered respiratory capacity with inhibition was only observed when oxygen flux was corrected to the approximate number of cells placed in the respiration chamber; correction of data to protein concentration did not reveal any significant change with inhibition. As mentioned previously, a high concentration of 2-mercaptoacetate resulted in a loss of cells and would be responsible in part for decreased flux at this concentration, since there would be fewer respiring mitochondria. Nevertheless, the additional decrease in oxygen flux with low inhibition concentration validates the use of octanoylcarnitine and malate substrate combination for detecting an MCAD specific β-oxidation dysfunction.

With the use of octanoylcarnitine and malate where MCAD was inhibited, our most significant finding was the decreased respiratory capacity at; a) routine state with low inhibitor concentration; b) $OXPHOS^{FAO}$ with both low and high inhibitor concentration; c) ETS^{FAO} with low inhibition; c) maximum

capacity ($ETS^{FAO+CI+CII}$) with both low and high inhibitor concentration. At $OXPHOS^{FAO}$, the oxidation of substrates accounts for the partial stimulation of the ETS and decreased respiration would mean decreased substrate oxidation (49, 51). Increased stimulation, after the addition of a protonophore (CCCP), indicates that both substrate oxidation, and electron transfer across the respiratory chain (including the working of complexes), would influence the rate of respiration at ETS^{FAO} and $ETS^{FAO+CI+CII}$ (49, 51). Results obtained reflect decreased respiratory capacity due to; a) blockage of octanoylcarnitine oxidation, and b) decreased reducing equivalents for the ETS where MCAD was inhibited (36, 107, 124). Reasons for this include; the MCAD catalysed step is rate limiting, it's partial or total inhibition would cause the accumulation of medium chain fatty acyl esters, and a reduction of the CoA pool. It was important for us to first measure the FAO contribution to OXPHOS and ETS capacities. This will assess the direct effect of MCAD inhibition on β-oxidation and resulting oxidative phosphorylation. After this state, the inclusion of pyruvate and glutamate at ETS^{FAO+CI} and succinate at $ETS^{FAO+CI+CII}$ allows the assessment of the maximum capacity of the mitochondrial for both β-oxidation and TCA cycle. Thus, the decreased respiration observed at $ETS^{FAO+CI+CII}$ is an indication that not only was β-oxidation impaired, but also the maximum respiratory capacity of the mitochondria, including TCA cycle-linked metabolism.

Importantly, we found that aside from respiratory capacity, the degree of coupling of substrate oxidation to ATP generation was decreased with MCAD inhibition (section 3.2.1.1; figure 3.4). The degree of coupling is a measure of energy efficiency, which is an index of dysfunction. It is sensitive to changes in all bioenergetics modules (substrate oxidation, electron transfer and oxidative phosphorylation) (51, 114). The degree of coupling of the mitochondria was assessed by calculating the ratio of each respiratory state to the maximum capacity, $ETS^{FAO+CI+CII}$ (represents convergent electron flow from FAO+CI+CII) or ETS^{FAO}. This ratio is not limited by error prone approximations of cell number or protein concentration. We found decreased coupling at routine, $OXPHOS^{FAO}$, ETS^{FAO} and ETS^{FAO+CI} respiratory states (Section 3.2.1a; Figure 3.4A). The decreased coupling after the addition of CI-linked substrate, shows that CI activity is altered with MCAD inhibition. The result of decreased coupling control indicates that where MCAD is inhibited (or in deficiency), and in the presence of maximum energetic substrate supply, the mitochondria is not efficient in converting this to energy. To our knowledge, this study is the first to show that MCAD inhibition affects the efficiency of the mitochondria to produce energy in skeletal muscle cells. Increased uncoupling proteins has been shown to be associated with free fatty acids in the failing heart where uncoupled respiration was associated with mitochondrial uncoupling and decreased cardiac efficiency (101). Interestingly, in many FAO defects and especially in MCAD deficiency, energetic substrate supplementation is unable to reverse or prevent

the symptom observed in some patients (170). These reports have shown that the disruption of mitochondrial homeostasis is compounded by deficient energy production and oxidative stress in β-oxidation defects (47, 131, 136, 161). The decreased energy efficiency reported here is not reflected in enzymatic determinations, contributing to the validation of HRR as an important technique for assessing mitochondrial dysfunction when MCAD specific β-oxidation is impaired.

A well-known causal effect of MCAD deficiency is the accumulation of toxic metabolites that fuel the production of reactive oxygen species (ROS), leading to oxidative stress (136, 138, 139). Oxidative stress further impairs mitochondrial function and contributes to the pathology of MCAD dysfunction (36, 104). Our study shows that MCAD inhibition increased citrate synthase activity (section 3.1.1, figure 3.1 E), which may be a consequence to increased citrate to combat oxidative stress and restore redox balance (75, 143). Mitochondrial alterations and disruption of redox homeostasis has been commonly observed in mouse models of fatty acid oxidation disorders (107, 140). In addition to disrupting mitochondrial function, increased oxidative stress contributes to the inactivation of sensitive aconitase and hence a limitation of the TCA cycle (75). Limitation of the TCA cycle would further impair the oxidation of octanoylcarnitine assessed when octanoylcarnitine and malate are used as substrates, since the metabolism of malate in the TCA cycle would be affected. Consequently, the supply of NADH to the ETS would be further decreased. Overall, oxidative phosphorylation and respiratory capacity especially complex I-linked contribution would be further attenuated contributing to mitochondrial dysfunction with MCAD inhibition.

4.4.1.2 The effect of MCAD inhibition on mitochondrial respiration using pyruvate, malate and glutamate substrate combination.

To support the hypothesis that MCAD inhibition resulted in decreased metabolism in the TCA cycle (especially CI-linked), we assessed respirometry separately with pyruvate, malate and glutamate substrate combination where MCAD was inhibited. The use of this substrate combination partially reconstitutes metabolism within the TCA cycle in assessment of HRR and their metabolism produces NADH that supplies electrons directly to CI and ultimately to CIV of the ETS with coupling sites at the ubiquinone pool and CIII, whilst only partially stimulating CII (49, 51). Thus, OXPHOS and ETS respiratory states were first assessed with the addition of only CI-linked substrates (at $OXPHOS^{CI}$ and ETS^{CI}), which was followed by addition of FAO substrates (ETS^{CI+FAO}) and then CII-linked substrate to give maximum capacity ($ETS^{CI+FAO+CII}$) (section 3.2.3, figure 3.16). Similar to octanoylcarnitine and malate substrate combination, pyruvate, malate and glutamate substrate combination were responsive to the SUIT

protocol in healthy C2C12 myotubes, additionally, reflecting altered respiration in response to inhibition. When respiration was corrected to the approximate number of cells we found decreased respiration with high MCAD inhibitor concentration at leak^{CI}, OXPHOS^{CI}, ETS^{CI}, ETS^{CI+FAO} and ETS$^{CI+FAO+CII}$ (figure 3.18A). Furthermore, for respiration corrected to protein concentration (figure 3.18B), we showed a decrease in respiration with low inhibitor concentration at ETS^{CI} and ETS^{CI+FAO}. Importantly, the decrease in respiratory capacity with MCAD inhibition were more pronounced here (with the use of pyruvate, malate and glutamate) than when substrates specific to FAO (octanoylcarnitine and malate) were used. Accordingly, pyruvate, malate and glutamate substrate combination proved to be the most sensitive for detecting MCAD inhibition. Our results confirm that MCAD inhibition indeed alters metabolism within the TCA cycle, thus showing that a primary β-oxidation inhibition caused a secondary TCA cycle inhibition.

Similar to our findings of decreased respiratory capacity with pyruvate, malate and glutamate, others have also found decreased ADP stimulated respiration with treatment with 2-mercaptoacetate (5) or in MCAD deficiency (2, 8). Our study showed that FCR was largely unaffected by MCAD inhibition when we used pyruvate, malate and glutamate substrate combination (figure 3.19). It appears there may be a mechanism that restores the uncoupling of substrate oxidation to oxidative phosphorylation that was observed when β-oxidation substrates (octanoylcarnitine and malate) were used. One possible mechanism for the observed intact coupling efficiency with CI-linked TCA cycle substrates may be the involvement of CI stability. It has been reported that CI reversibly alternates between an active and deactivated conformation that most likely depends on the cell respiratory status (13, 54, 55). For example, Grivennikova et al. (2003), found that in mitochondria where CI was inactivated by inhibition, exposure to malate/glutamate, NAD(+) and cytochrome C induced reactivation of the enzyme (54). On the other hand, loss of MCAD function has been shown to affects CI stability as well as the stability of OXPHOS super complexes (CI, CII and CIV). This may be an explanation for the uncoupling of respiration seen with MCAD inhibition with the use of octanoylcarnitine and malate. Thus, using pyruvate, malate and glutamate may have reactivated CI with the stability in turn affecting the other respiratory complexes. The arrangement of the mitochondrial respiratory chain complexes into super complexes is well established in different organisms (131), others have also found a physical association between CI and CIII (23, 74, 127). Hence although respiratory capacity was decreased, the coupling of respiration persisted. Therefore, the decreased respiratory capacity observed with the use of pyruvate, malate and glutamate substrate combination is limited to their impaired oxidation within the TCA cycle where MCAD is inhibited. This agrees with the earlier statement that a primary defect in MCAD (as well as resulting dysfunction in β-oxidation) results in secondary TCA cycle dysfunction.

The mechanism of decreased respiratory capacity from metabolism within the TCA cycle is not fully understood. As previously stated, we suspect that MCAD inhibition impairs aconitase activity, which was partly confirmed by reduced CI-linked respiration. Inhibition of aconitase would further limit the TCA cycle since aconitase functions as a regulator of the TCA cycle (5, 75, 85). The role of oxidative stress is very popular in the pathology of MCAD deficiency (107), indeed many researchers have investigated the role of accumulating toxic metabolites in MCAD deficiency on redox homeostasis (36, 104, 121, 130, 136, 138, 139). These studies have shown that toxic metabolites in MCAD deficiency cause oxidative stress leading to oxidative damage of proteins, inhibition of oxidative phosphorylation as well as diminished capacity of the anti-oxidant defence mechanism leading to overall mitochondrial bioenergetics dysfunction (3, 130, 136, 138, 161). This lends support to our hypothesis that the increase in citrate synthase activity with MCAD inhibition was not an indication of increased oxidative capacity, but rather a sign of oxidative stress and the cells machinery to restore homeostasis. In our study, TCA cycle-linked respiration associated with CI was decreased where MCAD was inhibited. Although no change in aconitase activity was reflected with spectrophotometric enzymatic analysis, other studies have shown that medium chain free fatty acids (from MCAD defect) decrease aconitase activity (137, 138). To our knowledge, the focus of secondary dysfunction with primary MCAD deficiency has been on oxidative phosphorylation even though different studies have shown that respiration in the presence of pyruvate, malate or glutamate is decreased as a result of the detrimental effects of MCAD dysfunction (3, 86, 121, 130, 137, 141). However, β-oxidation, the TCA cycle and OXPHOS are tightly linked, with OXPHOS being the ultimate outcome of substrate oxidation within either β-oxidation or the TCA cycle. We have proposed that a primary defect of either pathway would contribute to secondary dysfunction of the other. This is reflected in decreased TCA cycle-linked respiration where we have shown that MCAD was the primary defect.

4.4.1.3 The effect of MCAD inhibition on mitochondrial respiration using octanoylcarnitine and carnitine substrate combination

The use of octanoylcarnitine and carnitine substrate combination offers a similar support to FAO-linked respiration that octanoylcarnitine and malate provides. Inclusion of carnitine functions to lower the matrix level of catabolic intermediates. It regulates matrix acyl-CoA/CoA by exchange of cytosolic carnitine with matrix acylcarnitine catalysed by carnitine transferase (151). Our study shows that the addition of octanoylcarnitine and carnitine to control myotubes had minimal effect on oxygen consumption measured at LEAK, OXPHOS and ETS^{FAO}; the rates of respiration was only significantly increased after the addition of CI-linked (pyruvate, malate, glutamate) and CII-linked (succinate) substrates to uncoupled respiration in the presence of maximum amounts of protonophore (CCCP)

(figure 3.9). Similar patterns in respiratory capacity was observed when respiration was assessed in MCAD inhibited myotubes. Inhibition did not significantly decrease oxygen flux when corrected for either cell number or protein concentration (figure 3.10). The pattern of respiration we observed here questions the use of octanoylcarnitine and carnitine substrate combination.

Many studies using acylcarnitine and carnitine in assessing β-oxidation involve palmitoylcarnitine, a long chain acyl-carnitine. These studies have assessed respiration in isolated mitochondria from muscle, liver or brain tissue whereas we have used permeabilized skeletal muscle. Movement of substrates in and out of the inner mitochondrial matrix is different in intact cells versus isolated mitochondria and may have influenced the oxidation of octanoylcarnitine in our study perhaps accounting for disparity with other studies (1, 115, 141). For example, Seifert et al. (2010) using isolated mitochondria from male mice showed that increasing the concentration of palmitoylcarnitine from 4.5 µM to 18 µM did not increase respiration, and addition of 2 mM carnitine to 18 µM palmitoylcarnitine resulted in increased respiration (141). This indicates that addition of carnitine facilitates the oxidation of palmitoylcarnitine. However, in comparison, our study utilised a higher concentration of acylcarnitine (0.2 mM of octanoylcarnitine with 2 mM carnitine). Perhaps, the rate of oxidation of octanoylcarnitine and the resulting production of intermediates exceeds the rate of removal facilitated by carnitine leading to feed-back inhibition. Indeed, it has been shown that the ETS flux in skeletal muscle mitochondria can be inhibited with concentrations of palmitoylcarnitine above 5 µM (1). Although we have used octanoylcarnitine in our study this explanation may equally follow true. Regardless, the absence of further attenuation in respiration where MCAD is inhibited is questionable. We suspect that the use of octanoylcarnitine and carnitine at the concentrations used in this study in addition to functioning to inhibit flux, may produce a threshold effect, where up-regulating or down-regulating β-oxidation may not significantly cause further changes in oxygen flux.

Furthermore, this study explored the relationship between β-oxidation and the TCA cycle, and so we included pyruvate, malate and glutamate to octanoylcarnitine and carnitine after FAO-linked ETS (ETS^{FAO+CI}; figure 3.9); and in the reverse scenario, octanoylcarnitine and carnitine was added to pyruvate, malate and glutamate after CI-linked ETS (ETS^{CI+FAO}; figure 3.16). This expressed convergent electron flow from CI and β-oxidation in either instance. It is established that CI-linked substrates highly reduce the ETS compared to FAO-linked substrates (2, 141) and the addition of CI-linked substrates was expected to stimulate the ETS beyond FAO leading to increased respiration at ETS^{FAO+CI}. However, before now it was not known whether the inclusion of octanoylcarnitine and carnitine after CI-linked

substrates would increase respiration. As expected, oxygen consumption increased when CI-linked substrates were added to octanoylcarnitine and carnitine although, there was no significant change with MCAD inhibition (figure 3.10). This is in agreement with studies by Amaral et al. (2016) and Sauer et al. (2008), who reported that carnitine derivatives of toxic β-oxidation metabolites including octanoylcarnitine were unable to alter the activities of isolated respiratory chain complexes, membrane potential, oxidation within the TCA cycle and NAD(P)H/NAD(P)$^+$ ratio (2, 130). Interestingly, in the reverse scenario, we found that oxygen consumption decreased after the addition of octanoylcarnitine and carnitine to CI-linked substrates in both control and MCAD inhibited myotubes (figure 3.18). It seemed that octanoylcarnitine and carnitine acted as an inhibitor of oxidative phosphorylation in line with our earlier observations. Thus, the significant decrease observed with high inhibition compared to low at ETS^{CI+FAO} is most likely due to initial decrease in respiration at ETS^{CI}. Over all it seems that aspects of respiration involving the use of this substrate combination are unresolved and need to be explored further, especially with respect to the correct concentration of either octanoylcarnitine or carnitine for a specific sample type.

4.4.2 The effect of aconitase inhibition on mitochondrial respiration

4.4.2.1 The effect of aconitase inhibition on mitochondrial respiration using pyruvate, malate and glutamate substrate combination

The use of pyruvate, malate and glutamate substrate combination was the most sensitive combination for assessing the TCA cycle functioning where aconitase was inhibited. Previously, others have shown reduced mitochondrial respiration with both pyruvate and glutamate linked respiration. In isolated skeletal muscle mitochondria from fluorocitrate poisoned hearts, pyruvate linked mitochondrial respiration was ~80% inhibited (93). Gardener et al. (1994) also showed that basal, uncoupled and total respiration with malate was diminished in human epithelial A549 cells treated with either 10 mM sodium fluoroacetate or 0.1 mM sodium citrate when respiration was assessed using a Gilson oxygraph with a Clark electrode (43). In agreement with previous papers, we have shown that inhibition of aconitase significantly decreased all states of respiration (section 3.2.2.2; figure 3.21) with both correction to cell number and to protein concentration. Respiratory capacity at routine, $Leak^{CI}$, $OXPHOS^{CI}$, ETS^{CI}, ETS^{CI+FAO} and $ETS^{CI+FAO+CII}$ was significantly decreased with both high and low inhibition treatment. Firstly, the evidence of decreased respiratory capacity in response to aconitase inhibition adds validity to the use of HRR and pyruvate, malate and glutamate substrate combination for assessing dysfunction since we had only found trends for decreased aconitase activity with spectrophotometric

enzyme assays. Furthermore, these results rationalise our earlier discussions where CI-linked respiratory was implicated with aconitase inhibition indirectly from MCAD inhibition and we show with pyruvate, malate and glutamate substrate combination that direct inhibition of aconitase is reflected in decreased CI-linked respiration.

Even though we have inhibited aconitase in an attempt to limit the TCA cycle, it is known that where there is a defect in the cycle, its substrates may be generated from other anaplerotic reactions that allow for its partial continuation (51). Such supply can be generated from the oxidative decarboxylation of pyruvate catalysed by pyruvate dehydrogenase as well as oxidation of glutamate by glutamate dehydrogenase into 2-oxoglutarate. With both pyruvate and glutamate, extra support to oxidative phosphorylation from TCA cycle is supplied from the additional NADH produced. Notably, it has been shown that the reaction of pyruvate and glutamate are inhibited by fluorocitrate, and we have been able to limit the TCA cycle further by using this inhibitor. Furthermore, one of the mechanisms of reduced respiratory capacity with inhibition using fluorocitrate involves the transport of substrates into the mitochondrion. Decreased concentrations of aspartate and glutamate have been found in heart and skeletal muscle of fluorocitrate poisoned heart (93). In our study, the decrease in respiration may be explained by a limitation of the glutamate-aspartate carrier with the inclusion of glutamate. The glutamate-aspartate carrier catalyses the electrogenic antiport of glutamate and hydrogen in the ionic state for aspartate. It is also an important part of the malate-aspartate shuttle in many mitochondria (51), implicating not only the transport of glutamate but also malate with fluorocitrate poisoning. In addition, the 2-oxoglutarate carrier exchanges malate for 2-oxoglutarate in the ionic state (51).This transport may be further limited where the concentration of glutamate is decreased; glutamate oxidation supplies 2-oxoglutarate. In addition to limiting anaplerotic reactions, the direct inhibition of aconitase by fluorocitrate contributes to limiting downstream flux of the TCA cycle, exacerbating the impact of inhibition on the TCA cycle metabolism. By and large, oxidation of TCA cycle substrates are reduced leading to substantially decreased NADH production and ETS capacity.

An important mechanism for decreased respiratory capacity from TCA cycle metabolism is the effect of inhibition directly on aconitase. Its deactivation releases Fe^{2+} associated with subsequent production of free hydroxyl radicals via the Fenton reaction, which further oxidises mitochondrial proteins, DNA and lipids (27, 33, 66). Indeed, Dhami et al (2018) reported a marked increase in H_2O_2 production after aconitase knockdown in CHO mammalian cells (37). Likewise, Fe-S- cluster containing subunits of mitochondrial proteins are remarkably sensitive to free radical (includes complex I-III) (125), this may

further worsen the effect of inhibition of aconitase leading to not only impaired respiratory capacity but also contributing to uncoupling of respiration. In light of this, we showed that coupling efficiency was decreased with aconitase inhibition (figure 3.22). We first calculated the FCR to the maximum respiration, $ETS^{CI+FAO+CII}$; we showed that this ratio was significantly decreased at routine, $OXPHOS^{CI}$, ETS^{CI} and ETS^{CI+FAO} with both high and low inhibition (figure 3.22A). Remarkably, the reverse was the case when FCR was calculated as the ratio of each state to ETS^{CI} (figure 3.22B), this may indicate the CI exerts the most influence on the detrimental effects of decreased efficiency of the mitochondrial with aconitase inhibition. Collectively, aconitase inhibition lead to decreased respiratory capacity and decreased energetic efficiency of the mitochondria, causing overall mitochondrial dysfunction.

It has been reported that there is no known disease that is caused by a single deficiency of aconitase (53), although Friedrich's ataxia is characterised by combined aconitase and succinate dehydrogenase deficiency (125). However, several acquired conditions are characterised by alterations in electron transport respiratory chain proteins, compromised mitochondrial calcium handling and impaired TCA cycle enzymes (53). After pinpointing aconitase as a critical target where MCAD is inhibited (or in MCAD deficiency), we have shown that in direct inhibition of aconitase, respiratory capacity as well as energetic efficiency of the mitochondria is compromised. Therefore, reflecting that aconitase is key to TCA regulation and in the absence of primary aconitase deficiency, acquired defects that severely alter aconitase activity may be very detrimental to energy metabolism. Thus, aconitase may be a critical target for therapeutic interventions in diseases that affect oxidative metabolism.

4.4.2.2 The effect of aconitase inhibition on mitochondrial respiration using octanoylcarnitine and malate

Assessment of respiration with octanoylcarnitine and malate substrate combination involves the influence of the TCA cycle in addition to β-oxidation. Conditions affecting/limiting the TCA cycle would reduce oxygen flux, giving a false reading of the rate of β-oxidation when malate is used as a co-substrate (111). As previously mentioned, aconitase is a key regulator of the TCA cycle, its inactivation has been shown to inhibit mitochondrial respiration by inhibiting the TCA cycle (75). In this study, assessment of respiration after inhibition of aconitase lead to decreased oxygen flux at routine, $leak^{FAO}$, and $OXPHOS^{FAO}$ respiratory states when respiration was corrected to cell number (figure 3.7). The observations here is a fraction of what was observed with aconitase inhibition using pyruvate, malate and glutamate substrate combination. Although we recorded decreased respiratory capacities, this

decrease may have been related to decreased metabolism of malate in the TCA cycle, with β-oxidation minimising the effect of aconitase inhibition. Previously (section 4.1), we have shown increased MCAD activity in spectrophotometric analysis, which may have been an indication of increased β-oxidation in response to limitation of oxidative metabolism within the TCA cycle. As a result, there may be decreased burden of oxidative damage with this substrate combination since there is fewer reducing equivalents produced as a result of oxidation of octanoylcarnitine. In line with this, we only recorded significant changes in the FCR for each state to the maximum capacity ($ETS^{FAO+CI+CII}$) at routine and $OXPHOS^{FAO}$ states with both high and low inhibition (Figure 3.8). This may suggest that decreased respiratory capacity is mainly as a result of decreased substrate oxidation within the TCA cycle. Thus, our observation with this substrate combination may be mainly attributed to decreased flux through the TCA cycle.

4.4.2.3 The effect of aconitase inhibition on mitochondrial respiration using octanoylcarnitine and carnitine

Similar to the use of this substrate combination where MCAD was inhibited, there was no significant change in respiratory capacity with either high or low inhibition of aconitase when respiration was corrected for both cell number and protein concentration. As with MCAD inhibition, we added TCA cycle CI-linked substrates after FAO-linked ETS (ETS^{FAO+CI}; figure 3.9) and no significant change was observed. However, we observed a different pattern in contrast to where MCAD was inhibited. It appears that respiratory capacity was tending towards an increase at $Leak^{FAO}$, $OXPHOS^{FAO}$, ETS^{FAO} and $ETS^{FAO+CI+CII}$; the opposite pattern was noticed at ETS^{FAO+CI} with both high and low inhibitor concentrations (figure 3.14). Indeed, we know that the effect of aconitase inhibition is largely reflected in diminished CI-linked respiration, which explains the reversed graph indicating 'decrease' in respiration observed only after the addition of CI-linked substrates. This may be in agreement to the increased MCAD activity we found with aconitase inhibition in spectrophotometric analysis. In section 1.4.1.3 it was mentioned that the use of this substrate combination requires further optimization, perhaps this explains why the results here were not significant. It seems that β-oxidation may be enhanced to compensate for the loss of oxidative metabolism via the TCA cycle. Furthermore, we observed a significant increase in the flux control ratio of Leak to ETS^{FAO} (figure 3.15B) with low inhibition, contributing to the argument that beta-oxidative metabolism appears to be compensating for a limitation in the TCA cycle.

Additionally, we added octanoylcarnitine and carnitine after ETS respiratory state with CI-linked pyruvate, malate and glutamate to assess ETS^{CI+FAO} (figure 3.16). This assesses the convergent electron flow from both TCA cycle and FAO-linked oxidation. Respiratory capacity at this state was significantly decreased with low inhibitor concentration when respiration was corrected to number of cells (figure 3.21 A). This observation contrasts with the preceding paragraph where a role for increased β-oxidation when aconitase is inhibited was identified. However, because stimulation of the ETS from β-oxidation-linked substrates are a smaller fraction compared to that from TCA cycle-linked substrates, this decrease is most likely a carryover of that initially observed after the addition of pyruvate, malate and glutamate. Remarkably, addition of octanoylcarnitine and carnitine appears to have contributed to a loss in significant decreased observed initially at ETS^{CI} (figure 3.21B and 3.22A), which may support the hypothesis of increased β-oxidation where aconitase is inhibited. To our knowledge no other studies have measured the effect of aconitase inhibition (or deficiency) on β-oxidation. Here we show that where oxidation linked to the TCA cycle is compromised, β-oxidation is a likely alternative pathway to sustain fuel maintenance.

Despite these intriguing observations, we are unable to draw conclusions and it seems that the validity of octanoylcarnitine and carnitine substrate combination remains questionable. Further investigation is required to clarify reasons for inhibited respiration when this substrate combination is used. In our attempts to characterize the use of this substrate combination, we initially tested the effect of increasing octanoylcarnitine or carnitine and found that respiration remained the same. However, a follow up study is required to investigate the effect of decreasing the concentration of either octanoylcarnitine or carnitine on respiration.

4.5 Conclusion and future considerations

We investigated the effect of either MCAD or aconitase inhibition on the sensitivity of commonly used substrate combinations in HRR as well as the effect of inhibition on MCAD, aconitase and citrate synthase enzyme activities. We hypothesized that MCAD inhibition would lead to both a decrease in MCAD and aconitase activity while increasing citrate synthase activity. On the other hand inhibition of aconitase was predicted to decrease aconitase activity and increase citrate synthase activity. Furthermore, we predicted that this inhibition would be reflected by decreased mitochondrial respiration assessed with pyruvate, malate and glutamate as well as octanoylcarnitine and carnitine substrate combinations but not octanoylcarnitine and carnitine. To the knowledge of the author of this thesis, this is the first study to evaluate the sensitivity of commonly used HRR substrates in a β-oxidation or TCA cycle defective state. The major findings of this study are:

1. MCAD inhibition resulted in mitochondrial dysfunction reflected by decreased mitochondrial respiration and coupling control of respiration when pyruvate, malate and glutamate as well as octanoylcarnitine and malate substrate combinations were used in HRR assessment. Furthermore, with enzymatic spectrophotometric assay, MCAD inhibition increased citrate synthase activity. Contrary to the hypothesis, MCAD and aconitase activity remained unchanged with MCAD inhibition.
2. Aconitase inhibition resulted in mitochondrial dysfunction reflected by decreased mitochondrial respiration and coupling control of respiration when pyruvate, malate and glutamate as well as octanoylcarnitine and malate substrate combinations were used in HRR assessment. Furthermore, with enzymatic spectrophotometric assay, aconitase inhibition decreased aconitase activity, increased citrate synthase and unexpectedly increased MCAD activity.
3. Octanoylcarnitine and carnitine substrate combination was not sensitive to inhibition of either MCAD or aconitase

Overall, inhibition of either MCAD or aconitase was more apparent with pyruvate, malate and glutamate substrate combination, indicating a role for decreased CI-linked respiration and thus CI-activity where either of these enzymes are defective. Accordingly, pyruvate, malate and glutamate substrate combination may be the best choice for assessing a defect in either β-oxidation or the TCA cycle. HRR was sensitive to dysfunction that was undetected where spectrophotometric enzyme activity was measured, indicative of the effectiveness of HRR for assessing MCAD or TCA cycle dysfunction.

4.5.2 Future Considerations

The results of this study has demonstrated the importance of using HRR where there is a defect in either β-oxidation or the TCA cycle. However, HRR relies on fresh tissue from muscle biopsies, which limits its clinical applicability compared to other techniques that utilise less invasive samples such as blood or urine. It would be important in the future to explore the possibility of assessing mitochondrial respiration in blood samples of patients or animals where β-oxidation is defective. Completing HRR on blood samples would be less invasive and more cost effective. Furthermore, the use of octanoylcarnitine and carnitine substrate combination may prove useful in assessing defects in β-oxidation (or the effect of TCA cycle defect on β-oxidation) if the correct concentrations are used. To this effect, future studies may consider exploring the effect of using concentrations of octanoylcarnitine lower than 0.2 mM.

It is worth mentioning that the correction factor used in interpreting the results from HRR would be affected by the sample type and also by the treatment regime. This study discussed data normalised to approximate number of cells, protein concentration as well as flux control ratio. A limitation of using approximate number of cells here (since it was impossible to count fused myotubes) was that cell loss especially with inhibiting MCAD could not be accounted for. Thus correcting to protein concentration was more appropriate. However even better is the flux control ratio that acts as an internal control factor regardless of cell number or treatment used.

Lastly, this study has indicated that a primary defect in either β-oxidation or the TCA cycle could lead to a secondary defect in the other; a finding that has important therapeutic implications. However, future studies may benefit from exploring the exact mechanism through which this occurs, particularly assessing and investigating the role of oxidative stress and/or glycolysis under the conditions induced in this study

References

1. Abdul-Ghani MA, Muller FL, Liu Y, Chavez AO, Balas B, Zuo P, Chang Z, Tripathy D, Jani R, Molina-Carrion M, Monroy A, Folli F, Van Remmen H, Defronzo RA. Deleterious action of FA metabolites on ATP synthesis: possible link between lipotoxicity, mitochondrial dysfunction, and insulin resistance 266. *A J Physiol Endocrinol Metab* 295: E678–E685, 2008.

2. Amaral AU, Cecatto C, Da Silva JC, Wajner A, Godoy KDS, Ribeiro RT, Wajner M. Cis-4-Decenoic and decanoic acids impair mitochondrial energy, redox and Ca2 + homeostasis and induce mitochondrial permeability transition pore opening in rat brain and liver: Possible implications for the pathogenesis of MCAD deficiency. *Biochim Biophys Acta - Bioenerg* 1857: 1363–1372, 2016.

3. Amaral AU, Cecatto C, Da Silva JC, Wajner A, Godoy KDS, Ribeiro RT, Wajner M. Cis-4-Decenoic and decanoic acids impair mitochondrial energy, redox and Ca2 + homeostasis and induce mitochondrial permeability transition pore opening in rat brain and liver: Possible implications for the pathogenesis of MCAD deficiency. *Biochim Biophys Acta - Bioenerg* 1857: 1363–1372, 2016.

4. Andresen BS, Bross P, Udvari S, Kirk J, Gray G, Kmoch S, Chamoles N, Knudsen I, Winter V, Wilcken B, Yokota I, Hart K, Packman S, Harpey JP, Saudubray JM, Hale DE, Bolund L, Kølvraa S, Gregersen N. The molecular basis of medium-chain acyl-CoA dehydrogenase (MCAD) deficiency in compound heterozygous patients: Is there correlation between genotype and phenotype? *Hum Mol Genet* 6: 695–707, 1997.

5. Armstrong JS, Whiteman M, Yang H, Jones DP. The redox regulation of intermediary metabolism by a superoxide-aconitase rheostat. *BioEssays* 26: 894–900, 2004.

6. Bartlett K, Eaton S. Mitochondrial β-oxidation. *Eur J Biochem* 271: 462–469, 2004.

7. Bauche F, Sabourault D, Giudicelli Y, Nordmann J, Nordmann R. Effects of 2-mercaptoacetate in isolated liver mitochondria in vitro. *Biochem J* 206: 53–59, 1982.

8. Bauché F, Sabourault D, Giudicelli Y, Nordmann J, Nordmann R. 2-Mercaptoacetate administration depresses the beta-oxidation pathway through an inhibition of long-chain acyl-CoA dehydrogenase activity. *Biochem J* 196: 803–809, 1981.

9. Bauché F, Sabourault D, Giudicelli Y, Nordmann J, Nordmann R. Inhibition in vitro of acyl-CoA dehydrogenases by 2-mercaptoacetate in rat liver mitochondria. *Biochem J* 215: 457–64, 1983.

10. Bennett MJ. Assays of fatty acid beta-oxidation activity. *Methods Cell Biol* 80: 179–197, 2007.

11. Bier DM, Leake RD, Haymond MW, Arnold KJ, Gruenke LD, Sperling MA, Kipnis DM. Measurement of "true" glucose production rates in infancy and childhood with 6,6-dideuteroglucose. *Diabetes* 26: 1016–1023, 1977.

12. Bonnard C, Durand D, Peyrol S, Chanseaume E, Chauvin M a, Morio B, Vidal H, Rieusset J. Mitochondrial dysfunction results from oxidative stress in the skeletal muscle of diet-induced insulin resistant mice. *J Clin Invest* 118: 789–800, 2008.

13. Böttcher B, Scheide D, Hesterberg M, Nagel-Steger L, Friedrich T. A novel, enzymatically active conformation of the Escherichia coli NADH:ubiquinone oxidoreductase (complex I). *J Biol Chem* 277: 17970–17977, 2002.

14. Bourgeron T, Chretien D, Poggi-Bach J, Doonan S, Rabier D, Letouze P, Munnich IA, Rotig A, Landneu P, Rustin P. Mutation of the Fumarase Gene in Two Siblings with Progressive Encephalopathy and Fumarase Deficiency. *J Clin Invest* 93: 2514–2518, 1994.

15. Boushel R, Gnaiger E, Schjerling P, Skovbro M, Kraunsøe R, Dela F. Patients with type 2 diabetes have normal mitochondrial function in skeletal muscle. *Diabetologia* 50: 790–796, 2007.

16. Boutellier S, Lutz TA, Volkert M, Scharrer E. 2-Mercaptoacetate, an inhibitor of fatty acid oxidation, decreases the membrane potential in rat liver in vivo. *Am J Physiol Integr Comp Physiol* 277: R301–R305, 1999.

17. Bradford MM. Determinacion De Proteinas: Metodo De Bradford. *Anal Biochem* 72: 248–254, 1976.

18. Brand MD, Nicholls DG. Assessing mitochondrial dysfunction in cells. *Biochem J* 435: 297–312, 2011.

19. Brass EP, Hoppel CL. Effect of carnitine on mitochondrial oxidation of palmitoylearnitine. *Biochem J* 188: 451–458, 1980.

20. Brie J, Favier J, Rustin P. Tricarboxylic acid cycle dysfunction as a cause of human diseases and tumor formation. *AJP Cell Physiol* 291: C1114–C1120, 2006.

21. Brière J-J, Favier J, Gimenez-Roqueplo A-P, Rustin P. Tricarboxylic acid cycle dysfunction as a cause of human diseases and tumor formation. *Am J Physiol Physiol* 291: C1114–C1120, 2006.

22. Brzóska K, Męczyńska S, Kruszewski M. Iron-sulfur cluster proteins: Electron transfer and beyond. *Acta Biochim Pol* 53: 685–691, 2006.

23. Budde SMS, Van Den Heuvel LPWJ, Janssen AJ, Smeets RJP, Buskens CAF, DeMeirleir L, Van Coster R, Baethmann M, Voit T, Trijbels JMF, Smeitink JAM. Combined enzymatic complex I and III deficiency associated with mutations in the nuclear encoded NDUFS4 gene. *Biochem Biophys Res Commun* 275: 63–68, 2000.

24. Burattini S, Ferri R, Battistelli M, Curci R, Luchetti F, Falcieri E. C2C12 murine myoblasts as a model of skeletal muscle development: Morpho-functional characterization. *Eur J Histochem* 48: 223–233, 2004.

25. Burns J, Manda G. Metabolic Pathways of the Warburg Effect in Health and Disease: Perspectives of Choice, Chain or Chance. *Int J Mol Sci* 18: 2755, 2017.

26. Cabrero À, Alegret M, Sánchez RM, Adzet T, Laguna JC, Carrera MV. Increased reactive oxygen species production down-regulates peroxisome proliferator-activated α pathway in C2C12 skeletal muscle cells. *J Biol Chem* 277: 10100–10107, 2002.

27. Cantu D, Schaack J, Patel M. Oxidative inactivation of mitochondrial aconitase results in iron and H2O2-mediated neurotoxicity in rat primary mesencephalic cultures. *PLoS One* 4: e7095, 2009.

28. Chandra D, Singh KK. Genetic insights into OXPHOS defect and its role in cancer. *Biochim Biophys Acta - Bioenerg* 1807: 620–625, 2011.

29. Chase JFA, Tubbs PK. Specific Inhibition of Mitochondrial Fatty Acid Oxidation by 2-Bromopalmitate and its Coenzyme A and Carnitine Esters. *Biochem. J.* .

30. Chen TR. In situ detection of mycoplasma contamination in cell cultures by fluorescent Hoechst 33258 stain. *Exp Cell Res* 104: 255–262, 1977.

31. Dai L, Xu S, Choi SK, Ha CM, Thoudam T, Cha SK, Wiederkehr A, Wollheim CB, Lee IK, Park KS. Oxidative stress and calcium dysregulation by palmitate in type 2 diabetes. *Exp Mol Med* 49: e291-12, 2017.

32. Das AM, Fingerhut R, Wanders RJA, Ullrich K. Secondary respiratory chain defect in a boy with long-chain 3- hydroxyacyl-CoA dehydrogenase deficiency: Possible diagnostic pitfalls. *Eur J Pediatr* 159: 243–246, 2000.

33. David Cantu, Ruth E. Fulton, Derek A. Drechsel MP. Mitochondrial aconitase knockdown attenuates paraquat- induced dopaminergic cell death via decreased cellular metabolism and release of iron and H2O2. *J Neurochem* 118: 79–92, 2011.

34. Derks TGJ, Boer TS, Assen A, Bos T, Ruiter J, Waterham HR, Niezen-Koning KE, Wanders RJA, Rondeel JMM, Loeber JG, Te Kate LP, Smit GPA, Reijngoud DJ. Neonatal screening for medium-chain acyl-CoA dehydrogenase (MCAD) deficiency in The Netherlands: The importance of enzyme analysis to ascertain true MCAD deficiency. *J Inherit Metab Dis* 31: 88–96, 2008.

35. Derks TGJ, Reijngoud DJ, Waterham HR, Gerver WJM, van den Berg MP, Sauer PJJ, Smit GPA. The natural history of medium-chain acyl CoA dehydrogenase deficiency in the Netherlands: Clinical presentation and outcome. *J Pediatr* 148: 665–670, 2006.

36. Derks TGJ, Touw CML, Ribas GS, Biancini GB, Vanzin CS, Negretto G, Mescka CP, Reijngoud DJ, Smit GPA, Wajner M, Vargas CR. Experimental evidence for protein oxidative damage and altered antioxidant defense in patients with medium-chain acyl-CoA dehydrogenase deficiency. *J Inherit Metab Dis* 37: 783–789, 2014.

37. Dhami N, Trivedi DK, Goodacre R, Mainwaring D, Humphreys DP. Mitochondrial aconitase is a key regulator of energy production for growth and protein expression in Chinese hamster ovary cells. *Metabolomics* 14: 136, 2018.

38. Djouadi F, Bonnefont JP, Munnich A, Bastin J. Characterization of fatty acid oxidation in human muscle mitochondria and myoblasts. *Mol Genet Metab* 78: 112–118, 2003.

39. Dummel RJ, Kun E. Studies with Specific Enzyme Inhibitors. *J Biol Chem* 244: 2966–2969, 1969.

40. van Eunen K, Simons SMJ, Gerding A, Bleeker A, den Besten G, Touw CML, Houten SM, Groen BK, Krab K, Reijngoud DJ, Bakker BM. Biochemical Competition Makes Fatty-Acid β-Oxidation Vulnerable to Substrate Overload. *PLoS Comput Biol* 9: 2–9, 2013.

41. F. Feillet, G Steinmann, C. Vianey-Saban, C. de Chillou, N. Sadoul , E. Lefebvre, M. Vidailhet PEB. Adult presentation of MCAD deficiency revealed by coma and severe arrythmias. *Intensive Care Med* 29: 1594–1597, 2003.

42. Flandin P, Donati Y, Barazzone-Argiroffo C, Muzzin P. Hyperoxia-mediated oxidative stress increases expression of UCP3 mRNA and protein in skeletal muscle. *FEBS Lett* 579: 3411–3415, 2005.

43. Gardner PR, Nguyen DH, White CW. Aconitase is a Sensitive and Critical Target of Oxygen Poisoning in Cultured Mammalian Cells and in Rat Lungs. *Proc Natl Acad Sci* 91: 12248–12252, 1994.

44. Garedew A, Hütter E, Haffner B, Gradl P, Gradl L. High-resolution Respirometry for the Study of Mitochondrial Function in Health and Disease . The OROBOROS Oxygraph-2k. In: *11th Congress*

Eu. Shock Soc. 2005, p. 107–111.

45. Ghosh S, Kruger C, Wicks S, Simon J, Kumar KG, Johnson WD, Mynatt RL, Noland RC, Richards BK. Short chain acyl-CoA dehydrogenase deficiency and short-term high-fat diet perturb mitochondrial energy metabolism and transcriptional control of lipid-handling in liver. *Nutr Metab* 13: 1–17, 2016.

46. Gillingham MB, Scott B, Elliott D, Harding CO. Metabolic control during exercise with and without medium-chain triglycerides (MCT) in children with long-chain 3-hydroxy acyl-CoA dehydrogenase (LCHAD) or trifunctional protein (TFP) deficiency. *Mol Genet Metab* 89: 58–63, 2006.

47. Giselli Scaini, Kellen R. Simon AMT, Schuck, Estela N. B. Busanello, Alana P. Moura, Gustavo C. Ferreira, Moacir Wajner , Emilio L. Streck PF. Toxicity of octanoate and decanoate in rat peripheral tissues: evidence of bioenergetic dysfunction and oxidative damage induction in liver and skeletal muscle. *Mol Cell Biochem* 361: 329–335, 2012.

48. Gnaiger E. Bioenergetics at low oxygen: Dependence of respiration and phosphorylation on oxygen and adenosine diphosphate supply. *Respir Physiol* 128: 277–297, 2001.

49. Gnaiger E. Capacity of oxidative phosphorylation in human skeletal muscle. New perspectives of mitochondrial physiology. *Int J Biochem Cell Biol* 41: 1837–1845, 2009.

50. Gnaiger E. Mitochondrial Pathways and Respiratory control. *OROBOROS MiPNet Publ* 2: 43–53, 2009.

51. Gnaiger E. *Mitochondrial Pathways and Respiratory Control An Introduction to OXPHOS Analysis*. 2014.

52. Gnaiger E, Boushel R, Søndergaard H, Munch-Andersen T, Damsgaard R, Hagen C, Díez-Sánchez C, Ara I, Wright-Paradis C, Schrauwen P, Hesselink M, Calbet JAL, Christiansen M, Helge JW, Saltin B. Mitochondrial coupling and capacity of oxidative phosphorylation in skeletal muscle of Inuit and Caucasians in the arctic winter. *Scand J Med Sci Sport* 25: 126–134, 2015.

53. Goncalves S, Paupe V, Dassa EP, Brière J-J, Favier J, Gimenez-Roqueplo A-P, Bénit P, Rustin P. Rapid determination of tricarboxylic acid cycle enzyme activities in biological samples. *BMC Biochem* 17: 5, 2010.

54. Grivennikova VG, Kapustin AN, Vinogradov AD. Catalytic activity of NADH-ubiquinone oxidoreductase (Complex I) in intact mitochondria: Evidence for the slow active/inactive transition. *J Biol Chem* 276: 9038–9044, 2001.

55. Grivennikova VG, Serebryanaya D V, Isakova EP, Belozerskaya TA, Vinogradov AD. The transition between active and de-activated forms of NADH: ubiquinone oxidoreductase (Complex I) in the mitochondrial membrane of Neurospora crassa. *Biochem J* 369: 619–626, 2003.

56. Hailer RG, Henrikason KG, Jorfeldt L, Hultman E, Wibom R, Sahlin K, Areskog N, Gunder M, Ayyad K, Blomqvist CG, Hall RE, Thuillier P, Kennaway NG, Lewis SF. Deficiency of Skeletal Muscle Succinate Dehydrogenase and Aconitase. *J Clin Invest* 88: 1197–1206, 1991.

57. Haller RG, Henriksson KG, Jorfeldt L, Hultman E, Wibom R, Sahlin K, Areskog NH, Gunder M, Ayyad K, Blomqvist CG, Hall RE, Thuillier P, Kennaway NG, Lewis SF. Deficiency of skeletal muscle succinate dehydrogenase and aconitase. Pathophysiology of exercise in a novel human muscle oxidative defect. *J Clin Invest* 88: 1197–1206, 1991.

58. Han D, Canali R, Garcia J, Aguilera R, Gallaher TK, Cadenas E. Sites and Mechanisms of Aconitase Inactivation by Peroxynitrite : Modulation by. *Biochemistry* 44: 11986–11996, 2005.

59. Hocquette JF, Ortigues-Marty I, Pethick D, Herpin P, Fernandez X. Nutritional and hormonal regulation of energy metabolism in skeletal muscles of meat-producing animals. *Livest Prod Sci* 56: 115–143, 1998.

60. Hoeks J, Briedé JJ, de Vogel J, Schaart G, Nabben M, Moonen-Kornips E, Hesselink MKC, Schrauwen P. Mitochondrial function, content and ROS production in rat skeletal muscle: Effect of high-fat feeding. *FEBS Lett* 582: 510–516, 2008.

61. Houten SM, Violante S, Ventura F V., Wanders RJA. The Biochemistry and Physiology of Mitochondrial Fatty Acid β-Oxidation and Its Genetic Disorders. *Annu Rev Physiol* 78: 23–44, 2016.

62. Hutter E, Renner K, Pfister G, Ockl PS, Jansen-Urr P, Gnaiger E. Senescence-associated changes in respiration and oxidative phosphorylation in primary human fibroblasts. *Biochem J* 380: 919–928, 2004.

63. Huynh FK, Green MF, Koves TR, Hirschey MD. *Measurement of fatty acid oxidation rates in animal tissues and cell lines*. 2014.

64. I.D. Wexler, S.G. Hemalatha, J. McConnell, N.R.M. Buist, H-H.M. Dahl, S.A. Berry, S.D. Cederbaum, M.S. Patel and DSK. Outcome of pyruvate dehydrogenase deficiency treated with ketogenic diets: Studies in patients with identical mutations. *Neurology* 49: 1655–1661, 1997.

65. Ijlst L, Wanders RJ. A simple spectrophotometric assay for long-chain acyl-CoA dehydrogenase activity measurements in human skin fibroblasts. *Ann Clin Biochem* 30 (Pt 3): 293–297, 1993.

66. Kalyanaraman B, Claire M. Mitochondrial Aconitase Is a Source of Hydroxyl Radical. *J Biol Chem* 275: 14064–14069, 2000.

67. Kelley DE, Mandarin LJ, Mandarino LJ. Fuel selection in human skeletal muscle in insulin resistance: a reexamination. *Diabetes* 49: 677–683, 2000.

68. Kim JY, Hickner RC, Cortright RL, Dohm GL, Houmard J a. Lipid oxidation is reduced in obese human skeletal muscle. *Am J Physiol Endocrinol Metab* 279: E1039–E1044, 2000.

69. Kohn TA, Myburgh KH. Regional specialization of rat quadriceps myosin heavy chain isoforms occurring in distal to proximal parts of middle and deep regions is not mirrored by citrate synthase activity. *J Anat* 210: 8–18, 2007.

70. Kroemer G, Pouyssegur J. Tumor Cell Metabolism: Cancer's Achilles' Heel. *Cancer Cell* 13: 472–482, 2008.

71. Kumps A, Duez P, Mardens Y. Metabolic, nutritional, iatrogenic, and artifactual sources of urinary organic acids: A comprehensive table. *Clin Chem* 48: 708–717, 2002.

72. Kuznetsov A V, Schneeberger S, Seiler R, Brandacher G, Mark W, Steurer W, Saks V, Usson Y, Margreiter R, Gnaiger E. Mitochondrial defects and heterogeneous cytochrome c release after cardiac cold ischemia and reperfusion. *Am J Physiol Heart Circ Physiol* 286: H1633-41, 2004.

73. Lacobazzi V, Infantino V. Citrate-new functions for an old metabolite. *Biol Chem* 395: 387–399, 2014.

74. Lamantea E, Carrara F, Mariotti C, Morandi L, Tiranti V, Zeviani M. A novel nonsense mutation (Q352X) in the mitochondrial cytochrome b gene associated with a combined deficiency of complexes I and III. *Neuromuscul Disord* 12: 49–52, 2002.

75. Larsen FJ, Schiffer TA, Ørtenblad N, Zinner C, Morales-Alamo D, Willis SJ, Calbet JA, Holmberg HC, Boushel R. High-intensity sprint training inhibits mitochondrial respiration through aconitase inactivation. *FASEB J* 30: 417–427, 2016.

76. Larsen S, Danielsen JH, Søndergård SD, Søgaard D, Vigelsoe A, Dybboe R, Skaaby S, Dela F, Helge JW. The effect of high-intensity training on mitochondrial fat oxidation in skeletal muscle and subcutaneous adipose tissue. *Scand J Med Sci Sport* 25: e59–e69, 2015.

77. Larsen S, Kraunsøe R, Gram M, Gnaiger E, Helge JW, Dela F. The best approach: Homogenization or manual permeabilization of human skeletal muscle fibers for respirometry? *Anal Biochem* 446: 64–68, 2014.

78. Lauble H, Kennedy MC, Emptage MH, Beinert H, Stout CD. The reaction of fluorocitrate with aconitase and the crystal structure of the enzyme-inhibitor complex. *Proc Natl Acad Sci U S A* 93: 13699–13703, 1996.

79. Le W, Abbas AS, Sprecher H, Vockley J, Schulz H. Long-chain acyl-CoA dehydrogenase is a key enzyme in the mitochondrial β-oxidation of unsaturated fatty acids. *Biochim Biophys Acta - Mol Cell Biol Lipids* 1485: 121–128, 2000.

80. Lehman TC, Thorpe C. Alternate Electron Acceptors for Medium-Chain Acyl-CoA Dehydrogenase: Use of Ferricenium Salts. *Biochemistry* 29: 10594–10602, 1990.

81. Li J, Zhao S, Zhou X, Zhang T, Zhao L, Miao P, Song S, Sun X, Liu J, Zhao X, Huang G. Inhibition of lipolysis by mercaptoacetate and etomoxir specifically sensitize drug-resistant lung adenocarcinoma cell to paclitaxel. *PLoS One* 8: e746323, 2013.

82. Li W, Hu Z-F, Chen B, Ni G-X. Response of C2C12 Myoblasts to Hypoxia: The Relative Roles of Glucose and Oxygen in Adaptive Cellular Metabolism. *Biomed Res Int* 2013, 2013.

83. Lian XY, Stringer JL. Inhibition of aconitase in astrocytes increases the sensitivity to chemical convulsants. *Epilepsy Res* 60: 41–52, 2004.

84. Lian XY, Stringer JL. Astrocytes contribute to regulation of extracellular calcium and potassium in the rat cerebral cortex during spreading depression. *Brain Res* 1012: 177–184, 2004.

85. Liang-Jun Yan RLL and RSS. Oxidative damage during aging targets mitochondrial aconitase. *Proc Natl Acad Sci* 94: 11168–11172, 1997.

86. Lim SC, Tajika M, Shimura M, Carey KT, Stroud DA, Murayama K, Ohtake A, McKenzie M. Loss of the Mitochondrial Fatty Acid β-Oxidation Protein Medium-Chain Acyl-Coenzyme A Dehydrogenase Disrupts Oxidative Phosphorylation Protein Complex Stability and Function. *Sci Rep* 8: 1–17, 2018.

87. Lippel K, Beattie DS. The submitochondrial distribution of acid:CoA ligase (AMP) and acid:CoA ligase (GDP) in rat liver mitochondria. *Biochim Biophys Acta (BBA)/Lipids Lipid Metab* 218: 227–232, 1970.

88. López-Ríos F, Sánchez-Aragó M, García-Garía E, Ortega ÁD, Berrendero JR, Pozo-Rodríguez F, López-Encuentra Á, Ballestín C, Cuezva JM. Loss of the mitochondrial bioenergetic capacity underlies the glucose avidity of carcinomas. *Cancer Res* 67: 9013–9017, 2007.

89. Lu Z, Sack MN. ATF-1 is a hypoxia-responsive transcriptional activator of skeletal muscle

mitochondrial-uncoupling protein 3. *J Biol Chem* 283: 23410–23418, 2008.

90. Lunt SY, Vander Heiden MG. Aerobic Glycolysis: Meeting the Metabolic Requirements of Cell Proliferation. *Annu Rev Cell Dev Biol* 27: 441–464, 2011.

91. M. D. Brand, Susan M. Evans JM-M and JBC. Fluorocitrate Inhibition. *Biochem J* 134: 217–224, 1973.

92. Makrecka-Kuka M, Krumschnabel G, Gnaiger E. High-resolution respirometry for simultaneous measurement of oxygen and hydrogen peroxide fluxes in permeabilized cells, tissue homogenate and isolated mitochondria. *Biomolecules* 5: 1319–1338, 2015.

93. Margreth A, Azzone GF. A study of respiration in fluoroacetate-poisoned muscle preparations. *Biochem J* 92: 73–82, 1964.

94. Martines ACMF, van Eunen K, Reijngoud DJ, Bakker BM. The promiscuous enzyme medium-chain 3-keto-acyl-CoA thiolase triggers a vicious cycle in fatty-acid beta-oxidation. *PLoS Comput Biol* 13: e1005461, 2017.

95. Matsumura S, Saitou K, Miyaki T, Yoneda T, Mizushige T, Eguchi A, Shibakusa T, Manabe Y, Tsuzuki S, Inoue K, Fushiki T. Mercaptoacetate inhibition of fatty acid beta-oxidation attenuates the oral acceptance of fat in BALB/c mice. *Am J Physiol Regul Integr Comp Physiol* 295: R82-91, 2008.

96. De Meirleir LJ, Van Coster R, Lissens W. *Disorders of pyruvate metabolism and the tricarboxylic acid cycle*. 2006.

97. Mirsattari SM, Shen B, Leung LS, Rajakumar N. A gliotoxin model of occipital seizures in rats. *Seizure* 17: 483–489, 2008.

98. Mookerjee SA, Gerencser AA, Nicholls DG, Brand MD. Quantifying intracellular rates of glycolytic and oxidative ATP production and consumption using extracellular flux measurements. *J Biol Chem* 292: 7189–7207, 2017.

99. Morand C, Besson C, Demigne C, Remesy C. Importance of the Modulation of Glycolysis in the Control of Lactate Metabolism by Fatty Acids in Isolated Hepatocytes from Fed Rats. *Arch. Biochem. Biophys.* 309: 254–260, 1994.

100. Murphy SM, Jakeman PM, Kiely PA, Kiely M, Carson BP. Optimization of an in vitro bioassay to monitor growth and formation of myotubes in real time. *Biosci Rep* 36: e00330–e00330, 2016.

101. Murray AJ, Cole MA, Lygate CA, Carr CA, Stuckey DJ, Little SE, Neubauer S, Clarke K. Increased

mitochondrial uncoupling proteins, respiratory uncoupling and decreased efficiency in the chronically infarcted rat heart. *J Mol Cell Cardiol* 44: 694–700, 2008.

102. Nabben M, Hoeks J, Briedé JJ, Glatz JFC, Moonen-Kornips E, Hesselink MKC, Schrauwen P. The effect of UCP3 overexpression on mitochondrial ROS production in skeletal muscle of young versus aged mice. *FEBS Lett* 582: 4147–4152, 2008.

103. Nada MA, Chace DH, Sprecher H, Roe CR. Investigation of β-oxidation intermediates in normal and MCAD-deficient human fibroblasts using tandem mass spectrometry. *Biochem Mol Med* 54: 59–66, 1995.

104. Najdekr L, Gardlo A, Mádrová L, Friedecký D, Janečková H, Correa ES, Goodacre R, Adam T. Oxidized phosphatidylcholines suggest oxidative stress in patients with medium-chain acyl-CoA dehydrogenase deficiency. *Talanta* 139: 62–66, 2015.

105. Nima N. Naseri, Hui Xu, Joseph Bonica, Jean Paul G. Vonsattel, Etty P. Cortes, Larry C. Park, Jamshid Arjomand and GEG. Abnormalities in the Tricarboxylic Acid Cycle in Huntington Disease and in a Huntington Disease Mouse Model. *J Neuropathol Exp Neurol* 74: 527–537, 2016.

106. Nouws J, Te brinke H, Nijtmans LG, Houten SM. ACAD9, a complex I assembly factor with a moonlighting function in fatty acid oxidation deficiencies. *Hum Mol Genet* 23: 1311–1319, 2014.

107. Nsiah-Sefaa A, McKenzie M. Combined defects in oxidative phosphorylation and fatty acid -oxidation in mitochondrial disease. *Biosci Rep* 36: e00313–e00313, 2016.

108. O'Reilly LP, Andresen BS, Engel PC. Two novel variants of human medium chain acyl-CoA dehydrogenase (MCAD): K364R, a folding mutation, and R256T, a catalytic-site mutation resulting in a well-folded but totally inactive protein. *FEBS J* 272: 4549–4557, 2005.

109. Oezen I, Rossmanith W, Forss-Petter S, Kemp S, Voigtländer T, Moser-Thier K, Wanders RJ, Bittner RE, Berger J. Accumulation of very long-chain acids does not affect mitochondrial function in adrenoleukodystrophy protein deficiency. *Hum Mol Genet* 14: 1127–1137, 2005.

110. Ohta Shigeo IO. Contribution of dysfunction of mitochondria and oxidative stress in the pathogenesis of Alzheimer's disease: On defects in the cytochrome c oxidase complex and aldehyde detoxification. *J Alzheimer's Dis* 9: 155–166, 2006.

111. Ojuka E, Andrew B, Bezuidenhout N, George S, Maarman G, Madlala HP, Mendham A, Osiki PO. Measurement of beta-oxidation capacity of biological samples by respirometry: A review of

principles and substrates. *Am J Physiol Endocrinol Metab* 310: E715–E723, 2016.

112. Ott M, Gogvadze V, Orrenius S, Zhivotovsky B. Mitochondria, oxidative stress and cell death. *Apoptosis* 12: 913–922, 2007.

113. Owens KM, Kulawiec M, Desouki MM, Vanniarajan A, Keshav K. Impaired OXPHOS Complex III in Breast Cancer. *pone0023846* 6: 3–118, 2011.

114. Palmeira CM, Moreno AJ. *Mitochondrial Bioenergetics*. 2nd ed. Springer New York, 2018.

115. Perevoshchikova I V., Quinlan CL, Orr AL, Gerencser AA, Brand MD. Sites of superoxide and hydrogen peroxide production during fatty acid oxidation in rat skeletal muscle mitochondria. *Free Radic Biol Med* 61: 298–309, 2013.

116. Pesta D, Hoppel F, Macek C, Messner H, Faulhaber M, Kobel C, Parson W, Burtscher M, Schocke M, Gnaiger E. Similar qualitative and quantitative changes of mitochondrial respiration following strength and endurance training in normoxia and hypoxia in sedentary humans. *AJP Regul Integr Comp Physiol* 301: R1078–R1087, 2011.

117. Phielix E, Schrauwen-hinderling VB, Mensink M, Lenaers E, Meex R, Hoeks J, Kooi ME, Moonen-kornips E, Sels J, Hesselink MKC, Schrauwen P. Lower intrinsic ADP stimulated mitochondrial respirationin underlies in vivo mitochondrial dysfunction in muscle of male type 2 diabetic patients. *Diabetes* 57: 2943–2949, 2008.

118. Porter C, Hurren NM, Cotter M V., Bhattarai N, Reidy PT, Dillon EL, Durham WJ, Tuvdendorj D, Sheffield-Moore M, Volpi E, Sidossis LS, Rasmussen BB, Børsheim E. Mitochondrial respiratory capacity and coupling control decline with age in human skeletal muscle. *Am J Physiol - Endocrinol Metab* 309: E224–E232, 2015.

119. Puchowicz MA, Varnes ME, Cohen BH, Friedman NR, Kerr DS, Hoppel CL. Oxidative phosphorylation analysis: assessing the integrated functional activity of human skeletal muscle mitochondria—case studies. *Mitochondrion* 4: 377–385, 2004.

120. Rana Ziadeh, Eric P. Hoffman, David N. Finegold, Rita C. Hoop, Jeffrey C. Brackett, Arnold W. Strauss AEWN. Medium Chain Acyl-CoA Dehydrogenase Deficiency in Pennsylvania: Neonatal Screening Shows High Incidence and Unexpected Mutation Frequencies. *Pediatr Res* 37: 675–678, 1995.

121. Reis De Assis D, Maria RDC, Borba Rosa R, Schuck PF, Ribeiro CAJ, Da Costa Ferreira G, Dutra-Filho CS, Terezinha De Souza Wyse A, Duval Wannmacher CM, Santos Perry ML, Wajner M. Inhibition of energy metabolism in cerebral cortex of young rats by the medium-chain fatty

acids accumulating in MCAD deficiency. *Brain Res* 1030: 141–151, 2004.

122. Rena E. Falk, M.D., Stephen D. Cederbaum, M.D., John P. Blass, M.D., Ph.D., Gary E. Gibson, Ph.D., R. A. Pieter Kark, M.D., and Robert E. Carrel MD. Ketonic Diet in the Management of Pyruvate Dehydrogenase Deficiency. *Pediatr Res* 58: 713–721, 1976.

123. Rinaldo P, Matern D. Disorders of fatty acid transport and mitochondrial oxidation: Challenges and dilemmas of metabolic evaluation. *Genet Med* 2: 338–344, 2000.

124. Rinaldo P, Matern D, Bennett MJ. Fatty Acid Oxidation Disorders. *Annu Rev Physiol* 64: 477–502, 2002.

125. Rotig A, de Lonlay P, Chretien D, Foury F, Koenig M, Sidi D, Munnich A RP. Aconitase and mitochondrial iron–sulphur protein deficiency in Friedreich ataxia. *Nat Genet* 17: 215–217, 1997.

126. Rustin P, Bourgeron T, Parfait B, Chretien D, Munnich A, Rotig A. Inborn errors of the krebs cycle: a group of unusual mitochondrial diseases in human. *Biochim Biophys Acta* 1361: 185–197, 1997.

127. S. M. S. Budde, L.P.W.J.van den Heuvel, R.J.P. Smeets, D.Skladal, J. A. Mayr, C. Boelen, V. Petruzzella SP and JAMS 1Nijmegen. Clinical heterogeneity in patients with mutations in the NDUFS4 gene of mitochondrial complex I. *j.inherit.metab* 26: 813–815, 2003.

128. Sakai C, Yamaguchi S, Sasaki M, Miyamoto Y, Matsushima Y, Goto Y ichi. ECHS1 mutations cause combined respiratory chain deficiency resulting in leigh syndrome. *Hum Mutat* 36: 232–239, 2015.

129. Saks VA, Veksler VI, Kuznetsov A V., Kay L, Sikk P, Tiivel T, Tranqui L, Olivares J, Winkler K, Wiedemann F, Kunz WS. Permeabilized cell and skinned fiber techniques in studies of mitochondrial function in vivo. In: *Bioenergetics of the Cell: Quantitative Aspects*. 1998.

130. Sauer SW, Okun JG, Hoffmann GF, Koelker S, Morath MA. Impact of short- and medium-chain organic acids, acylcarnitines, and acyl-CoAs onmitochondrial energy metabolism. *Biochim Biophys Acta - Bioenerg* 1777: 1276–1282, 2008.

131. Scha¨gger H. Respiratory chain supercomplexes of mitochondria and bacteria Hermann. *Biochim Biophys Acta* 1555: 154–159, 2002.

132. Schlichtholz B, Turyn J, Goyke E, Biernacki M, Jaskiewicz K, Sledzinski Z, Swierczynski J. Enhanced citrate synthase activity in human pancreatic cancer. *Pancreas* 30: 99–104, 2005.

133. Scholte HR, Ross JD, Blom W, Boonman AMC, van Diggelen OP, Hall CL, Huijmans JGM, Luyt-Houwen IEM, Kleijer WJ, de Klerk JBC, Przyrembel H, Verduin MHM, Verstegen JCM. Assessment of deficiencies of fatty acyl-CoA dehydrogenases in fibroblasts, muscle and liver. *J Inherit Metab Dis* 15: 347–352, 1992.

134. Schönfeld P, Wieckowski MR, Lebiedzińska M, Wojtczak L. Mitochondrial fatty acid oxidation and oxidative stress: Lack of reverse electron transfer-associated production of reactive oxygen species. *Biochim Biophys Acta - Bioenerg* 1797: 929–938, 2010.

135. Schöpf B, Schäfer G, Weber A, Talasz H, Eder IE, Klocker H, Gnaiger E. Oxidative phosphorylation and mitochondrial function differ between human prostate tissue and cultured cells. *FEBS J* 283: 2181–2196, 2016.

136. Schuck PF, Ceolato PC, Ferreira GC, Tonin A, Leipnitz G, Dutra-Filho CS, Latini A, Wajner M. Oxidative stress induction by cis-4-decenoic acid: Relevance for MCAD deficiency. *Free Radic Res* 41: 1261–1272, 2007.

137. Schuck PF, da Costa Ferreira G, Tonin AM, Viegas CM, Busanello ENB, Moura AP, Zanatta Â, Klamt F, Wajner M. Evidence that the major metabolites accumulating in medium-chain acyl-CoA dehydrogenase deficiency disturb mitochondrial energy homeostasis in rat brain. *Brain Res* 1296: 117–126, 2009.

138. Schuck PF, Ferreira G da C, Tahara EB, Klamt F, Kowaltowski AJ, Wajner M. Cis-4-decenoic acid provokes mitochondrial bioenergetic dysfunction in rat brain. *Life Sci* 87: 139–146, 2010.

139. Schuck PF, Ferreira GC, Moura AP, Busanello ENB, Tonin AM, Dutra-Filho CS, Wajner M. Medium-chain fatty acids accumulating in MCAD deficiency elicit lipid and protein oxidative damage and decrease non-enzymatic antioxidant defenses in rat brain. *Neurochem Int* 54: 519–525, 2009.

140. Schuler AM, Wood PA. Mouse models for disorders of mitochondrial fatty acid beta-oxidation. *ILAR J* 43: 57–65, 2002.

141. Seifert EL, Estey C, Xuan JY, Harper ME. Electron transport chain-dependent and -independent mechanisms of mitochondrial H2O2 emission during long-chain fatty acid oxidation. *J Biol Chem* 285: 5748–5758, 2010.

142. Shen JJ, Matern D, Millington DS, Hillman S, Feezor MD, Bennett MJ, Qumsiyeh M, Kahler SG, Chen YT, Van Hove JLK. Acylcarnitines in fibroblasts of patients with long-chain 3-hydroxyacyl-CoA dehydrogenase deficiency and other fatty acid oxidation disorders. *J Inherit Metab Dis* 23:

27–44, 2000.

143. Shigenaga MK, Hagen TM, Ames BN. Oxidative damage and mitochondrial decay in aging. *Proc Natl Acad Sci* 91: 10771–10778, 2006.

144. Silberstein L, Webster SG, Travis M, Blau HM. Developmental progression of myosin gene expression in cultured muscle cells. *Cell* 46: 1075–1081, 1986.

145. Simon Eaton KB and MP. Mammalian mitochondrial β-oxidation. *Biochem J* 320: E1039-E1044A345-357, 1996.

146. Sofou K, Dahlin M, Hallböök T, Lindefeldt M, Viggedal G, Darin N. Ketogenic diet in pyruvate dehydrogenase complex deficiency: short- and long-term outcomes. *J Inherit Metab Dis* 40: 237–245, 2017.

147. Spiekerkoetter U. Effects of a fat load and exercise on asymptomatic VLCAD deficiency. *J Inherit Metab Dis* 30: 405, 2007.

148. Spiekerkoetter U, Lindner M, Santer R, Grotzke M, Baumgartner MR, Boehles H, Das A, Haase C, Hennermann JB, Karall D, de Klerk H, Knerr I, Koch HG, Plecko B, Röschinger W, Schwab KO, Scheible D, Wijburg FA, Zschocke J, Mayatepek E, Wendel U. Management and outcome in 75 individuals with long-chain fatty acid oxidation defects: Results from a workshop. *J Inherit Metab Dis* 32: 488–497, 2009.

149. Spiekerkoetter Ute PAW. Mitochondrial fatty acid oxidation disorders: Pathological studies in mouse models. 33: 539–546, 2010.

150. Stadlmann S, Rieger G, Amberger A, Kuznetsov A V., Margreiter R, Gnaiger E. H2O2-mediated oxidative stress versus cold ischemia-reperfusion: Mitochondrial respiratory defects in cultured human endothelial cells. *Transplantation* 74: 1800–18003, 2002.

151. Steiber A, Kerner J, Hoppel CL. Carnitine: A nutritional, biosynthetic, and functional perspective. *Mol Aspects Med* 25: 455–473, 2004.

152. Steinlechner-Maran R, Eberl T, Kunc M, Margreiter R, Gnaiger E. Oxygen dependence of respiration in coupled and uncoupled endothelial cells. *Am J Physiol Physiol* 271: C2053–C2061, 1996.

153. Sugden MC, Holness MJ, Palmer TN. Fuel selection and carbon flux during the starved-to-fed transition. *Biochem J* 263: 313–23, 1989.

154. Sumegi B, Srere PA. Complex I binds several mitochondrial NAD-coupled dehydrogenases. *J Biol*

Chem 259: 15040–15045, 1984.

155. Tajima G, Sakura N, Yofune H, Nishimura Y, Ono H, Hasegawa Y, Hata I, Kimura M, Yamaguchi S, Shigematsu Y, Kobayashi M. Enzymatic diagnosis of medium-chain acyl-CoA dehydrogenase deficiency by detecting 2-octenoyl-CoA production using high-performance liquid chromatography: A practical confirmatory test for tandem mass spectrometry newborn screening in Japan. *J Chromatogr B Anal Technol Biomed Life Sci* 823: 122–130, 2005.

156. Taylor RW, Jackson S, Pourfarzam M, Bartlett K, Turnbull DM. Measurement of acyl-CoA dehydrogenase activity in cultured skin fibroblasts and blood platelets. *J Inherit Metab Dis* 15: 727–732, 1992.

157. Taylor WA, Mejia EM, Mitchell RW, Choy PC, Sparagna GC, Hatch GM. Human Trifunctional Protein Alpha Links Cardiolipin Remodeling to Beta-Oxidation. *PLoS One* 7: e48628, 2012.

158. Tein I. *Handbook of Clinical Neurology: Disorders of fatty acid oxidation*. 3rd ed. Elsevier B.V., 2013.

159. Tein I. Impact of fatty acid oxidation disorders in child neurology: From Reye syndrome to Pandora's box. *Dev Med Child Neurol* 57: 304–306, 2015.

160. Tetreault M, Fahiminiya S, Antonicka H, Mitchell GA, Geraghty MT, Lines M, Boycott KM, Shoubridge EA, Mitchell JJ, Michaud JL, Majewski J. Whole-exome sequencing identifies novel ECHS1 mutations in Leigh syndrome. *Hum Genet* 134: 981–991, 2015.

161. Tonin AM, Grings M, Knebel LA, Zanatta Â, Moura AP, Ribeiro CAJ, Leipnitz G, Wajner M. Disruption of redox homeostasis in cerebral cortex of developing rats by acylcarnitines accumulating in medium-chain acyl-CoA dehydrogenase deficiency. *Int J Dev Neurosci* 30: 383–390, 2012.

162. Tremblay LA, Fisher P, Leusch FDL, Heuvel MR Van Den, Nicolas J, Pillon A, Balaguer P. Potential of Sodium Fluoroacetate (1080) and Fluorocitrate to Bind to Androgen and Oestrogen Receptors. *Australas J Ecotoxicol* 1080: 155–162, 2004.

163. Tremblay LA, Fisher P, Leusch FDL, Heuvel MR Van Den, Nicolas J, Pillon A, Balaguer P. Potential of Sodium Fluoroacetate (1080) and Fluorocitrate to Bind to Androgen and Oestrogen Receptors. *Australas J Ecotoxicol* 1080: 155–162, 2005.

164. Turner N, Bruce CR, Beale SM, Hoehn KL, So T, Rolph MS, Cooney GJ. Excess lipid availability increases mitochondrial fatty acid oxidative capacity in muscle: Evidence against a role for reduced fatty acid oxidation in lipid-induced insulin resistance in rodents. *Diabetes* 56: 2085–

2092, 2007.

165. Tyni T, Majander A, Kalimo H, Rapola J, Pihko H. Pathology of skeletal muscle and impaired respiratory chain function in long-chain 3-hydroxyacyl-CoA dehydrogenase deficiency with the G1528C mutation. *Neuromuscul Disord* 6: 327–337, 1996.

166. Villani G, Attardi G. In vivo control of respiration by cytochrome c oxidase in wild-type and mitochondrial DNA mutation-carrying human cells. *Proc Natl Acad Sci U S A* 94: 1166–71, 1997.

167. Villarreal-Pérez JZ, Villarreal-Martínez JZ, Lavalle-González FJ, Torres-Sepúlveda MDR, Ruiz-Herrera C, Cerda-Flores RM, Castillo-García ER, Rodríguez-Sánchez IP, Martínez de Villarreal LE. Plasma and urine metabolic profiles are reflective of altered beta-oxidation in non-diabetic obese subjects and patients with type 2 diabetes mellitus. *Diabetol Metab Syndr* 6: 129, 2014.

168. Vockley J, Whiteman DAH. Defects of mitochondrial β-oxidation: A growing group of disorders. *Neuromuscul. Disord.* 12: 235–246, 2002.

169. Votion DM, Gnaiger E, Lemieux H, Mouithys-Mickalad A, Serteyn D. Physical fitness and mitochondrial respiratory capacity in horse skeletal muscle. *PLoS One* 7: e34890, 2012.

170. Wajner M, Amaral AU. Mitochondrial dysfunction in fatty acid oxidation disorders: insights from human and animal studies. *Biosci Rep* 36: e00281–e00281, 2016.

171. Wanders RJ, Vreken P, den Boer ME, Wijburg F a, van Gennip a H, IJlst L. Disorders of mitochondrial fatty acyl-CoA beta-oxidation. *J Inherit Metab Dis* 22: 442–87, 1999.

172. Wanders RJA, Ruiter JPN, IJlst L, Waterham HR, Houten SM. The enzymology of mitochondrial fatty acid beta-oxidation and its application to follow-up analysis of positive neonatal screening results. *J Inherit Metab Dis* 33: 479–494, 2010.

173. Wang H, Sreenivasan U, Gong D-W, O'Connell K a, Dabkowski ER, Hecker P a, Ionica N, Konig M, Mahurkar A, Sun Y, Stanley WC, Sztalryd C. Cardiomyocyte-specific perilipin 5 overexpression leads to myocardial steatosis and modest cardiac dysfunction. *J Lipid Res* 54: 953–65, 2013.

174. Wang Y, Mohsen AW, Mihalik SJ, Goetzman ES, Vockley J. Evidence for physical association of mitochondrial fatty acid oxidation and oxidative phosphorylation complexes. *J Biol Chem* 285: 29834–29841, 2010.

175. Ward PF, Peters RA. The chemical and biochemical properties of fluorocitric acid. *Biochem J* 78: 661–668, 1961.

176. Warren BE, Lou P-H, Lucchinetti E, Zhang L, Clanachan AS, Affolter A, Hersberger M, Zaugg M, Lemieux H. Early mitochondrial dysfunction in glycolytic muscle, but not oxidative muscle, of the fructose-fed insulin-resistant rat. *AJP Endocrinol Metab* 306: E658–E667, 2014.

177. Winterbourn CC. Toxicity of iron and hydrogen peroxide: the Fenton reaction. *Toxicol Lett* 82–83: 969–974, 1995.

178. Yaffe D, Saxel O. Serial passaging and differentiation of myogenic cells isolated from dystrophic mouse muscle. *Nature* 270: 725–727, 1977.

179. Zheng J. Energy metabolism of cancer: Glycolysis versus oxidative phosphorylation (review). *Oncol Lett* 4: 1151–1157, 2012.

Appendix

A.1 Determination of the effective concentration of inhibitors: Protocol for MTT Assay

The purpose of this experiment is to determine the effective concentrations of inhibitors to be used as well as time of treatment for each. Three biological repeats to be applied for this determination.

- Grow 3000 cells per well in a 96 well plate
- For the two inhibitors, use the following concentrations; (0, 0.25, 0.5, 1, 2, 4, 6, 8, 10 mM).
- Plate each concentration in triplicate; 27 wells (9 x 3) for each inhibitor; 54 wells for both inhibitor (see figure A.1)
- Fill the edges of the plate with 200µL of media to prevent evaporation of media in the remaining wells.

	1	2	3	4	5	6	7	8	9	10	11	12
A						200UL						
B												
C				FIRST	INHIBITOR		90UL					
D										BLANK	200UL	
E										100UL		
F				SECOND	INHIBITOR		90UL					
G												
H					200UL							

Figure A.1: Plate layout for MTT assay

<u>Plating of cells</u>

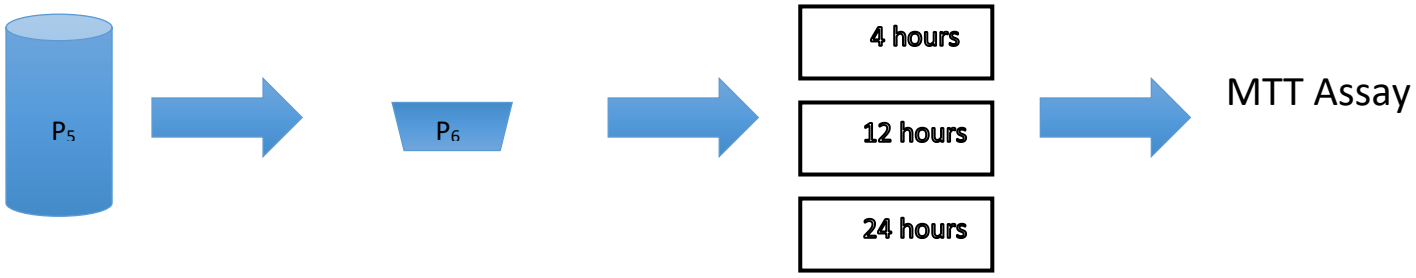

- Use a plate per treatment time point (4, 12 & 24 hrs), hence 3 plates in total
- The 3 plates would be plated with cells at the same time
- Suspend cells in 90µL of Dmem^{++}. Hence to get 3000 in 90µL;

54 wells per plate; 3 plates X 54 wells = 162 wells ≈ 200 wells

90µL in 200 wells = 18, 000µL

Want; 3000 cells in 90µL

Hence, 60 X 10^4 cells in 18000µL

Therefore, will need to have 600, 000 cells in 18ml to get 3000 cells in 90µL of Dmem^{++} (Differentiation media).

Concentration of Inhibitors

- The inhibitors are miscible in DMEM
- Make up 1M of main stock solution.
- Re-dilute to 100mM

Using $C_1V_1=C_2V_2$: C_1= 1M, C_2=100mM, V_2=1000µL, V_1= ?

V_1= 100µL

Therefore, 100µL of 1M stock solution into 900µL of Dmem^{++}.

- 10µL of the inhibitor will be added to 90µL of Dmem^{++} (fig 1)
- For each concentration there will be 30µL/plate (each concentration is done in triplicate). Hence, for the three plates, there will be 90µL/conc. To account for errors and easy pipetting, number would be rounded off to 150µL.
- Hence, prepare a 150µL stock solution such that on adding 10µL of this to each well, should obtain the desired final concentration. See Table A.1 below.
- Dilute 10X concentration in 150µL of Dmem^{++}

- To get 1X concentration, add 10µL of the 10X concentration into the 90µL media containing seeded cells.

For example:

For 0.25mM; 1x = 0.25mM and 10X = 2.5mM

To make a 10X solution; Using $C_1V_1=C_2V_2$: C_1= 100mM, C_2=2.5mM, V_2=150µL, V_1= ?

V_1=3.75µL

Therefore; 3.75µL of 100mM inhibitor stock will be added to 146.25µL $Dmem^+$.

To make 1X solution; $C_1V_1=C_2V_2$: C_1= 2.5mM, C_2=0.25mM, V_2=100µL, V_1= ?

V_1= 10µL

Therefore; 10µL of 2.5mM 10X inhibitor solution will be added to 90µL $Dmem^+$ cell suspension in well.

The same calculation repeated for all the remaining concentrations and shown in table A.1.

Table A.1: Concentration and volume of inhibitor

	1XmM (final concentration required)	10XmM (starting concentration)	Media (µL)	Inhibitor (µL)
A	0	0	150	0
B	0.25	2.5	146.25	3.75
C	0.5	5.0	142.5	7.5
D	1	10	135	15
E	2	20	120	30
F	4	40	90	60
G	6	60	60	90
H	8	80	30	120
	10	100	0	150

6.1.2 Steps to be followed on each day of experiment

Day 1:

- Cell lines used- C2C12, passage number of 5
- Defrost 1 vial of frozen cells quickly at room temperature
- Combine with 5ml of $Dmem^{++}$ in a 15ml falcon tube, centrifuge to get pellets
- Re-suspend pellets in 1ml of $Dmem^{++}$ and add to 6ml of $Dmem^{++}$ in a flask
- Return flask to the incubator

Day 2:

- Once the cells from day 1 have reached about 80% confluency (about 700,000cells), trypsinize to lift cells off tissue culture flask, re-suspend in 5ml of $Dmem^{++}$ in a 15ml falcon tube, centrifuge to get pellets
- Pellets will be resuspended in 18ml of fresh media. Pipette several times to obtain single cell suspensions.
- Load Neubaur haemocytometer with 20 µL of cell suspension for cell counting.
- Record and average cell counts for each of the 4 segments of the counting chamber.
- Use average count for preparing the cell suspension to be used for plating.
- Add $Dmem^{++}$ to each well of the 96-well plate according to figure A.1
- For wells containing cells, after thorough mixing of cell suspension, add 90 µL of this to each as per figure 1.
- Return plates to the incubator

Day 3:

- Once the cells have reached 90% confluency, switch growth media, $Dmem^{++}$ to a differentiation medium- $Dmem^{+}$.

Day 5-9:

- Change differentiation media every second day till the cells have differentiated for 7 days.

Day 9:

- Treat cells with the respective inhibitor concentrations as per table A.1
- Add 150 µL of the inhibitor solution into a new 96-well plate; this would ensure ease of transfer of the solution by multi pipetting into each well as detailed in figure A.1 and table A.1.

0.0mM (150µL)	0.25mM (150µL)	0.5mM (150µL)	1mM (150µL)	2mM (150µL)	4mM (150µL)	6mM (150µL)	8mM (150µL)	10mM (150µL)

- Add 10 µL of inhibitor solution to each well of the three 96-well plates and note the time of treatment
- Treat Each plate for the next step after its incubation period is over
- Plate 1: 4 hrs, Plate 2: 12 hrs, Plate 3: 24 hrs.

E.G after 24 hours:

- Add 10µL of MTT solution to each of the wells containing cells as well as the blank well
- 4 hours later, add 100µL of solubilisation solution to the wells and incubate overnight
- The next morning, read the absorbance using a microplate reader at 595nm, analyse with Graph pad Prism software

Solubilisation solution (250ml)

25g of SLS (Sodium lauryl Sulphate)

250ml of distilled water

76.6ul Conc. HCL

- Follow the same steps for all the other time points.

A.2 Optimization of digitonin for permeabilizing cells

The purpose of this is to get the effective concentration of digitonin that would completely permeabilize cells. Digitonin concentration for permeabilization of cells must be optimized for each cell type/cell line and cell concentration used in respirometry. A single experiment is sufficient to determine this concentration.

- Grow myotubes for 6 days and collect pellets
- Place pellets (10^6 cells) in two Oxygraphy-2K chambers
- The following protocol will be used;

SUIT Protocol

i. First, observe routine respiration after cells have been placed into the O2K
ii. Add rotenone, 1µg/ml (inhibitor of complex I) to block respiration
iii. Add Substrates; 20µl succinate (10mM) and 10µl ADP (2.5mM). These do not stimulate respiration in intact cells, slight increase will represent damaged cells
iv. Digitonin (5mg/ml) is add in 1µl steps up to 10µg/ml. This is to progressively permeabilize the plasma membrane up to an optimum allowing access of substrates to the mitochondria, while leaving the membrane intact.

Respiration is expected to increase with progressive addition of digitonin, once a decrease begins to occur, it signifies over titration of digitonin and thus the maximum concentration needed to permeabilize the cells can be determined.

A.3 Aconitase assay Methodology

Principle

This assay monitors the activity of aconitase indirectly by monitoring the reduction of NAD-dependent isocitrate dehydrogenase. Citrate is converted by aconitase into isocitrate, which is further broken into α-ketoglutarate by isocitrate dehydrogenase. The reduction of NADP at 340nm is monitored kinetically over an hour.

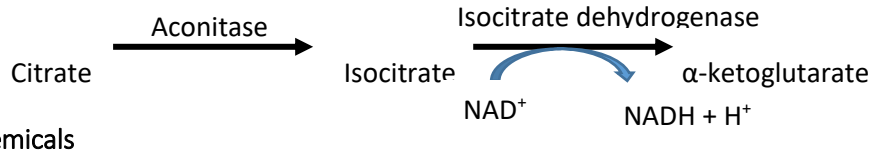

Chemicals

Tri-sodium citrate (Uviv AR 58225000), β-$NADP^+$ (Sigma N050), $MgCl_2$ (Merck), isocitrate dehydrogenase (ICDH) (Sigma 94596), $MgCl_2$ (Merck), Tris-Cl (Sigma 77861)

Stock solutions

Tris-buffer 0.2 M, Mw = 121.14 g/mol (1.21 g in 50ml dH_2O) pH 7.4

Tri-sodium citrate 0.5 M, Mw = 294.10 g/mol (1.47 g in 10 ml DH_2O)

$MgCl_2$ 0.5 M, Mw = 203.3 g/mol (2.03 g in 20 ml dH_2O)

B-$NADP^+$ 0.1 M, Mw = 743.4 g/mol (74.34 mg in 1 ml dH_2O)

ICDH 100 Units/ml

Table A.2: Aconitase assay reagent solutions:

Reagents	Stock Concentration	1 ml	10 ml	25 ml	Final Concentration
Tris-Buffer	0.2 M	250 µl	2.5 ml	6.25 ml	50 mM
Tri-sodium citrate	0.5 M	4 µl	40 µl	100 µl	2 mM
$MgCl_2$	0.5 M	1 µl	10 µl	25 µl	0.5 mM
B-$NADP^+$	0.1 M	2 µl	20 µl	50 µl	0.2 mM
ICDH	100 U/ml	15 µl	150 µl	375 µl	1.5 U/ml

Fill up with DH_2O, pH 7.4

Generating NADPH standard

Chemicals:

NADPH Sigma N7505

Na_2CO_3 Merck 6392

$NaHCO_3$ Merck 6329

Buffer:

Na_2CO_3 0.08 M Mw 105.99 0.848 g

$NaHCO_3$ 0.02 M Mw 84.01 0.168 g

Make up to 100 ml dH_20

NADPH ± 5 mM Mw 833.4 25 mg

Dissolve in 6 ml buffer

Heat NADPH solution for 10 min in a water bath at 60°C to destroy $NADP^+$

Standardising NADPH:

- Add 1 ml 0.1 M TRIS buffer pH 8.0 (or any other buffer between pH 8 – 12) to 4 quarts cuvettes.
- Read the blanks at 340 nm and write down the values. (NB remember which cuvette is which)
- Pipette 20 µl NADH or NADPH solution into 2 of the cuvettes, invert to mix and read.

Correction factor: Reading 2 – Reading 1

$$\frac{\text{NADH}}{6270} \times \frac{\text{Total volume}}{\text{Volume NADH}} = \text{mM NADH or NADPH}$$

Generating NADPH standard curve:

1. Using clear 96-well plates; make sure the microplate reader is switched on for at least 20 minutes. Set the wavelength to 340nm.
2. Make a solution of 50mM Tris Buffer from 0.2M stock, pH 7.4
3. Dilute the original NADPH standard whose concentration has been measured above serially to get concentrations for a standard curve.
4. By using the table below, pipette the required volumes in duplicate into each well.
5. Add 250 µl 0.05 M (Tris or Imidazole) buffer to each well and read.
6. Subtract the blank value from the rest of the measurements.
7. Draw a graph with the absorbance values on the Y-axis and NADPH concentration (µM) on the X-axis.
8. Determine the slope, expressed as absorbance units / µM

NADPH Stock Solution: 4.89mM.

Doing 1:1 serial dilutions; e.g. 50 µl 4.89 mM in 50 µl DH_2O; this gives 2.44 mM. For three serial dilutions the concentrations of stock solutions are: 4.89 mM, 2.44 mM, 1.22 mM, 0.61 mM

Table A.3: NADPH Standard Curve

Standard	Initial concentration (mM)	Vol. Stock	Vol. 0.5 Mm Tris	Final concentration (µM)
Blank	-	0	250	-
1	0.61	10	240	24.4
2	1.22	10	240	48.8
3	2.44	10	240	97.6
4	4.89	10	240	195.6

Procedure for kinetic determination for aconitase activity

1. Under “Protocol”, Open Aconitase-protocol
2. SETTINGS: wavelength (340 nm), shaking duration 5secs before measurements, 25°C, Kinetics: read every min for 2 hrs.
3. Add 15µl of each sample; 240 µl complete reaction Mix to each well
4. Place the plate on the plate reader and Start readings immediately
5. Repeat procedure until all samples are done.

Export raw data to Aconitase template on excel sheet

A.4 MCAD activity assay Methodology

Principle

This is a sensitive assay that detects the activity of FAD-dependent MCAD by monitoring the transfer of electrons from FAD to electron transferring flavoprotein (ETF) of the electron transport system (ETS). Octanoyl-CoA is the substrate that binds tightly to the enzyme active site and is oxidized to trans-Δ^2-enoyl-CoA. The organometallic oxidant ferricenium hexafluorophosphate ($Fe^+PF_6^-$) is an excellent alternative electron acceptor that mimics the activity of physiology ETF. $Fe^+PF_6^-$ is reduced during this reaction and the rate of its reduction is measured at 300nm.

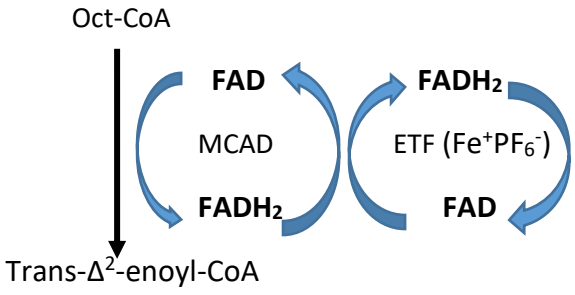

Chemicals

KH_2PO_4 (Sigma P5379), EDTA (Sigma E5134), Sodium tetrathionate (Sigma S5758), ferrocenium hexafluorophosphate (Sigma 388297), Octanoyl-CoA (Sigma 06877)

Reaction Mix/Buffer: KH_2PO_4 + EDTA + Sodium tetrathionate + ferrocenium hexafluorophosphate

Stock solutions

Each component of the reaction mix except $Fe^+PF_6^-$ is measured and added together; made up to 100ml DH_2O (pH 7.4). Complete reaction mix is made after determining $FE^+PF_6^-$.

KH_2PO_4	100mM, Mw 136.086g/mol (1.36g in 100ml DH_2O)
EDTA	1mM, Mw 372.24g/mol (0.0372g in 100ml DH_2O)
Sodium tetrathionate	0.5mM, Mw 306.27g/mol (0.0153g in 100ml DH_2O)
Octanoyl-CoA	0.5mM, Mw 898.73g/mol (5mg in 11.19 DH_2O)
$Fe^+PF_6^-$	71.6µM, Mw 330.999g/mol (determined in spectrophotometer)

In the spectrophotometer

To make up a solution of $Fe^+PF_6^-$ that contains 71.6 µM, add a spatula (~10 mg) of $Fe^+PF_6^-$ powder in a 1.5 ml microfuge tube, to this add 50 ml con HCL. Allow to dissolve for about 10minutes on bench, thereafter vortex vigorously for ~ 30 seconds then centrifuge at 10000 g X for 10minutes, 4°C. Collect the supernatant into a clean microfuge tube. Blank a cuvette containing 996.8 µl DH_2O then add 3.25 µl $Fe^+PF_6^-$. Based on the extinction coefficient for $Fe^+PF_6^-$ a 71.6 µM concentration should read 0.308 Au at 300 nm. The method formula indicates how much $Fe^+PF_6^-$ to add to bring up to 1 ml.

In the microplate reader

The same steps as in the above for spectrophotometric reading of the absorbance are followed; however, the absorbance of 71.6 µM should read as 0.230 Au.

In order to perform subsequent experiments using the microplate reader, a standard curve for $Fe^+PF_6^-$ should be generated according to the table below.

Table A.4: Determination of Ferrocenium ($Fe^{+}PF_6^{-}$) standard

Vol Concentrated $Fe^{+}PF_6^{-}$ (µl)	Vol of reaction mix - $Fe^{+}PF_6^{-}$ (µl)	Concentration (µM)
0	290	0
40	250	9.88
90	200	22.2
140	150	34.6
190	100	46.9
240	50	59.3
290	0	71.6

Procedure

1. Turn on the BIOTEK Synergy (microplate reader), select Gen5 on the computer
2. Under "Protocol", Open Ferrocenium standard-protocol
3. SETTINGS: wavelength (340 nm), shaking duration 5secs before measurements, 35°C
4. Pipette volumes in table above to generate standard curve
5. Read the plate
6. Under "Protocol", Open MCAD-protocol
7. SETTINGS: wavelength (340 nm), shaking duration 5secs before measurements, 35°C, Kinetics: read every 5 mins for 30 mins.
8. Add 20 µl of each sample; 220 µl complete reaction Mix to each well
9. Place the plate on the plate reader and immediately add 50 µl Oct-CoA to each well using a 8-channel pipette
10. Start readings immediately
11. Repeat procedure until all samples are done.
12. Export raw data to MCAD template on excel sheet.

A.5 Citrate synthase Assay Methodology

Principle

This assay monitors the activity of citrate synthase indirectly by monitoring the reduction of NAD^+-dependent conversion of malate to oxaloacetate. Oxaloacetate condenses with acetyl-CoA to form citrate, a reaction catalysed by citrate synthase. This is a fluorometric assay that measures the production of NADH at known time intervals for 10 mins.

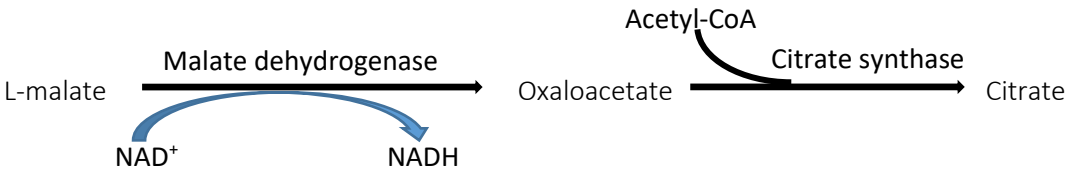

Chemicals

Tris Base	Sigma T-1503
Ethylenediaminetetraacetic acid (EDTA)	Sigma E-5134
NAD^+	Roche 127 965
L-Malate	Sigma M-1125
Malate dehydrogenase (MDH)	Roche 127 256
Acetyl-CoA	Sigma A-2056
NADH	Roche 107 735

Stock solutions

Tris-buffer: Mw 121.1, 0.2 M pH 8.0, 12.11 g/100 ml dH_2O

EDTA: MW 372.2, 0.1 M, 3.722 g/100 ml dH_2O

NAD^+: MW 663.4, 69 mg/1 ml dH_2O, freeze at -80^{0}C in aliquots

L-malate: MW 156.1, 78 mg/5 ml dH_2O, freeze at -80^{0}C in aliquots

Acetyl-CoA: MW 809.6, 3 mM, 5 mg/2 ml dH_2O

NADH: MW 709.3, 36 mg/10 ml buffer, heat NADH solution for 10 min in a water bath at 60^0C to destroy NAD^+

Reagent solutions:

	Initial concentration	25 ml:	50 ml:	120 ml:	Final concentration
Tris buffer	1 M	2.5 ml	5 ml	12 ml	0.1 M
EDTA	0.1 M	625 µl	1.25 ml	3 ml	2.5 M
NAD^+	0.1 M	125 µl	250 µl	600 µl	0.5 M
L-malate	0.1 M	250 µl	500 µl	1.2 ml	1.0 mM
MDH	5 mg/ml	40 µl	80 µl	192 ml	8 µg/ml

Fill up with dH_2O to desired volume; pH 8.0

Standardising NADH

- Add 1ml 0.1 M Tris buffer pH8 to 4 quarts cuvettes
- Read the blanks at 340 nm and write down the values
- Pipette 20 µl NADH solution into 2 of the cuvettes, invert to mix and read.

Correction factor: Reading 2 – reading 1

$$\frac{NADH}{6270}\ X\ \frac{Total\ volume}{Volume\ NADH} = mM\ NADH$$

Generating NADH standard curve

1. Use black plates; make sure the fluorometer is switched on for at least 20 minutes. Set the excitation wavelength to 340/11 nm and the emission wavelength to 460/40 nm.
2. Read the background fluorescence of each well
3. Dilute the original NADH standard 11 times (1:10) with dH_2O
4. By using the table below, pipette the required volumes in duplicate into each well.
5. Add 250 µl 0.05 M tris buffer to each well and read
6. Subtract the blank value from each NADH read
7. Subtract the blank volume from the rest of the measurements

8. Draw a graph with the fluorescence values on the Y-axis and NADH concentration (µM) on the X-axis
9. Determine the slope, expressed as fluorescent units/µM

Table A.5: Development of NADH standards

Standards	Vol. NADH (µl)
A	0
B	2
C	4
D	6
E	8
F	10

Procedure

1. Turn on the BIOTEK synergy and start Gen5 on the computer
2. Under "protocol", open the citrate synthase-protocol
3. Settings:
    a. Excitation wavelength: 340/11
    b. Emission wavelength: 460/40
    c. Optics position: top; sensitivity:100
    d. Shaking intensity = 3, shaking duration = 3 seconds before measurements
    e. Temperature: 25^0C
    f. Kinetics: read every 30seconds for 3 minutes
4. Into the side of the plate, pipette 5 µl sample; 5 µl acetyl-CoA in the other side
5. Place the plate on the reader and add 250 µl reagent solution to each using a 8-channel pipette
6. Start the readings
7. After completion, export to Microsoft excel
8. Repeat procedure until all samples are done